

AMERICAN UNIVERSITY OF BEIRUT

PROCESS-BASED FLOW AND TRANSPORT MODELS FOR
KARST AQUIFERS

by
CHRISTIANE ANTOINE ZOGHBI

A dissertation
submitted in partial fulfillment of the requirements
for the degree of Doctor of Philosophy
to the Department of Civil and Environmental Engineering
of the Faculty of Engineering and Architecture
at the American University of Beirut

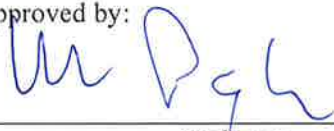
Beirut, Lebanon
May 2016

AMERICAN UNIVERSITY OF BEIRUT

PROCESS-BASED FLOW AND TRANSPORT MODELS FOR
KARST AQUIFERS

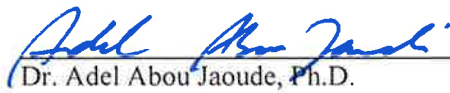
by
CHRISTIANE ANTOINE ZOGHBI

Approved by:



Dr. Habib Basha, Professor
Civil and Environmental Engineering

Advisor



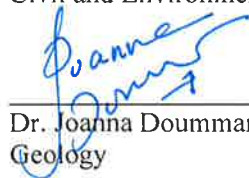
Dr. Adel Abou Jaoude, Ph.D.
Khatib & Alami

Member of Committee



Dr. Majdi Abou Najm, Assistant Professor
Civil and Environmental Engineering

Member of Committee



Dr. Joanna Doummar, Assistant Professor
Geology

Member of Committee

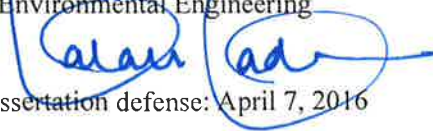
Dr. Wajdi Najem, Professor
Université Saint Joseph

Member of Committee



Dr. Salah Sadek, Professor
Civil and Environmental Engineering

Member of Committee



Date of dissertation defense: April 7, 2016

AMERICAN UNIVERSITY OF BEIRUT

DISSERTATION RELEASE FORM

Student Name: Zoghbi Christiane Antoine
Last First Middle

Master's Thesis Master's Project Doctoral Dissertation

I authorize the American University of Beirut to: (a) reproduce hard or electronic copies of my thesis, dissertation, or project; (b) include such copies in the archives and digital repositories of the University; and (c) make freely available such copies to third parties for research or educational purposes.

I authorize the American University of Beirut, **three years after the date of submitting my dissertation** to: (a) reproduce hard or electronic copies of it; (b) include such copies in the archives and digital repositories of the University; and (c) make freely available such copies to third parties for research or educational purposes.

Signature _____ Date _____

ACKNOWLEDGEMENTS

I would like to thank the Lebanese National Council for Scientific Research (NCSR) and the Faculty of Engineering and Architecture for their financial support throughout my graduate studies. This work would not have been possible without the three-year scholarship obtained through the "NCSR PhD Award program". Additional financial support from NCSR through the project entitled "Groundwater Flow and Contaminant Transport Modeling in a Karst Environment" is also acknowledged.

I express my gratitude to the members of the dissertation committee: Drs. Adel Abou Jaoude, Majdi Abou Najm, Joanna Doummar, Wajdi Najem and Salah Sadek for generously offering their time and efforts to review this work and provide insightful comments that significantly improved the thesis. Last but not least, I deeply thank my thesis advisor Dr. Habib Basha for his encouragement and patience throughout this karst journey.

AN ABSTRACT OF THE DISSERTATION OF

Christiane Antoine Zoghbi for Doctor of Philosophy
Major: Environmental and Water Resources
Engineering

Title: Process-Based Flow and Transport Models for Karst Aquifers

Karst aquifers are characterized by the presence of highly developed subterranean conduits embedded in a low porosity matrix. The conduits are hydraulically connected to the matrix and act either as a source or drain depending on the recharge conditions. Distributive models generally face several difficulties in simulating karst aquifers due to the high data requirements and often unknown location and geometry of the conduits. In the present study, simplified process-based flow and transport models are proposed using a one-dimensional conduit system embedded in a two-dimensional matrix domain. The flow in the conduit can be under pressurized or free-surface flow conditions, and it is driven by a diffuse aquifer recharge as well as a concentrated recharge applied at the conduit entrance. The governing equation is a coupled system of nonlinear differential equations that is solved numerically using the method of finite differences. Analytical and Laplace transform solutions are also obtained for given initial and boundary conditions using linearizing assumptions. The linear solutions simulate the typical shape of a spring hydrograph using physical parameters rather than empirical ones. They are computationally advantageous and reproduce the response of more complex numerical models while requiring less data than two- or three-dimensional dual-hydraulic models. The proposed models are successfully applied to real karst aquifer systems thus demonstrating their effectiveness in simulating observed spring hydrographs. A transport model is also proposed using the same conceptual framework as the flow models. It takes into account the physical representation of the matrix and its parameters, and serves to simulate tracer breakthrough curves. The transport model is applied to actual karst systems and effectively reproduced measured tracer breakthrough curves using physically meaningful parameters.

CONTENTS

| | Page |
|-----------------------------|------|
| ACKNOWLEDGEMENTS | v |
| ABSTRACT | vi |
| LIST OF ILLUSTRATIONS | xii |
| LIST OF TABLES | xvi |

Chapter

| | |
|---|----|
| 1. INTRODUCTION | 1 |
| 1.1. Karst Aquifers: Definition and Importance | 1 |
| 1.2. Developments in Karst Modeling..... | 2 |
| 1.3. Thesis Objectives | 5 |
| 1.4. Thesis Scope..... | 6 |
| 1.5. Thesis Organization..... | 7 |
| 2. PIPE FLOW MODEL – THEORY..... | 8 |
| 2.1. Flow Processes | 8 |
| 2.1.1 Pipe flow..... | 10 |
| 2.1.2 Matrix flow..... | 11 |
| 2.1.3 Exchange flow | 12 |
| 2.2. Combined Pipe-Matrix Flow | 12 |
| 2.3. Auxiliary Conditions | 13 |
| 2.3.1 Boundary conditions in the conduit domain..... | 13 |
| 2.3.2 Boundary conditions in the aquifer domain | 14 |
| 2.3.3 Initial conditions | 14 |
| 2.3.4 Diffuse recharge variation | 15 |
| 2.4. Dimensionless Forms | 15 |

| | | |
|--|--|-----------|
| 2.5. | Numerical Solution..... | 16 |
| 2.6. | Karst Pipe Flow Models..... | 19 |
| 2.6.1 | Bound conduit and finite aquifer (BB)..... | 19 |
| 2.6.2 | Bound conduit and semi-infinite aquifer (BU)..... | 21 |
| 2.6.3 | Unbound conduit and finite aquifer (UB)..... | 21 |
| 2.6.4 | Unbound conduit and semi-infinite aquifer (UU)..... | 22 |
| 2.7. | Optimal Coefficient..... | 23 |
| 2.8. | Summary of Important Results..... | 24 |
| 3. PIPE FLOW MODEL – ANALYSIS AND RESULTS | | 26 |
| 3.1. | Salient Results | 26 |
| 3.1.1 | Key model parameters..... | 26 |
| 3.1.2 | Hypothetical setup | 27 |
| 3.1.3 | Spring hydrograph..... | 28 |
| 3.1.3.1 | Concentrated recharge | 28 |
| 3.1.3.2 | Diffuse aquifer recharge | 31 |
| 3.1.4 | Sensitivity Analysis | 32 |
| 3.1.5 | Effect of conduit nonlinearity..... | 34 |
| 3.1.6 | Effect of aquifer boundary conditions | 36 |
| 3.1.7 | Effect of conduit boundary conditions | 36 |
| 3.2. | Comparison to Other Models | 39 |
| 3.2.1 | Lumped and process-based models | 39 |
| 3.2.2 | Distributive models | 40 |
| 3.3. | Parameter Estimation | 41 |
| 3.3.1 | Parameter ranges | 41 |
| 3.3.2 | Nonlinear least square fitting..... | 42 |
| 3.4. | Model Application and Results | 42 |
| 3.4.1 | Santa Fe River Sink/Rise system..... | 42 |
| 3.4.2 | Model assumptions..... | 44 |
| 3.4.3 | Initial parameter estimates and dimensionless system | 45 |
| 3.4.4 | Model results and analysis..... | 46 |
| 3.4.4.1 | Flood A | 46 |
| 3.4.4.2 | Flood B | 49 |
| 3.4.4.3 | Flood C | 50 |
| 3.5. | Summary of Important Results..... | 51 |

| | |
|---|----|
| 4. CHANNEL FLOW MODEL – THEORY | 52 |
| 4.1. Flow Processes | 52 |
| 4.2. Combined Channel-Aquifer Flow | 54 |
| 4.3. Auxiliary Conditions | 55 |
| 4.3.1 Boundary conditions in the conduit domain..... | 55 |
| 4.3.2 Boundary conditions in the aquifer domain | 55 |
| 4.3.3 Initial conditions..... | 55 |
| 4.4. Dimensionless Forms | 56 |
| 4.5. Numerical Solution..... | 57 |
| 4.6. Karst Channel Flow Models..... | 58 |
| 4.6.1 Semi-infinite aquifer solution (KWU)..... | 58 |
| 4.6.2 Finite aquifer solution (KWB)..... | 60 |
| 4.7. Optimal Coefficient..... | 60 |
| 4.8. Summary of Important Results..... | 62 |
| 5. CHANNEL FLOW MODEL–ANALYSIS AND RESULTS .63 | |
| 5.1. Salient Results | 63 |
| 5.1.1 Key model parameters | 63 |
| 5.1.2 Hypothetical Scenario | 64 |
| 5.1.3 Spring hydrograph | 65 |
| 5.1.3.1 Concentrated recharge | 65 |
| 5.1.3.2 Diffuse aquifer recharge | 66 |
| 5.1.4 Sensitivity analysis | 67 |
| 5.1.5 Effect of conduit nonlinearity..... | 71 |
| 5.1.6 Effect of boundary conditions | 73 |
| 5.2. Comparison to existing models | 75 |
| 5.3. Parameter Estimation | 76 |
| 5.4. Model Applications and Results..... | 77 |
| 5.4.1 Bluegrass Spring, Missouri..... | 77 |
| 5.4.2 Lurbach Karst System, Austria..... | 82 |
| 5.4.2.1 Area description..... | 82 |
| 5.4.2.2 Model Assumptions | 83 |
| 5.4.2.3 Model results | 85 |
| 5.5. Summary of Important Results..... | 88 |

| | |
|---|-----|
| 6. TRANSPORT MODEL – THEORY | 89 |
| 6.1. Transport Processes | 89 |
| 6.1.1 Conduit transport | 89 |
| 6.1.2 Matrix transport | 90 |
| 6.1.3 Exchange solute flux | 90 |
| 6.2. Combined Conduit-Aquifer Transport | 91 |
| 6.3. Boundary Conditions..... | 91 |
| 6.4. Dimensionless System..... | 92 |
| 6.5. Karst Transport Models | 93 |
| 6.5.1 Semi-infinite aquifer (KTM) | 94 |
| 6.5.2 Finite aquifer (KTMB) | 96 |
| 6.6. Summary of Important Results..... | 96 |
| 7. TRANSPORT MODEL – ANALYSIS AND RESULTS | 97 |
| 7.1. Salient Results | 97 |
| 7.1.1 Key model parameters | 97 |
| 7.1.2 Effect of non-constant velocities | 98 |
| 7.1.3 Effect of boundary conditions | 99 |
| 7.1.3.1 Aquifer..... | 99 |
| 7.1.3.2 Instantaneous input pulse..... | 100 |
| 7.2. Comparison to other models..... | 102 |
| 7.3. Parameter Estimation | 103 |
| 7.4. Model Applications | 104 |
| 7.4.1 Dyers and Quarry springs | 104 |
| 7.4.2 Sagebach spring..... | 107 |
| 7.4.3 Olaorta spring | 108 |
| 7.4.4 Villanueva del Rosario spring | 111 |
| 7.5. Summary of Important Results..... | 115 |
| 8. CONCLUSIONS..... | 116 |
| 8.1. Important Conclusions | 116 |
| 8.2. Future Work | 118 |
| 8.2.1 Branched systems solutions..... | 118 |
| 8.2.2 Matrix water levels simulation | 119 |

| | | |
|-------|---|-----|
| 8.2.3 | Hydrological models | 119 |
| 8.2.4 | Synthesized flow and transport modeling approach..... | 119 |

Appendix

| | |
|-------------------------------|-----|
| A – RECHARGE EXPRESSIONS..... | 121 |
|-------------------------------|-----|

| | |
|---------------------------------------|-----|
| B – FINITE DIFFERENCE EQUATIONS | 122 |
|---------------------------------------|-----|

| | |
|-------------------|-----|
| BIBLIOGRAPHY..... | 125 |
|-------------------|-----|

ILLUSTRATIONS

| | Page |
|---|------|
| Figure 1. Typical karst aquifer conceptual layout..... | 9 |
| Figure 2. Schematic of the model domain: cross-section along x-axis (top left), top view (bottom left) and pressurized conduit cross section (right) | 10 |
| Figure 3. Mesh schematic: The conduit upstream boundary is located at point (0, 0). The flow in the conduit and matrix are in the X- and Y-directions respectively. The model boundaries are L_c and L_m . The distance between horizontal and vertical lines represents ΔX and $\Delta Y_{j+1/2}$. respectively. The interface is located along the line $[0, L_c]$ in the X-direction..... | 17 |
| Figure 4. Fully bound model (BB) predictions for a concentrated recharge event given select values of the model parameters. The model response is almost instantaneous. As the exchange parameter increases, the peak is reduced and the spring recession becomes longer. Also shown is the finite difference solution (FD) for the linear numerical model. | 30 |
| Figure 5. Fully bound model (BB) predictions for a diffuse recharge event given selected values of the model parameters. The conduit drains the surrounding conduit and is able to transfer a diffuse aquifer recharge towards the spring. | 31 |
| Figure 6. Sensitivity of the hydrograph peak to the model parameters given a concentrated recharge. The model is most sensitive to κ . The coalesced parameter ω results are also shown. | 33 |
| Figure 7. Sensitivity of the hydrograph peak to the model parameters given a diffuse recharge. The model is most sensitive to the specific yield S_y | 34 |
| Figure 8. Comparison between linear (BB) and nonlinear models for a concentrated type of pulse. The linear model is found an acceptable approximation of the nonlinear one..... | 35 |
| Figure 9. Effect of conduit and aquifer boundary conditions on spring hydrograph given a concentrated type of recharge (upper subplot). The unbound conduit models are not able to capture the more complex behavior of bound conduit models thus highlighting the importance of the downstream boundary condition. The semi-infinite aquifer models (BU and UU) are found as acceptable approximations of the finite ones (BB and UB) for $L_m > 2.5$ (lower subplot)..... | 38 |
| Figure 10. . Effect of conduit and aquifer boundary conditions on spring hydrograph given a diffuse type of recharge. As the recharge is applied over larger widths ($L_r = 2.5$ instead of 1), the volume of water recovered at the spring decreases significantly. | 39 |

| | |
|--|----|
| Figure 11. Observed and simulated discharge of the Santa Fe karst system for Flood A. The UU model is able to simulate the observed River Rise with a high goodness of fit and shows a better performance than BB..... | 48 |
| Figure 12. Observed and simulated discharge of the Santa Fe karst system for Flood B using optimized parameters from Flood A. Note that Flood A is also featured (between July 08 and February 09 time ticks)..... | 49 |
| Figure 13. Observed and simulated discharge of the Santa Fe karst system for Flood C. | 50 |
| Figure 14. Open-channel conduit cross section. The conduit either drains the surrounding aquifer (right) or acts as a source (left)..... | 53 |
| Figure 15. KWB (linear) and numerical (nonlinear) model predictions for a concentrated recharge event for selected values of the exchange parameter κ . As the exchange parameter increases, the peak is reduced and the pulse arrival is further delayed. Also shown is the finite difference solution (FD) for the linear model. KWB fails to capture the rising limb and recession period of the nonlinear model. .. | 66 |
| Figure 16. KWB (linear) and numerical (nonlinear) model predictions for a diffuse recharge event. The linear model with a constant conduit velocity can capture either the peak or the whole hydrograph using the selected minimizing equations (KWB-1 corresponds to 4-21, and KWB-2 corresponds to 4-23) | 67 |
| Figure 17. Sensitivity of the model to the parameters in terms of peak outflow for a concentrated recharge. The model is most sensitive to the exchange parameter κ | 68 |
| Figure 18. Sensitivity of the model to the parameters in terms of peak arrival for a concentrated recharge. The velocity parameter α has the highest influence on the peak delay. | 69 |
| Figure 19. Sensitivity of the model to the parameters in terms of outflow volume for a concentrated recharge. The exchange parameter κ is the most sensitive. The change in volume is not as significant as the one observed for the hydrograph peak and peak delay because the volume recovered during the recession compensates the volume lost due to peak reduction..... | 69 |
| Figure 20. Sensitivity of the model to the parameters in terms of peak outflow for a diffuse recharge. The model is most sensitive to the specific yield..... | 70 |
| Figure 21. Sensitivity of the model to the parameters in terms of peak outflow for a diffuse recharge. The model is insensitive to S_y but most sensitive to α | 70 |
| Figure 22. Sensitivity of the model to the parameters in terms of outflow volume for a diffuse recharge. The specific yield has the most influence on the volume of water reaching the spring from the diffuse recharge. | 71 |

| | |
|---|-----|
| Figure 23. Comparison between KWB (linear) and numerical (nonlinear) models for a concentrated input pulse. The linear model with a non-constant conduit velocity can capture the whole shape of the hydrograph using the selected minimizing equations (KWB-1 corresponds to 4-21, and KWB-2 corresponds to 4-23).... | 73 |
| Figure 24. Comparison between the bound (KWB) and unbound (KWU) channel models for a concentrated recharge. The results are simulated for a constant conduit velocity $c = 65$. The aquifer boundary either affects the recession ($L_m = 7$), the peak and recession ($L_m = 4$) or the whole shape of the hydrograph ($L_m = 2$). The semi-infinite aquifer simplification is valid for $L_m > 7$ where the two models are nearly superimposed..... | 74 |
| Figure 25. Comparison between the finite (KWB) and semi-infinite (KWU) aquifer models for a diffuse aquifer recharge. The results are simulated for a constant conduit velocity $c = 65$. The finite aquifer model is a good approximation of the unbound one for $L_r = L_m > 10$. As the recharge is applied over larger widths, the volume of water recovered at the spring decreases while KWB shows a greater recovery than the semi-infinite aquifer model KWU..... | 75 |
| Figure 26. Observed vs. simulated discharge at the Bluegrass spring for the February 2001 event. KWU is more effective than UU in simulating the long recession. It also compares well to another process-based model (C&W) that simplifies the conduit hydraulics and recharge conditions..... | 81 |
| Figure 27. Observed vs. simulated discharge at the Bluegrass spring for the March 2001 event..... | 82 |
| Figure 28. Schematic representation of the Lurbach karst system | 83 |
| Figure 29. Simulated and observed discharge values at Schmelzbach spring for Event 1. The KWU model is able to simulate the SB's spring hydrograph and is particularly able to capture the delay in pulse arrival from the overflow station (OS). The pressurized pipe model UU simulated an instantaneous response and had a lower performance than KWU's. | 87 |
| Figure 30. Effect of the model parameters on the breakthrough curve. When the advective exchange parameter α increases, the solute mass is lost to the aquifer (compare solid line to coarsely dotted line). Conversely, the diffusive exchange parameter β shows a later recovery of solute (compare solid line to finely dotted line)..... | 98 |
| Figure 31. Comparison between the unbound and bound aquifer models for $S = 200$. The unbound aquifer model is found valid for small aquifer widths that are at least 50 times shorter than the conduit length..... | 101 |
| Figure 32. Comparison between a Dirac-type and short-pulse rectangular input functions. The Dirac-type input approximation is found acceptable for a wide range of pulse durations. | 102 |

| | |
|---|-----|
| Figure 33. Observed vs. simulated Dyers Spring breakthrough curve. | 106 |
| Figure 34. Observed vs. simulated Quarry Spring breakthrough curve..... | 107 |
| Figure 35. Observed vs. simulated Sagebach spring breakthrough curve. | 108 |
| Figure 36. Observed vs. simulated Olaorta, Test 1 spring breakthrough curve..... | 110 |
| Figure 37. Observed vs. simulated Olaorta, Test 2 spring breakthrough curve..... | 111 |
| Figure 38. Schematic representation of the Villanueva del Rosario Spring. Tracers are released in swallow holes (P-arrows) at five locations. Connections were proven between the designated karst windows and spring (i.e. dotted lines). | 112 |
| Figure 39. Computed and measured concentrations for the Sulforhodamine-B tracer test | 114 |
| Figure 40. Computed and measured concentrations for the Pyranine tracer test..... | 115 |

TABLES

| | Page |
|---|------|
| Table 1. Parameter values of pipe flow models' hypothetical run..... | 28 |
| Table 2. Input data for Santa Fe River Sink and Rise karst system..... | 47 |
| Table 3. Estimated dimensionless parameters for Flood A and Flood C..... | 47 |
| Table 4. Parameter values of open channel flow models' hypothetical run | 64 |
| Table 5. Input data for Bluegrass karst system | 80 |
| Table 6. KWU results for the Bluegrass karst system | 80 |
| Table 7. Input data for Lurbach karst system..... | 86 |
| Table 8. Input data for Villanueva del Rosario Spring tracer tests | 112 |

CHAPTER 1

INTRODUCTION

1.1. Karst Aquifers: Definition and Importance

Karst aquifers are characterized as dual-flow systems comprised of a highly conductive conduit network embedded in a low porosity matrix. The conduits are hydraulically connected to the matrix and behave either as a drain or source depending on the recharge conditions. Modeling flow and solute transport in karst aquifers is difficult to achieve due to the heterogeneity of the medium and the existence of different flow processes within the same aquifer [Bakalowicz, 2005]. These include laminar or turbulent flow in the porous matrix, partial or full flow in the subterranean conduit and conduit-matrix exchange at the interface. The flow in a karst system is driven by a groundwater recharge referred to as diffuse aquifer recharge herein as well as a concentrated conduit recharge in form of sinking streams. Both recharge mechanisms originate in the epikarst which is a highly fissured surface layer that facilitates the slow (diffuse) or fast (concentrated) water infiltration to the subterranean saturated zone. These different flow processes are in contrast to the well-developed field of groundwater flow in porous media where the system recharge is mainly diffuse and the flow is described by a simple law (Darcy's). Other modeling challenges in karst arise from the often unknown location and geometry of the underground conduits as well as the high data requirements necessary to reach robust predictions.

Globally, karst aquifers constitute an important fresh water source and supply drinking water to nearly 25% of the world population. However, they are particularly vulnerable to contamination due to the fast conduit flow towards the springs. As a

result, modeling groundwater flow and solute transport in karst aquifers becomes both an essential and challenging task. Although the topic is considered important due to the vulnerability of karst aquifers, the construction of models that describe the flow, transport and interaction of the aquifer's components has received attention only recently [*White, 2002*].

1.2. Developments in Karst Modeling

Karst flow models generally aim to simulate the spring hydrograph that represents the system's response to a recharge event. They are classified into two categories: lumped or physical models. Lumped models rely on an empirical approach to analyze the spring hydrograph recession [e.g. *Maillet, 1905; Mangin, 1975*] or on mathematical relationships between the rainfall and spring discharge [e.g. *Jukić and Denić-Jukić, 2006; Jukić and Denić-Jukić, 2008*]. Conversely, distributive flow models are built in two- or three-dimensional domains and are used for the spatial simulation of aquifer flow. They are usually based on Darcy's equation and are divided into three categories: equivalent porous media (EPM), double continuity (DC) and combined discrete-continuum (CDC) models.

The EPM approach is seldom used in the study of karst systems because it averages the hydraulic heterogeneities into an equivalent porous medium and thus loses the karst flow duality representation. Yet, it has been applied to large scale systems where conduit influences become diluted and where matrix water levels are available for model calibration [*Scanlon et al., 2003*]. In DC models, both matrix and conduit network are represented by continuum formulations or Darcy's equation. The fluid interface exchange is calculated based on the hydraulic head difference between two

continua using a linear exchange formula. DC models have been tested through several studies [e.g. *Maréchal et al.*, 2008; *Doummar*, 2012] and generally show a good correlation to field conditions. In CDC models, the highly conductive karst conduits are considered as one-dimensional discrete elements embedded in a three-dimensional low-permeability matrix. This type of models has an enhanced physical representation of karst duality as compared to others. A more thorough review of lumped and distributive models is available in *Hartmann et al.* [2014].

Existing CDC models assume a pressurized conduit flow that is coupled to a laminar matrix. The flow in the conduit is either laminar or turbulent while the matrix flow is laminar and Darcian. The interface exchange is induced by the hydraulic gradient and is a function of an exchange coefficient. Among these models is CAVE [*Clemens et al.*, 1996] which is the precursor to MODFLOW-CFP [*Shoemaker et al.*, 2008; *Reimann and Hill*, 2009]. Yet, the aforementioned CDC models can only handle pressurized and time-independent conduit flow and are thus unable to simulate open-channel flow in karst conduits. As a result, existing studies either used EPA's SWMM that is designed for urban stormwater drainage [*Chen and Goldscheider*, 2014] or built on the existing MODFLOW-CFP to simulate conduits flowing under various saturated conditions [e.g. *Reimann et al.*, 2011b; *de Rooij et al.*, 2013]. The latter approach is conceptually advantageous because the models have a physical representation of the matrix. Although these models are numerically tested on hypothetical scenarios, they have not been validated and calibrated on actual karst systems because the level of data requirements prevents their usage.

The main limitation of lumped models is their empirical parameters. On the other hand, distributive models are difficult to apply in the absence of information about

the conduits' location, aquifer physical properties and recharge conditions. In order to overcome these difficulties, process-based models combine both lumped and distributive approaches in order to simulate a karst system response to a recharge event. The latter is achieved by simplifying the domain geometry and offering a system conceptualization that is physically meaningful. Consequently, a process-based model's parameters are a function of the system's physical properties and are often derived from the spring hydrograph or its recession limb [e.g. *Baedke and Krothe, 2001; Cornaton and Perrochet, 2002; Kovacs et al., 2005; Birk and Hergarten, 2010*].

Simulating transport in a karst environment can achieve a better understanding of the system hydrodynamics and recharge conditions. However, the encountered difficulties in simulating the flow have hindered the development of transport modules especially in CDC-based models. Yet, tracer tests have proven useful in determining flow paths and underground connections. Their aim is to reduce flow models' uncertainties and get preliminary estimations of conduit flow velocities and dispersion coefficients by simulating the tracer breakthrough curve. The selected modeling approaches depend on the amount of field information available and include (1) time series analysis of natural or artificial spring tracers through correlation or auto-correlation methods, (2) physically-based models that rely on the advection-diffusion equation and (3) process-based simulations that involve a certain conceptualization of the system hydrodynamics.

The one-dimensional advection-diffusion equation gave acceptable estimates of the conduit's physical properties but failed to capture the long tailing of the breakthrough curves. On the other hand, process-based models were more successful in this endeavor by following the partitioning approach. For example, *Field and Pinsky*

[2000] used the two-region (mobile and immobile) non-equilibrium model 2RNE [Toride *et al.*, 1993] to simulate the long tailing of breakthrough curves. However, 2RNE was originally developed to simulate transport in porous media rather than karst. The analogy between karst and 2RNE conceptual models is that conduits represent mobile regions with high flow velocities while the surrounding aquifer, conduit pools and sediments are considered immobile regions with stagnant flows. However, this conceptual approach underrepresents the matrix physical domain and thus prevents the estimation of the aquifer's physical properties from the breakthrough curves. The matrix role is already discussed in Katz *et al.* [1998] and Martin and Dean [2001] who recorded a change of water chemistry in the surrounding matrix after conduit flood events implying a transport of solutes across the conduit/aquifer interface.

1.3. Thesis Objectives

In the present study, a simplified process-based approach to analyze the response of karst aquifers is proposed. The main objective is to develop computationally inexpensive models that are able to simulate karst spring hydrographs and tracer breakthrough curves. The proposed models are based on the physical processes that govern the flow and transport in the main conduit and the surrounding matrix. A second objective is to compare the developed models to existing ones in terms of their performance, simplicity, and versatility. A third objective is to apply the models on real karst systems subject to various recharge and boundary conditions.

1.4. Thesis Scope

Two types of process-based flow models are proposed: pressurized pipe and open-channel flow models. Their conceptual framework consists of a single conduit embedded in a two-dimensional matrix and subject to a concentrated recharge at its entrance and a diffuse aquifer recharge along its length. The flow is described by a coupled system of partial differential equations. For the pipe flow model, the equations are the Darcy-Weisbach for turbulent conduit flow and the Boussinesq equation for the groundwater flow in the matrix. On the other hand, the kinematic wave approximation of the Saint-Venant equations is used in the open-channel model. The analytical models simulate the typical shape of a spring hydrograph using physical parameters rather than empirical ones, and require less data than two- and three-dimensional discrete-continuum models. The pipe flow model simulates almost instantaneous responses to a recharge event while the open-channel flow model captures delays in pulse arrival to a spring. Applications of the models to real karst aquifer systems demonstrate their effectiveness in simulating the observed spring hydrographs.

Finally, a process-based transport model is proposed and aims to simulate tracer breakthrough curves and capture their long tailing. The transport in the conduit and matrix is governed by the advection-diffusion equation while the two elements exchange solute at their common interface. The model is validated using real breakthrough curves and effectively estimates conduit and matrix physical properties.

1.5. Thesis Organization

This thesis is organized as follows:

In *Chapter 2*, the pipe flow model is presented. This chapter deals with the governing equations, their simplifications as well as the mathematical solutions to the coupled system of pipe/matrix flow equations.

In *Chapter 3*, the different approximations and simplifications introduced to the pipe flow model are discussed and assessed. The model is subsequently applied to a karst system.

In *Chapter 4*, process-based flow models for unpressurized conduits are presented.

In *Chapter 5*, the process-based channel flow model is discussed along with its application to the several karst systems subject to various recharge conditions.

In *Chapter 6*, the mathematical formulation and solutions of the process-based transport model are presented.

In *Chapter 7*, the transport model is used to analyze the breakthrough curves obtained from various tracer tests.

Chapter 8 summarizes the important conclusions and discusses future work.

CHAPTER 2

PIPE FLOW MODEL – THEORY

In this chapter, process-based flow models describing the flow in a coupled pipe/matrix karst system are derived. First, the different flow processes occurring in the system are defined and include the pipe, matrix and exchange flow at the interface. Second, the combined system of nonlinear differential equations is obtained for a simplified two-dimensional aquifer domain. A numerical solution is then proposed to solve the system of nonlinear equations for given initial and boundary conditions. Consequently, the system of governing equations is linearized and the Laplace transform method is used to derive computationally advantageous solutions for various conduit and matrix boundary conditions. Finally, an estimation of the optimal linearizing parameter relating nonlinear and linear models is proposed.

2.1. Flow Processes

This study considers a karst conduit embedded in a low porosity matrix with the two elements interacting at their common interface. As shown in Figure 1, the underground conduit receives a concentrated recharge originating from sinkholes, sinking streams or rivers while the aquifer is subject to a diffuse recharge. The conduit flow is turbulent and pressurized. The matrix is assumed a porous medium with prevailing laminar flow conditions.

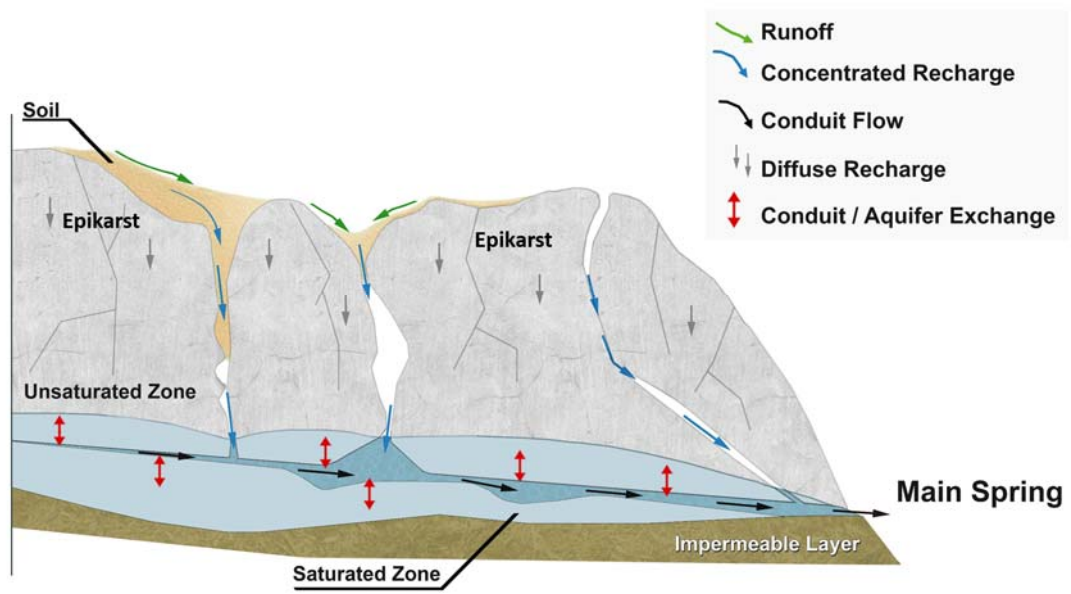


Figure 1. Typical karst aquifer conceptual layout

For the mathematical analysis, the model's physical domain is made of a single conduit of length l_c [L] located at the center of a matrix of width w_m [L] and semi-width l_m [L]. The aquifer diffuse recharge r_* [L/T] is applied over a distance l_r [L] from the conduit's centerline and on its each side. The conduit's upstream boundary is subject to a concentrated recharge referred to as Q_u [L³/T]. The outflow at the lower boundary is the spring hydrograph denoted by Q_* [L³/T]. The model domain being two-dimensional, the conduit and aquifer flows are thus assumed to be in the Cartesian x – and y – directions respectively. A schematic of the model domain is shown in Figure 2. The conduit and aquifer hydraulic heads, h_c and h_m , are measured above the conduit's bottom. The system is under saturated conditions with the water table being higher than the conduit's bottom.

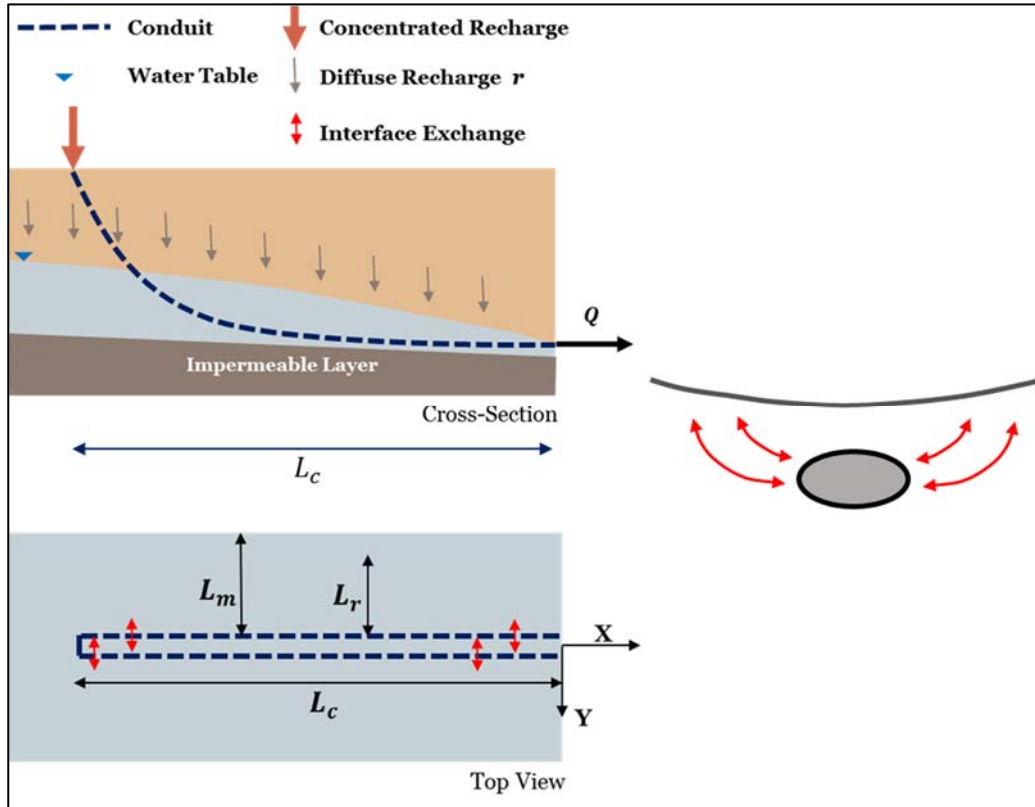


Figure 2. Schematic of the model domain: cross-section along x-axis (top left), top view (bottom left) and pressurized conduit cross section (right)

2.1.1 Pipe flow

The continuity equation for conduit flow Q_* is given by

$$\frac{\partial Q_*}{\partial x} = 2q_{ex} \quad 2-1$$

where q_{ex} is the lateral input [L^2/T] and the coefficient 2 is added to account for exchange on both sides of the conduit. The relationship between the hydraulic gradient and conduit velocity u_* is defined by the Darcy-Weisbach equation for turbulent flows

$$-\frac{\partial h_c}{\partial x} = \frac{f}{4R_h} \frac{u_*^2}{2g} \quad 2-2$$

where R_h is the hydraulic radius [L], g the gravitational acceleration [L/T^2] and f the pipe friction factor [-]. The pipe discharge is thus equal to

$$Q_* = u_* A_* = \beta_* \sqrt{-\frac{dh_c}{dx}} \quad 2-3$$

where $\beta_* = \sqrt{8gR_h A_*^2 / f}$ and A_* is the cross-sectional area of flow [L^2].

2.1.2 Matrix flow

The flow in the aquifer is one-dimensional, in the lateral y -direction and thus perpendicular to the conduit or pipe's centerline. The groundwater flow equation for an unconfined homogenous aquifer is described by

$$\frac{\partial h_m}{\partial t} = \frac{K_m}{S_y} \frac{\partial}{\partial y} \left(h_m \frac{\partial h_m}{\partial y} \right) + \frac{r_*}{S_y} \quad 2-4$$

where K_m is the aquifer's hydraulic conductivity [L/T], S_y the specific yield or drainable porosity [-], h_m the hydraulic head measured from the base of the conduit [L], y – the Cartesian coordinate in the aquifer flow direction [L] and r_* the recharge to groundwater referred to as diffuse aquifer recharge [L/T]. The aquifer recharge originates from the slow infiltration in the epikarst layer and reaches the water table as a pulse r_* .

Equation (2-4) is known as the Boussinesq equation for horizontal aquifers and is obtained by coupling the continuity equation with Darcy's discharge equation.

Equation (2-4) is nonlinear due to the presence of h_m in the diffusion term. However, its linearization facilitates the application of the Laplace transform method and the subsequent derivation of analytical solutions. One way to linearize it is to assume an average aquifer depth \tilde{h}_m . The product $K_m \tilde{h}_m$ is herein defined as the aquifer transmissivity denoted by $T_m [L^2/T]$. The linearized form of Equation (2-4) becomes

$$\frac{\partial h_m}{\partial t} = \frac{T_m}{S_y} \frac{\partial^2 h_m}{\partial y^2} + \frac{r_*}{S_y} \quad 2-5$$

2.1.3 Exchange flow

The pipe and matrix exchange water at their common interface that is located at $y = 0$. The interface flow is proportional to the difference in hydraulic heads and a linear exchange coefficient as expressed by Darcy's law

$$q_{ex} = K_m D \left. \frac{\partial h_m}{\partial y} \right|_{y=0} \quad 2-6$$

where D is the height of the interface [L].

2.2. Combined Pipe-Matrix Flow

The coupled conduit-aquifer flow equation is obtained by combining Equations (2-3) and (2-1) using (2-6). The governing equation becomes

$$-\frac{\beta_*^2}{2Q_*} \frac{\partial^2 h_c}{\partial x^2} = \kappa_* \frac{\partial h_m}{\partial y} \Big|_{y=0} \quad 2-7$$

where $\kappa_* = 2K_m D$.

In order to simplify Equation (2-7), a linear relationship between the discharge and hydraulic head gradient is proposed

$$Q_* = -\beta_{l_*} \frac{dh_c}{dx} \quad 2-8$$

where β_{l_*} is the conduit conductivity parameter for a linearized flow.

Combining Equations (2-8) and (2-1) through (2-6), one obtains

$$-\beta_{l_*} \frac{\partial^2 h_c}{\partial x^2} = \kappa_* \frac{\partial h_m}{\partial y} \Big|_{y=0} \quad 2-9$$

The linear parameter can be expressed in terms of a linearizing coefficient Q_{m*} such that $\beta_{l_*} = \beta_*^2 / 2Q_{m*}$.

2.3. Auxiliary Conditions

2.3.1 Boundary conditions in the conduit domain

The upstream boundary condition at $x = 0$ is the input hydrograph referred to as the dimensionless discharge Q_u . The downstream boundary is either unbound or bound at $x = l_c$ and $x \rightarrow \infty$ respectively. Therefore, the conduit's boundaries are

$$\frac{dh_c}{dx} = -Q_u/\beta_{l^*} \quad x = 0 \quad 2-10$$

$$h_c = h_d(t) \quad x = l_c \quad 2-11$$

$$h_c = h_i \quad x \rightarrow \infty \quad 2-12$$

where $h_d(t)$ represents the temporal variation of the downstream boundary.

The time functions used for the conduit's upstream flux boundary Q_u and downstream head boundaries $h_d(t)$ are defined in Appendix A.

2.3.2 *Boundary conditions in the aquifer domain*

The aquifer is considered either semi-infinite or finite. At the interface or $y = 0$, the heads in the aquifer are equal to the ones in the conduit. The boundary conditions become

$$h_m = h_c \quad y = 0 \quad 2-13$$

$$\frac{dh_m}{dy} = 0 \quad y = l_m \quad 2-14$$

$$h_m = h_i \quad y \rightarrow \infty \quad 2-15$$

2.3.3 *Initial conditions*

The model assumes zero or uniform initial conditions. It is spatially constant when the conduit's downstream end is unbound

$$h_c = h_m = Q_u(0)[l_c - x]/\beta_{l^*} + h_d(0) \quad t = 0 \quad 2-16$$

2.3.4 Diffuse recharge variation

The aquifer recharge term $r(T)$ is considered as a piecewise recharge

$$r_*(t) = \begin{cases} r_0, & 0 \leq t < t_1 \\ r_1, & t_1 \leq t < t_2 \\ \dots & \dots \\ r_n, & t_n \leq t < t_{n+1} \end{cases} \quad 2-17$$

where n is the number of recharge pulses.

2.4. Dimensionless Forms

Define the following dimensionless variables

$$\frac{x}{X} = \frac{y}{Y} = \frac{h}{H} = d_0; \quad \frac{t}{T} = t_0; \quad u = \frac{u_*}{u_0}; \quad u_0 = \frac{Q_0}{d_0^2}; \quad Q_0 = \frac{d_0^3}{t_0}; \quad Q = \frac{Q_*}{Q_0} \quad 2-18$$

where d_0 [L], t_0 [T] and u_0 [L/T] are the characteristic depth, time and velocity respectively and Q_0 is the normalizing flow [L^3/T]. The dimensionless aquifer flow Equation (2-5) becomes

$$\frac{\partial H_m}{\partial T} = \sigma \frac{\partial^2 H_m}{\partial Y^2} + \frac{r}{S_y} \quad 2-19$$

and the dimensionless linear conduit flow Equation (2-9)

$$-\beta_l \frac{\partial^2 H_c}{\partial X^2} = \kappa \frac{\partial H_m}{\partial Y} \Big|_{Y=0} \quad 2-20$$

where $\beta_l = \beta^2/2Q_m$, $\beta = \beta_*/Q_0$, $\kappa = \kappa_*/(u_0d_0)$ and $Q_m = Q_{m^*}/Q_0$.

The above dimensionless forms of the equations simplify the analysis of the system. If t_0 and d_0 are chosen as equal to the time to the input pulse's peak t_p and conduit length l_c (or $0.1 \times l_c$, etc...), one can simplify the physical domain as $L_c = 1$ (or $L_c = 10$, etc...) and easily capture the pulse arrival delay by comparing to $T_p = 1$.

2.5. Numerical Solution

The system of nonlinear governing equations (2-5) and (2-7) is solved numerically using the Crank-Nicolson scheme. The finite difference equations for the conduit and aquifer equations have a tri-diagonal form that is efficiently solved using the Thomas algorithm. The finite difference forms of the equations are presented in Appendix B and the mesh is shown in Figure 3. The discretization in the conduit flow direction (X –direction) is uniform and equal to ΔX while the one in the matrix is non-uniform and equal to $\Delta Y_{j+1/2}$. The latter's values are small near the interface and increase as one moves away in the Y –direction (i.e. $[0, L_c]$ in Figure 3). The no-flow aquifer boundary condition is applied at $Y = L_m$.

The nonlinear pipe module is validated using a simple analytical solution with a constant exchange flow q_{ex} while the matrix subroutine is tested against particular analytical solutions [e.g. *Bruggeman*, 1999]. However, the main challenge remains in coupling the time-independent pipe flow equation (2-7) to the unsteady groundwater flow equation (2-5). As a result, a fictitious time-dependent term is added to Equation (2-7) in order to enhance the coupling process. Each equation is solved in a separate subroutine following the discretizations in Appendix B and are coupled according to the

following algorithm. At each time step, the heads in the pipe are calculated by (1) updating the upstream boundary condition at the first node, (2) using the exchange flux from the previous time step and (3) iterating until convergence is achieved. After the pipe heads converge within a given time step, they are set as a boundary condition in the matrix subroutine in order to calculate the exchange flux at the current time step. The latter is replaced into the pipe subroutine to get a new conduit head distribution using the averaged fluxes from the current and previous time steps. Finally, the calculations are repeated for all time steps. After the system's hydraulic heads h_c are obtained, the spring discharge is calculated using Equation (2-3). This coupling algorithm also applies for the finite difference solution of the linearized model or coupled equations (2-19) and (2-20).

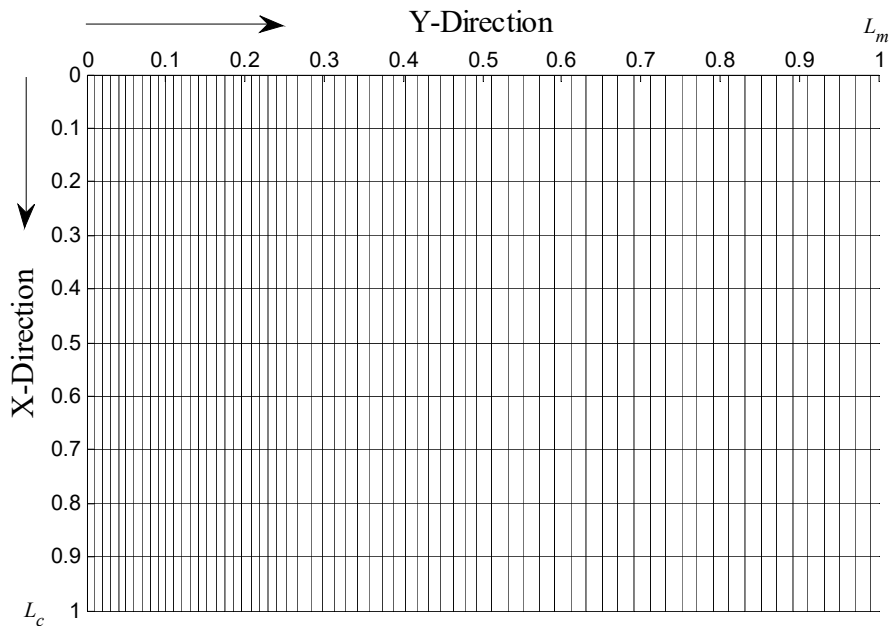


Figure 3. Mesh schematic: The conduit upstream boundary is located at point (0, 0). The flow in the conduit and matrix are in the X- and Y-directions respectively. The model boundaries are L_c and L_m . The distance between horizontal and vertical lines represents ΔX and $\Delta Y_{j+1/2}$ respectively. The interface is located along the line $[0, L_c]$ in the X-direction.

Existing numerical models that couple pipe and matrix flow such as MODFLOW-CFP are highly sensitive to the interface discretization as revealed by hypothetical runs [Reimann *et al.*, 2011a]. Furthermore, the coupling of a time-independent conduit flow (fast flow) with a time-dependent matrix flow (slow flow) is numerically challenging. Therefore, numerical solutions for dual-hydraulic models should be used with careful considerations of time and space discretizations and have to satisfy the Courant number in conduit and matrix. The number of iterations for the conduit and matrix heads should be high and the error tolerance low. Furthermore, the fictitious time-dependent term should be carefully selected as it introduces further numerical dispersion. However, this technique allows the simulation of the spring hydrograph particularly for high exchange coefficients.

Given the above model evaluation and numerical difficulties, there is a need for more computationally advantageous solutions. The latter can be derived for the linearized system of governing equations using the Laplace transform method as shown in the upcoming section. Although the resulting models are exact and fast solutions, they are not able to handle system nonlinearities and heterogeneities as effectively as a numerical or distributive model. They can, however, provide a good approximation of the nonlinear models for a set of assumptions such as homogeneous matrices, linear conduit flow and constant diameter conduit.

2.6. Karst Pipe Flow Models

The proposed pipe flow model consists of solving the simplified system of governing equations (2-19) and (2-20) using the Laplace transform method. The Laplace transform is first applied to the aquifer flow Equation (2-19) and the resulting differential equation is solved for the given aquifer boundary conditions. An expression for the interface flux is therefore obtained and replaced into the conduit flow governing equation. The latter is subsequently solved for the conduit boundary conditions and the solution is either analytically or numerically inverted.

In the upcoming sections, four Laplace transform solutions are derived for a combination of boundary conditions. These include: bound conduit/finite aquifer (BB), bound conduit/semi-finite aquifer (BU), unbound conduit/finite aquifer (UB) and unbound conduit/semi-finite aquifer (UU). The first model BB is the most general case while the others (BU, UB and UU) consist of simplifying either the conduit's or aquifer's boundary conditions.

2.6.1 Bound conduit and finite aquifer (BB)

Taking the Laplace transform on T for the linearized aquifer governing Equation (2-19), one gets

$$p\bar{H}_m - \sigma \frac{d^2\bar{H}_m}{dY^2} = \frac{\bar{r}(p, Y)}{S_y} \quad 2-21$$

where p is a complex parameter and \bar{H}_m is the Laplace transform of H_m

$$\bar{H}_m = \int_0^{\infty} e^{-pT} H_m dT \quad 2-22$$

Solving for a finite aquifer and bound conduit subject to the conditions in (2-10), (2-11), (2-13) and (2-14), one gets

$$\begin{aligned} \bar{H}_c = \bar{H}_i + \operatorname{sech}(L_c \bar{\omega}_b) \left\{ (\bar{Q}_u - \bar{Q}_i) \frac{\sinh[(L_c - X) \bar{\omega}_b]}{\beta_l \bar{\omega}_b} \right. \\ \left. + (\bar{H}_d - \bar{H}_i) \cosh(X \bar{\omega}_b) \right. \\ \left. + \frac{\bar{r}}{pS_y} [\cosh(L_c \bar{\omega}_b) - \cosh(X \bar{\omega}_b)] \right\} \end{aligned} \quad 2-23$$

where $\bar{\omega}_b = \omega p^{1/4} \sqrt{\tanh(L_m \sqrt{p/\sigma})}$, $\omega^2 = \kappa/\beta_l \sqrt{\sigma}$ and \bar{H}_c is the Laplace transform of the conduit hydraulic heads H_c . Differentiating with respect to X and setting $X = L_c$, one gets

$$\bar{Q}_l = \bar{Q}_i + (\bar{Q}_u - \bar{Q}_i) \operatorname{sech}(L_c \bar{\omega}_b) + \beta_l \bar{\omega}_b \tanh(L_c \bar{\omega}_b) \left[\frac{\bar{r}}{pS_y} - (\bar{H}_d - \bar{H}_i) \right] \quad 2-24$$

where \bar{Q}_l is the Laplace transform of the dimensionless linear pipe discharge Q_l . \bar{Q}_u , \bar{H}_d and \bar{r} are expressed in function of the complex parameter p as shown in Appendix A. \bar{Q}_i and \bar{H}_i are constant values and can be replaced by Q_i/p and H_i/p .

Equation (2-24) relates the spring discharge Q_l to the model parameters (β_l , κ , σ and S_y), the model domain (L_c and L_m) as well as the boundary conditions (Q_u , H_d) and diffuse aquifer recharge (r). The equation can also serve as a benchmark for testing the numerical solution's coupling algorithm introduced in Section 2.5 for the linear

system of governing equations. The solution can be evaluated by numerical inversion using the *de Hoog et al.* [1982] algorithm and the routine developed by *Hollenbeck* [1998].

2.6.2 Bound conduit and semi-infinite aquifer (BU)

Applying the conditions in (2-10), (2-11), (2-13) and (2-15), the downstream hydraulic heads become

$$\begin{aligned} \bar{H}_c = \bar{H}_i + \operatorname{sech}(L_c \bar{\omega}_u) & \left\{ (\bar{Q}_u - \bar{Q}_i) \frac{\sinh[(L_c - X) \bar{\omega}_u]}{\beta_l \bar{\omega}_u} \right. \\ & + (\bar{H}_d - \bar{H}_i) \cosh(X \bar{\omega}_u) \\ & \left. + \frac{\bar{r}}{pS_y} \left(1 - e^{-L_r \sqrt{p/\sigma}} \right) [\cosh(L_c \bar{\omega}_u) - \cosh(X \bar{\omega}_u)] \right\} \end{aligned} \quad 2-25$$

where $\bar{\omega}_u = \omega p^{1/4}$ and the discharge is expressed as

$$\begin{aligned} \bar{Q}_l = \bar{Q}_i + (\bar{Q}_u - \bar{Q}_i) \operatorname{sech}(L_c \bar{\omega}_u) \\ + \beta_l \bar{\omega}_u \tanh(L_c \bar{\omega}_u) \left[\frac{\bar{r}}{pS_y} \left(1 - e^{-L_r \sqrt{p/\sigma}} \right) \right. \\ \left. - (\bar{H}_d - \bar{H}_i) \right] \end{aligned} \quad 2-26$$

2.6.3 Unbound conduit and finite aquifer (UB)

Solving for the boundary conditions in (2-10), (2-12), (2-13) and (2-14), the downstream hydraulic heads become

$$\bar{H}_c = \bar{H}_i + \frac{(\bar{Q}_u - \bar{Q}_i) e^{-X \bar{\omega}_b}}{\beta_l \bar{\omega}_b} + \frac{\bar{r}}{S_y} \left[\frac{1 - e^{-L_c \bar{\omega}_b} \cosh(X \bar{\omega}_b)}{p} \right] \quad 2-27$$

and the discharge is equal to

$$\bar{Q}_l = \bar{Q}_i + e^{-L_c \bar{\omega}_b} \left[(\bar{Q}_u - \bar{Q}_i) + \frac{\bar{r} \beta_l}{p S_y} \bar{\omega}_b \sinh(L_c \bar{\omega}_b) \right] \quad 2-28$$

2.6.4 Unbound conduit and semi-infinite aquifer (UU)

For an unbound conduit coupled to an unbound or semi-infinite aquifer (Equations 2-10, 2-12, 2-13 and 2-15), the solution becomes

$$\bar{H}_c = \bar{H}_i + \frac{(\bar{Q}_u - \bar{Q}_i) e^{-X \bar{\omega}_u}}{\beta_l \bar{\omega}_u} + \frac{\bar{r}}{S_y} \left(1 - e^{-L_r \sqrt{p/\sigma}} \right) \left[\frac{1 - e^{-L_c \bar{\omega}_u} \cosh(X \bar{\omega}_u)}{p} \right] \quad 2-29$$

And the discharge is equal to

$$\bar{Q}_l = \bar{Q}_i + e^{-L_c \bar{\omega}_u} \left[(\bar{Q}_u - \bar{Q}_i) + \frac{\bar{r} \beta_l}{p S_y} \bar{\omega}_u \left(1 - e^{-L_r \sqrt{p/\sigma}} \right) \sinh(L_c \bar{\omega}_u) \right] \quad 2-30$$

Equations (2-26), (2-28) and (2-30) are simplifications of the fully bound model BB and serve to study the effect of the downstream boundary condition and aquifer width on the spring hydrograph. The unbound aquifer solutions (BU and UU) are a function of the model parameters, conduit length, boundary conditions, diffuse recharge and recharge length. In the bound aquifer models (BB and UB), the recharge length is equal to the matrix width $L_r = L_m$ and is incorporated in the coalesced

parameter $\bar{\omega}_b$. The downstream boundary condition H_d only shows up in the bound conduit models BB and BU. All aforementioned Laplace transform solutions are numerically inverted using the *Hollenbeck* [1998] routine.

2.7. Optimal Coefficient

The linearizing coefficient Q_m is yet to be determined in order to relate the nonlinear and linear parameters β_l and β^2 . This is achieved by minimizing the residual between the original Equation (2-7) and its linear approximation (2-9)

$$R = -\beta_l \frac{\partial^2 H_c}{\partial X^2} + \frac{\beta^2}{2Q} \frac{\partial^2 H_c}{\partial X^2} = 0 \quad 2-31$$

Equation (2-31) can be rewritten in terms of Q as

$$R = \left(\frac{\beta^2}{2Q} - \beta_l \right) \frac{d^2 H_c}{dX^2} = \left(\frac{Q}{Q_m} - 1 \right) \frac{dQ}{dX} = 0 \quad 2-32$$

Minimizing Equation (2-32) over space and time gives

$$\int_0^T \int_0^{L_c} \left[\left(\frac{Q}{Q_m} - 1 \right) \frac{dQ}{dX} \right] dX dT = 0 \quad 2-33$$

Integrating between 0 and L_c

$$\int_0^T \frac{Q^2}{2Q_m} - Q \Big|_0^{L_c} dT = 0 \quad 2-34$$

Equation (2-34) is rewritten as

$$\int_0^T \left\{ \frac{Q^2(L_c, T) - Q^2(0, T)}{2Q_m} - [Q(L_c, T) - Q(0, T)] \right\} dT = 0 \quad 2-35$$

Or

$$Q_m = \frac{1}{2} \frac{\int_0^T [Q^2(L_c, T) - Q^2(0, T)] dT}{\int_0^T [Q(L_c, T) - Q(0, T)] dT} \quad 2-36$$

Equation (2-36) provides a useful relationship between the linear and nonlinear models. The computationally advantageous Laplace transform solutions can thus be related to the nonlinear numerical one using $\beta_l = \beta^2/2Q_m$. The value of the linearizing parameter Q_m is well-defined because the boundary values at $X = 0$ and $X = L_c$ are known in inverse problems. The integrals in Equation (2-36) can be evaluated numerically between time $T = 0$ and $T = T_m$ or at a defined time $T = T_m$.

2.8. Summary of Important Results

A conceptual coupled pipe/matrix model is proposed to simplify a real karst aquifer. It consists of a single conduit coupled to the surrounding matrix at their common interface. The pipe flow is described by the Darcy-Weisbach equation and the matrix flow by the Boussinesq equation for unconfined aquifer flow. The interface

exchange flow is governed by Darcy's law. The coupled system of governing equations is consequently linearized and solutions are derived using the Laplace transform method for different boundary conditions. The latter include finite and semi-infinite aquifer conditions as well as bound and unbound conduit downstream conditions.

The Laplace transform solutions provide a relationship between the spring discharge, conduit/matrix physical properties as well as the boundary and recharge conditions. They thus combine all flow processes occurring in a karst aquifer in one single equation. They can be numerically inverted using efficient algorithms and provide a computationally inexpensive method to simulating spring hydrographs.

Finally, an optimal relationship between the linear and nonlinear model's parameters is obtained. The latter facilitates the approximation of the nonlinear model using the computationally advantageous linear ones and allows a better interpretation of the parameters.

CHAPTER 3

PIPE FLOW MODEL – ANALYSIS AND RESULTS

In this chapter, the outflow of the various models is generated for specific recharge mechanisms and boundary conditions. First, the key pipe flow model parameters and their effect on the spring hydrograph are discussed. Consequently, the linear model is compared to the nonlinear numerical one in order to validate the linear conduit flow simplification. Then, a comparison between the finite and semi-infinite aquifer solutions is carried out in order to assess the effect of aquifer width on the spring hydrograph. Similarly, the free conduit discharge models are compared to the bound conduit ones. Finally, the models are applied to a real karst system located in Florida, USA that is subject to a concentrated recharge in form of a sinking river that emerges further downstream as a perennial spring.

3.1. Salient Results

3.1.1 Key model parameters

The models' parameters are the exchange coefficient κ , aquifer coefficient σ , drainable porosity S_y and pipe conductivity β (nonlinear) or β_l (linear). The linear and nonlinear β or β_l are related through the linearizing coefficient Q_m that is calculated using Equation (2-36). An additional coalesced parameter ω was also introduced and combines all four parameters. When the aquifer diffuse recharge r and downstream boundary condition H_d are zero, simpler relationships of the spring discharge are obtained. Indeed, UU becomes a function of ω while UB, BB and BU are in terms of both ω and σ . Consequently, a smaller number of fitting parameters is required for

systems undergoing a concentrated recharge (Q_u) as compared to a diffuse aquifer recharge.

In case of diffuse recharge, the interface depth D should be less or equal to the average depth in the aquifer \tilde{h}_m . After algebraic manipulations of the parameters, one finds that the parameter κ should be less or equal to the product $2\sigma S_y$.

3.1.2 Hypothetical setup

In order to evaluate the output of the different models, assess their performance and simplifications, the following study setup is proposed. A single circular conduit of length $l_c = 1,000 \text{ m}$ is coupled to an aquifer of semi-width $l_m = 1,000 \text{ m}$. The aquifer's properties are $K_m = 0.006 \text{ m/s}$ and $T_m = 0.03 \text{ m}^2/\text{s}$. The average conduit/matrix interface length is assumed equal to $D = 5 \text{ m}$. The conduit's cross-sectional area is assumed as $A_* = 50 \text{ m}^2$ and the conductivity factor as $\beta_*/A_* = 1.5 \text{ m/s}$. Given the above values of the system's properties, the dimensional model parameters become equal to: $\beta_* = 75 \text{ m}^3/\text{s}$; $\kappa_* = 1 \text{ m}^2/\text{s}$ and $\sigma_* = 0.75 \text{ m}^2/\text{s}$. The system is subject to a concentrated isosceles triangular pulse with $Q_i = 15 \text{ m}^3/\text{s}$, $Q_p = 150 \text{ m}^3/\text{s}$ where Q_i and Q_p are the baseflow and peak flow respectively. The downstream boundary condition is assumed fixed and equal to zero throughout the simulation. Using the dimensionless system $Q_0 = Q_p$ and $d_0 = l_c$, the model domain and parameters become: $L_c = 1$; $L_m = 1$; $\beta = 0.5$; $\kappa = 0.4$ and $\sigma = 1$. The dimensionless pulse characteristics are $Q_p = 1$, $T_p = 1$ and the total simulation duration is $T_d = 4$. Later, the system is subject to a rectangular diffuse aquifer recharge where $r = 0.1$ and $T_r = 1$ with T_r being the pulse duration. A summary of all dimensional and dimensionless parameters is available in Table 1.

Table 1. Parameter values of pipe flow models' hypothetical run

| Dimensional Parameter | Dimensional Value | Dimensionless Parameter | Dimensionless Value |
|-----------------------|----------------------------|----------------------------|---------------------|
| l_c | 1000m | L_c | 1 |
| l_m | 1000m | L_r | 1 |
| K_m | 0.006m/s | | |
| T_m | 0.03 m ² /s | | |
| S_y | 0.2 | S_y | 0.2 |
| D | 5m | | |
| β_* | 75 m ³ /s | $\beta = \beta_*/Q_0$ | 0.5 |
| $\kappa_* = 2K_mD$ | 0.06 m ² /s | $\kappa = \kappa_*/u_0d_0$ | 0.4 |
| $\sigma_* = T_m/S_y$ | 0.15 m ² /s | $\sigma = T_m/S_y u_0d_0$ | 1 |
| H_d | 0m | β_l | 1 |
| Dimensionless system | | Recharge Type | Concentrated |
| Q_0 | 150 m ³ /s | T_p | 1 |
| d_0 | 1000m | T_d | 4 |
| u_0 | 1.5 × 10 ⁻⁴ m/s | Q_i | 0.1 |
| | | Q_{max} | 1 |
| | | Recharge Type | Diffuse |
| | | r | 0.1 |
| | | T_r | 1 |

3.1.3 Spring hydrograph

3.1.3.1 Concentrated recharge

Figure 4 shows the fully bound linear model (BB) outflow for the selected parameters values in Table 1. The numerical solution of the linearized system of equations agrees with the numerically inverted Laplace transform solution thus validating the coupling algorithm proposed in Section 2.5. The discretization values are as follows: $\Delta X_i = 0.02$; $(\Delta Y_{j+1/2})_{j=1} = 0.001$ at the interface and gradually increases as one moves away towards the boundary with $(\Delta Y_{j+1/2})_{max} = 0.0029$, $\Delta T = 2 \times 10^{-4}$ and $\epsilon = 0.005$. The tolerance level is 10^{-5} and the maximum number of conduit and matrix hydraulic head iterations is 10. The mesh is previously shown in Figure 3.

The conduit-aquifer exchange reduces the peak of the triangular concentrated input pulse and changes its shape into a fast flood followed by a slow baseflow recession. Given that the conduit flow is pressurized, one notices an almost instantaneous response at the spring. When $\kappa = 0$, no conduit/matrix exchange occurs such that the input pulse and resulting spring hydrograph are nearly superimposed. As the exchange coefficient κ increases, the spring outflow peak is reduced and the duration of the baseflow recession becomes longer (Figure 4). Lower pipe conductivities β_l (smaller pipe diameter or higher friction factors) also induce more exchange with the aquifer. As for the matrix parameter σ , it is proportional to the aquifer transmissivity and inversely proportional to the matrix porosity or specific yield S_y . Therefore, as σ is lowered and κ is kept constant (K_m is constant), more exchange occurs with the aquifer due to higher specific yield.

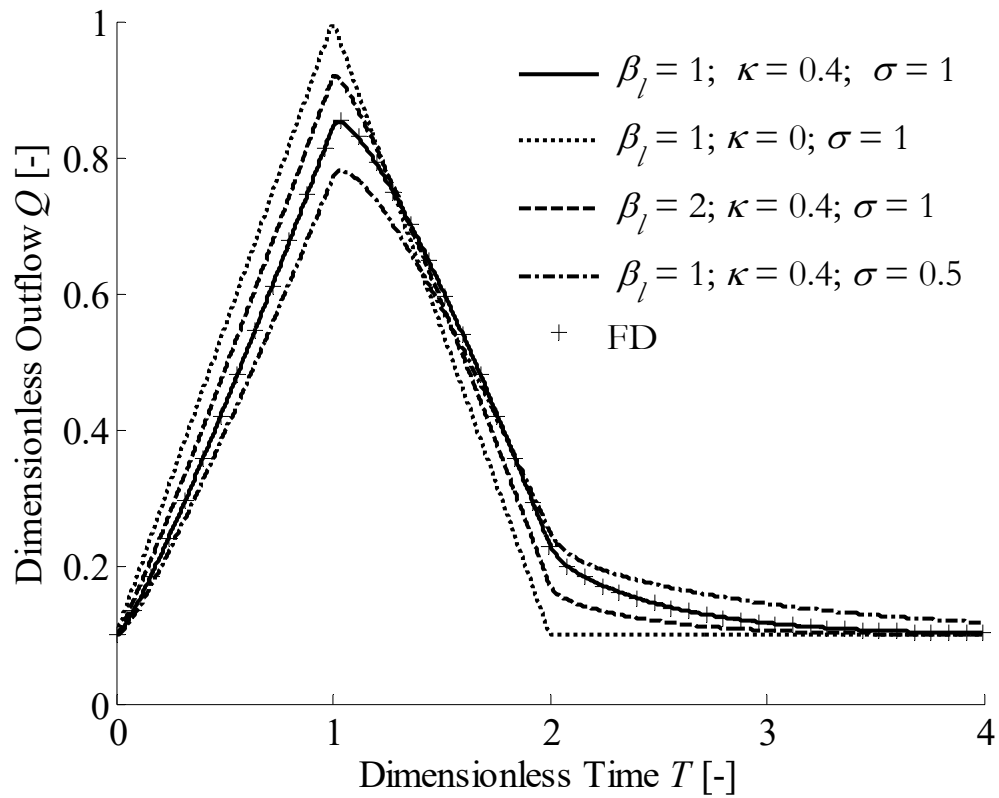


Figure 4. Fully bound model (BB) predictions for a concentrated recharge event given select values of the model parameters. The model response is almost instantaneous. As the exchange parameter increases, the peak is reduced and the spring recession becomes longer. Also shown is the finite difference solution (FD) for the linear numerical model.

3.1.3.2 Diffuse aquifer recharge

The spring hydrograph is also simulated using a diffuse recharge for a range of model parameters (Figure 5). The diffuse aquifer recharge represents the As the exchange coefficient κ is increased, more water crosses the interface and the hydrograph achieves a higher peak. The effect of the matrix parameter σ and specific yield S_y are also shown. As S_y decreases, the velocity in the aquifer decreases and less water is retrieved at the spring. The maximum dimensionless volume retrieved at the spring from a rectangular diffuse pulse is equal to $rT_r(2L_cL_r) = 0.2$.

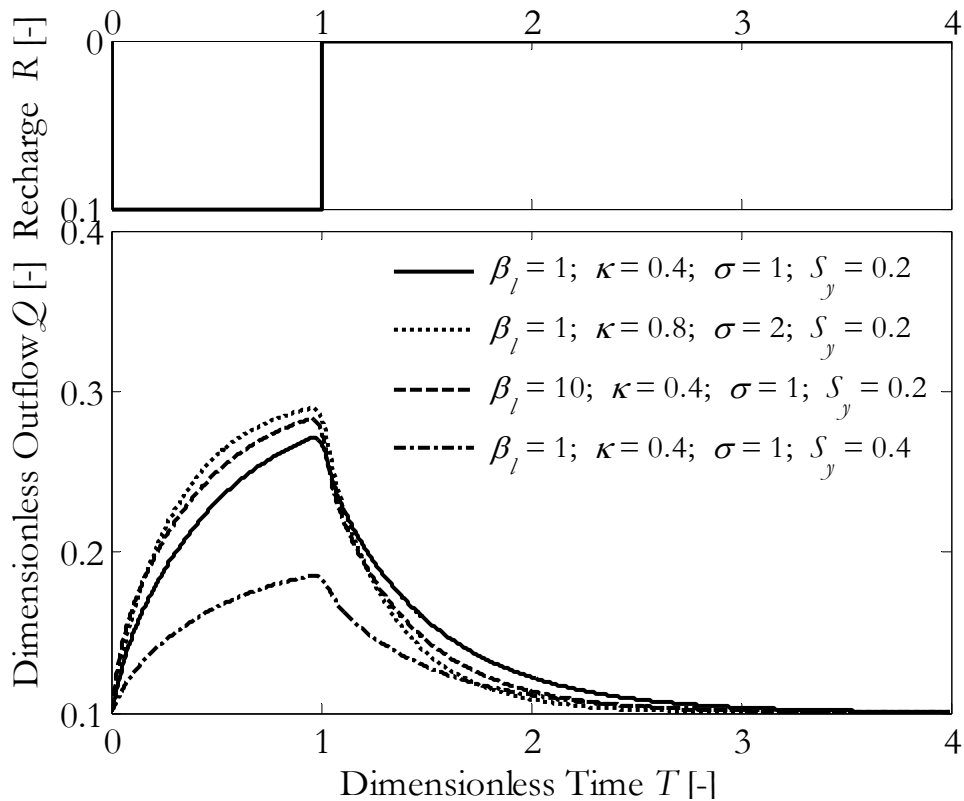


Figure 5. Fully bound model (BB) predictions for a diffuse recharge event given selected values of the model parameters. The conduit drains the surrounding conduit and is able to transfer a diffuse aquifer recharge towards the spring.

3.1.4 Sensitivity Analysis

In order to study the sensitivity of the model results to the calibration parameters κ , β_l and σ , the latter are varied by $\pm 10\%$ from the standard values presented in Table 1. Consequently, the standard and simulated hydrographs are compared by assessing the parameters' effect on the hydrograph peak and volume retrieved at the spring. The fully unbound model UU is used to generate the results.

For a concentrated type of recharge, the results are shown in Figure 6 with the most sensitive parameter being plotted in blue. The figure depicts the change in the peak hydrograph and output volume versus the change in parameter value. The results reveal that κ and σ are the most and least sensitive parameters respectively. This is determined by comparing the slopes of peak variation for each parameter. Furthermore, the figure shows the influence of the coalesced parameter ω which turned out to be more sensitive than the individual parameters κ , β_l and σ . As previously mentioned, ω can be considered as the only calibration parameter in the UU model for concentrated recharge applications. Also, the parameters have more effect on the change in hydrograph peak rather than the change in output volume because the volume lost during the peak reduction period is later recovered during the recession period.

A similar analysis is carried out for the case of a diffuse aquifer recharge. Figure 7 shows that S_y and β_l are the most and least sensitive parameters respectively. Conversely, β_l showed a more significant effect in case of a concentrated recharge. In numbers, a 5% increase in the values of β_l , κ and σ led to a peak change of 0.6%, 1.7% and 1.5% for a diffuse recharge and 1.3%, 1.35% and 0.7% for a concentrated recharge.

However, the sensitivity analysis results reveal that a variation of $\pm 10\%$ in parameter values did not have a significant effect on the peak outflow and output

volume. Indeed, the change was still minimal (i.e. < 5%) for both concentrated and diffuse types of recharge.

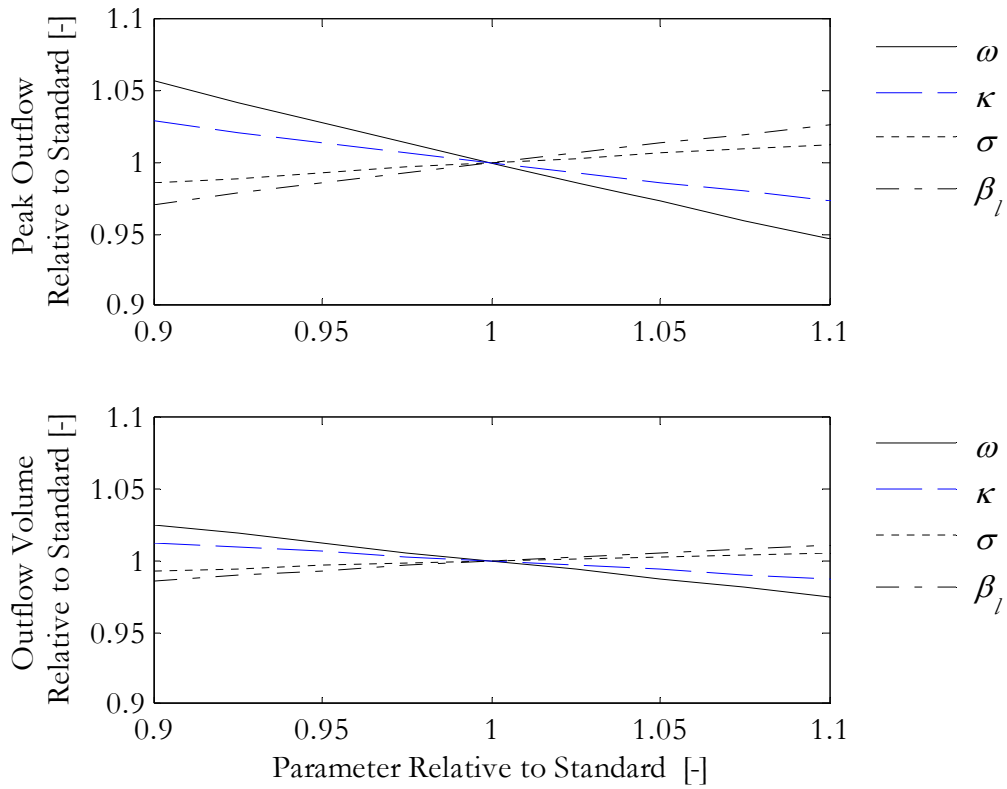


Figure 6. Sensitivity of the hydrograph peak to the model parameters given a concentrated recharge. The model is most sensitive to κ . The coalesced parameter ω results are also shown.

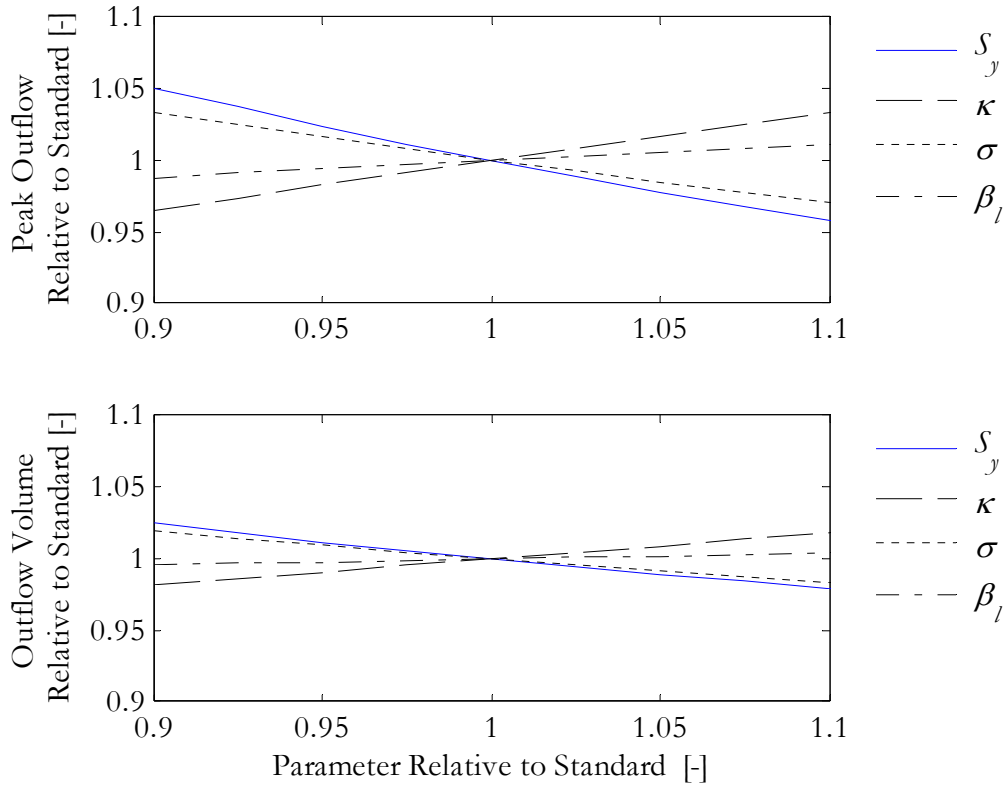


Figure 7. Sensitivity of the hydrograph peak to the model parameters given a diffuse recharge. The model is most sensitive to the specific yield S_y .

3.1.5 Effect of conduit nonlinearity

The effect of the conduit flow linearization is assessed by comparing the behavior of the fully bound model BB to the nonlinear model or coupled Equations (2-5) and (2-7) that are solved numerically. The linearizing coefficient Q_m is evaluated using Equation (2-36) and is a function of the nonlinear model's boundary conditions.

For simplicity reasons, it is hereby suggested to evaluate Equation (2-36) at the peak

outflow with $Q_m = \frac{1}{2} \frac{[Q_p^2(L_c, T_p) - Q_p^2(0, T_p)]}{[Q_p(L_c, T_p) - Q_p(0, T_p)]}$.

Figure 8 shows the simulation results of the study setup introduced in the previous section. The nonlinear numerical solution is evaluated for the following

discretization values: $\Delta X_i = 0.02$; $(\Delta Y_{j+1/2})_{j=1} = 5 \times 10^{-4}$ at the interface and gradually increases as one moves away towards the boundary with $(\Delta Y_{j+1/2})_{max} = 0.001$, $\Delta T = 1 \times 10^{-4}$ and $\epsilon = 0.05$. The tolerance level is 10^{-5} and the maximum number of conduit and matrix hydraulic head iterations is 50.

Consequently, the linearizing coefficient is found equal to $Q_m = 0.58$ and the evaluation of β_l gives $\beta^2/2Q_m = 0.22$. The error in the peak value is nearly 10% while the mass balance error is 3.8%. One thus concludes that the linear models conserve the effect of conduit nonlinearity through the linearizing coefficient Q_m and are able to simulate the response of the nonlinear model with an acceptable error range.

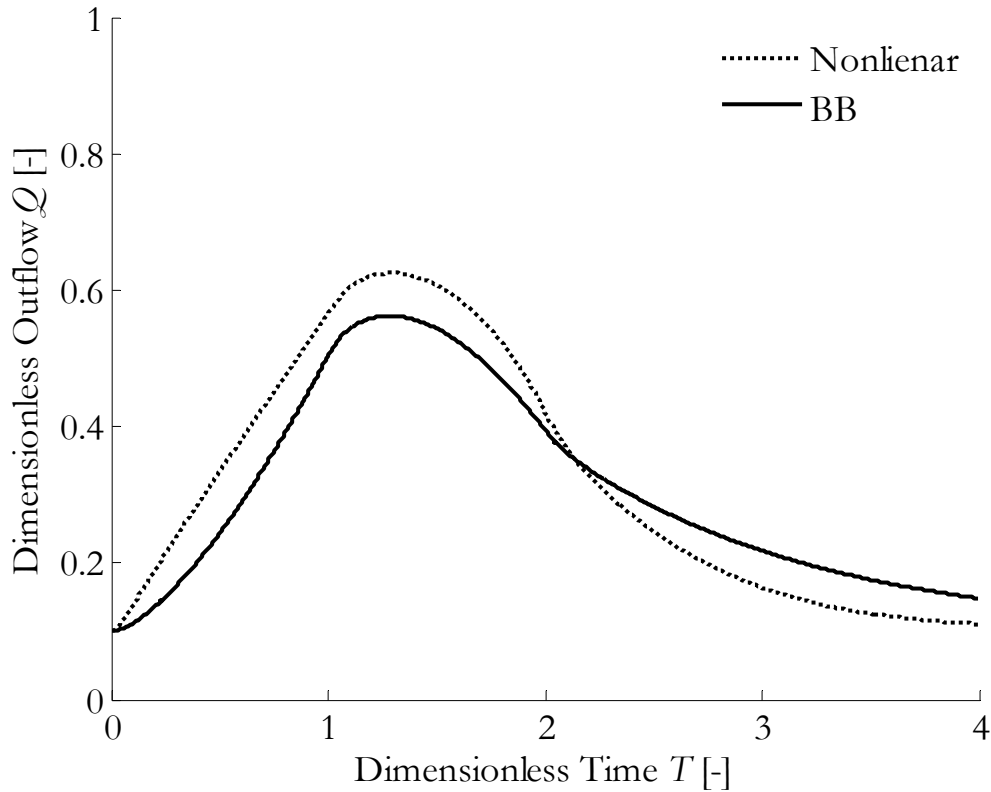


Figure 8. Comparison between linear (BB) and nonlinear models for a concentrated type of pulse. The linear model is found an acceptable approximation of the nonlinear one.

3.1.6 Effect of aquifer boundary conditions

By comparing BB to BU (or UB and UU) given a concentrated recharge (Figure 9), it is noticed that smaller aquifer widths generate a higher hydrograph peaks and larger mass recovery at the spring. As the aquifer width increases, the fluid slug is allowed to travel further into the matrix and consequently gets trapped without the possibility of being flushed at the spring. This leads to a potential mass imbalance between input pulse and output spring hydrograph and, as a result, a sequestered water volume in the matrix.

The unbound aquifer models (UU and BU) were found as acceptable simplifications to the more complex BB and BU for $L_r > 2.5$. This value is in good agreement with the condition proposed by *Hunt* [1990] who showed that $\sigma T_p / L_m^2 < 0.2$ (or $L_m \geq \sqrt{5}$ for current conditions) should be satisfied for the semi-infinite aquifer approximation to be valid.

3.1.7 Effect of conduit boundary conditions

When unbound downstream boundary conditions prevail (UB and UU), the spring hydrograph has a lower peak and a longer recession because the extent of conduit/aquifer exchange is no longer controlled by the downstream boundary. In systems where the spring freely discharges into a natural water course, the unbound conduit solutions (UB and UU) are generally more applicable than the bound ones (BB and BU). However, the latter are useful in applications where a weir, man-made structure or natural obstruction affect the downstream discharge. They are also advantageous when downstream water level measurements are available thus allowing improved estimations of the parameters.

Similar conclusions about the effects of boundary conditions are reached for a diffuse aquifer recharge pulse (Figure 10). The effect of recharge length and matrix width is assessed by applying a diffuse recharge over a length $L_r = 1$ and $L_r = 2.5 > \sqrt{5}$. Figure 10 also shows that the boundary condition either affects the recession period ($L_r = 2.5$) or the whole shape of the hydrograph ($L_r = 1$). For very large aquifer widths, it takes an indefinite time to retrieve the diffuse aquifer recharge at the spring ($L_r \geq 2.5$). Therefore, a simple mass balance approach between a recharge pulse and spring outflow is often not satisfied due to the spatial variability of recharge. An enhanced parameter estimation can thus be achieved by a careful assessment of the recharge term using either karst infiltration models or field methods that are beyond the scope of this work.

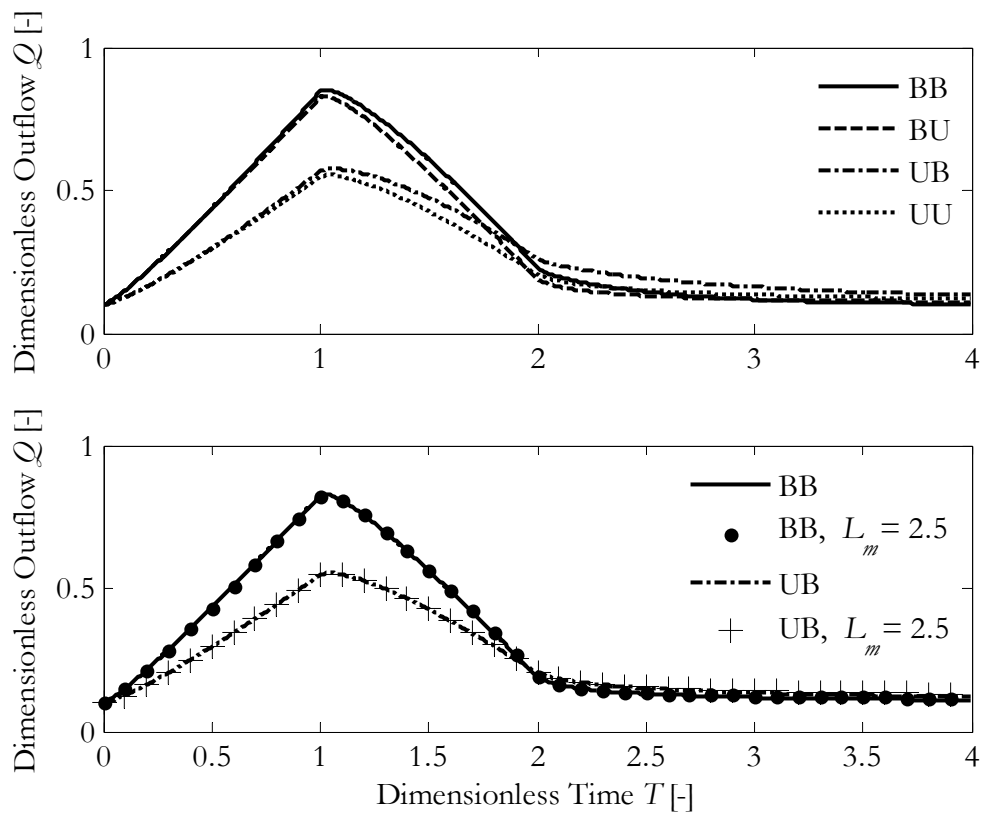


Figure 9. Effect of conduit and aquifer boundary conditions on spring hydrograph given a concentrated type of recharge (upper subplot). The unbound conduit models are not able to capture the more complex behavior of bound conduit models thus highlighting the importance of the downstream boundary condition. The semi-infinite aquifer models (BU and UU) are found as acceptable approximations of the finite ones (BB and UB) for $L_m > 2.5$ (lower subplot).

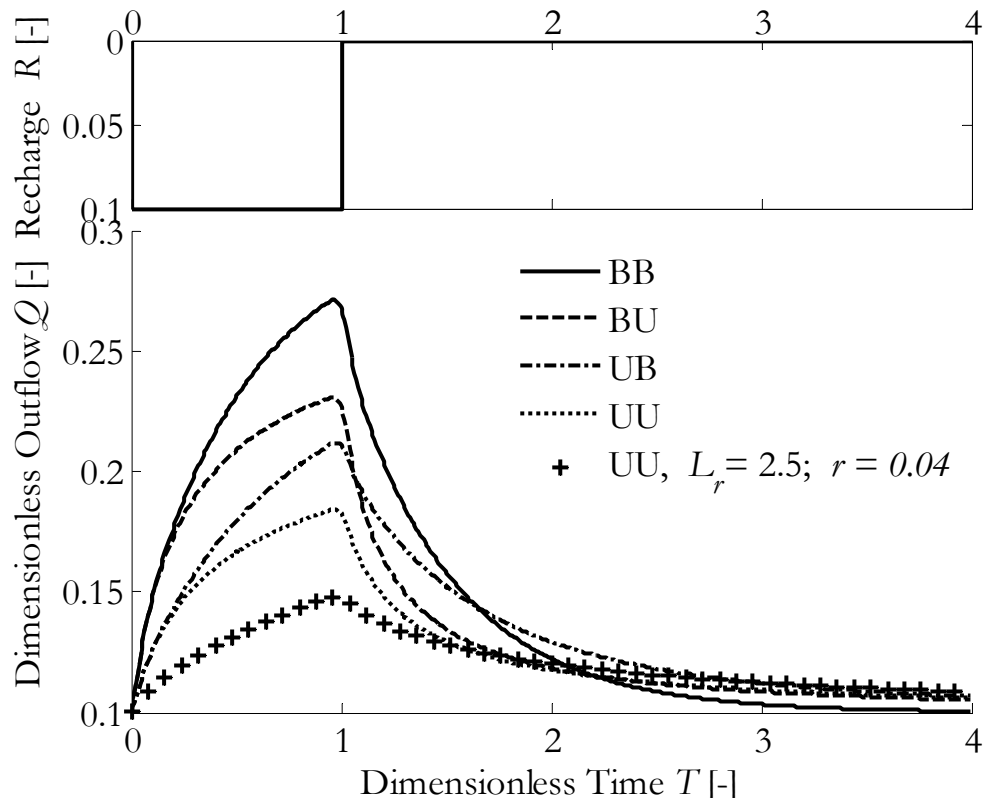


Figure 10. Effect of conduit and aquifer boundary conditions on spring hydrograph given a diffuse type of recharge. As the recharge is applied over larger widths ($L_r = 2.5$ instead of 1), the volume of water recovered at the spring decreases significantly.

3.2. Comparison to Other Models

3.2.1 Lumped and process-based models

The empirical models by *Maillet* [1905], *Drogue* [1972] and *Mangin* [1975] are widely used in simulating karst aquifers by decomposing the spring hydrograph recession. *Maillet* [1905] derived an exponential function that represents the drainage of a reservoir and has one empirical parameter referred to as the recession coefficient α . *Drogue* [1972] proposed a function with a quadratic denominator that was found adequate for simulating recession curves. *Mangin* [1975] introduced a hyperbolic function that was more suited in simulating the early and fast recession limb. In comparison, the proposed process-based models are able to simulate the whole spring

hydrograph and not only its recession. They are a function of physically meaningful parameters instead of empirical ones and have the ability to transform a measured diffuse or concentrated recharge into a spring hydrograph. They thus take into account the recharge mechanisms and boundary conditions that are largely ignored in lumped models.

On the other hand, existing process-based models express the early recession [Birk and Hergarten, 2010] or the whole recession curve [Kovacs *et al.*, 2005; Kovacs and Perrochet, 2008; Fu *et al.*, 2016] in terms of the matrix and conduit properties. Although their physical meaning improved over lumped models, their mathematical form is often similar to *Maillet's* exponential function which was not successful in simulating real recession curves [Fu *et al.*, 2016]. Furthermore, the karst system recharge mechanism is often simplified as a fully saturated matrix being drained by a conduit which is not representative of actual field conditions.

Fewer process-based models have an enhanced representation of interface exchange and are able to simulate a spring hydrograph given a concentrated recharge [e.g. Cornaton and Perrochet, 2002]. However, these models adopt a DC rather than a CDC approach and neglect the diffuse recharge mechanisms. Conversely, the proposed models take into account the effect of conduit turbulence and are capable of approximating the nonlinear numerical model's response with linear ones using computationally advantageous solutions.

3.2.2 *Distributive models*

The proposed process-based models have an improved physical representation of the system as compared to EPM and DC approaches because the conduit is treated as

a discrete element rather than a continuum. On the other hand, they are computationally advantageous to existing CDC numerical models. They also offer more flexibility with respect to the conduit's upstream and downstream boundary conditions. For example, the existing MODFLOW-CFP does not have a limiting flux boundary condition in the conduit cells and can feed the system with large amounts of water if used without proper care [Reimann and Hill, 2009].

Though numerically challenging, distributive CDC models are more suited than the proposed ones for studying matrix, conduit as well as recharge heterogeneities. Nonetheless, a simulation of complex karst systems can be achieved by combining the proposed process-based and distributive CDC models. The simplified equations presented herein can be used to get preliminary parameter estimates whose values are further refined using distributive models.

3.3. Parameter Estimation

3.3.1 Parameter ranges

An initial estimate of the parameters can be obtained from literature reported values. The parameter β_*/A_* was reported to range between 5 and 11 m/s [Jeannin, 2001] but can be as high as 50 m/s in large, smooth and straight conduits [Lauritzen, 1985]. Baedke and Krothe [2001] calculated the ratio of the aquifer transmissivity to the specific yield or σ_* from hydrograph recession analysis and found that it varies between 0.015 and 0.07 m^2/s with some sites yielding values as high as 0.19 to 0.26 m^2/s . A typical karst aquifer's specific yield or drainable porosity ranges between 5.4×10^{-5} and 2×10^{-3} [Shevenell, 1996; Baedke and Krothe, 2001]. The aquifer transmissivity (i.e. σ_*S_y) was estimated from slug, pumping and hydrograph

analysis tests for several karst aquifers by *Powers and Shevenell* [2000] and was found to vary between 1.1 to 226 m^2/day . Other studies reported significantly higher values of the transmissivity and specific yield for an eogenetic karst aquifer which ranged from 950 to 160,000 m^2/day and 0.2 to 0.4 respectively [*Martin and Dean*, 2001; *Martin et al.*, 2006].

3.3.2 Nonlinear least square fitting

The above ranges can be refined from field-specific information such as slug or aquifer tests and used as a starting point in the parameter optimization procedure. Knowing the upper and lower ranges of the parameters, one can use the nonlinear least square method to minimize the sum of the squared differences between the observed and simulated hydrographs and obtain an optimized value of the parameters. The model performance is evaluated using the Nash-Sutcliffe Efficiency or N-S [*Nash and Sutcliffe*, 1970]. Furthermore, a simultaneous fitting of spring hydrographs Q_l , downstream $H_c(L_c)$ and matrix $H_m(X, Y)$ hydraulic heads can achieve enhanced estimates of the parameters.

3.4. Model Application and Results

3.4.1 Santa Fe River Sink/Rise system

The Santa Fe River Basin covers an area of 3,583 km^2 and is located in north-central Florida, USA. The Santa Fe River runs approximately 60 km to the west of its headwaters at Lake Santa Fe then sinks in a 36 m deep sinkhole known as the River Sink [*Martin and Dean*, 2001]. The river flows underground, reappears intermittently and finally reemerges 5 km downstream as a perennial spring called the River Rise.

Extreme flow variations are observed at both Sink and Rise locations. Within the area separating the River Sink and Rise, a total of seven sinkholes (20– 36 m thick) are present as well as a major sinkhole lake known as the Sweetwater Lake that represents a small section of the Santa Fe River [*Martin and Dean, 2001*]. Previous tracer tests run by *Hisert [1994]* proved a connection between the River Rise, Sweetwater Lake and the various karst windows.

The average dimensions of the conduits linking River Rise and Sink are 18 to 24 m in width and 12 to 18 m in height [*Screaton et al., 2004*]. The conduits are typically 30– 40 m below the ground surface level. Through the Old Bellamy Cave Project [2005], 15 km of caves and conduits were mapped by cave divers. The main underground conduit that connects the River Rise and Sink is approximately 8 km long, with an intermediate length of 5 km between the River Sink and Sweetwater Lake [*Moore et al., 2009; Moore et al., 2010*].

During low-flow conditions, the conduit appears to be draining the surrounding aquifer as indicated by the higher flow values observed at the River Rise as opposed to the River Sink [*Martin and Dean, 2001; Screaton et al., 2004; Martin et al., 2006; Moore et al., 2009; Ritorto et al., 2009; Langston et al., 2012*]. Conversely, the conduits lose water to the aquifer during high-flow or flood conditions. This exchange is facilitated by the high aquifer permeability or porosity which is estimated around 20% [*Martin et al., 2006; Bailly-Comte et al., 2011*].

The conduit-aquifer exchange flow at the Santa Fe River system has been monitored through several wells and discharge measurements at the Sink and Rise. The August 2008 flood [*Bailly-Comte et al., 2011; Langston et al., 2012*] is hereby used for parameter estimation and model validation. It is referred to as Flood A herein. The

hydrological years 2008-2009 [Langston *et al.*, 2012] are consequently used for model calibration (Flood B). An additional flood from 2002 is also fitted (Flood C) [Martin, 2003; Martin *et al.*, 2006]. Flood A is available in water levels that are converted to discharge using the corresponding rating curves for River Sink and Rise. According to Bailly-Comte *et al.* [2011], Langston *et al.* [2012] and Martin [2003], the River Sink (RS) rating curve is developed by the Suwannee River Water Management District (SRWMD, Figure 1, rating 3 for station 02321898) and is applicable to all three floods A, B and C. The equation of this rating curve is available in Ritorto [2007]. As for River Rise (RR), the rating curve developed by Sreaton *et al.* [2004] is used in previous studies featuring the same three floods [Martin, 2003; Martin *et al.*, 2006; Bailly-Comte *et al.*, 2011; Langston *et al.*, 2012]. The two rating RS and RR rating curves are as follows:

$$Q_{m^3/s} = 4.1363H_{masl}^2 - 63.642H_{masl} + 224.59 \text{ at RS} \quad 3-1$$

$$Q_{m^3/s} = 7.36H_{masl}^2 - 127.23H_{masl} + 545.18 \text{ at RR} \quad 3-2$$

3.4.2 Model assumptions

The Santa Fe conduits are located well below the water table and are believed to be under pressurized conditions. The linearized pipe flow models are thus suitable to simulate the conduit/aquifer interaction observed at the site. The River Sink inflows constitute the upstream boundary condition Q_u of the main karst conduit. The distance between the two stations is set equal to $L_c = 8,000$ m. The aquifer width and recharge length are hereby assumed equal to double the conduit length such that $L_r = L_m = 8,000$ m. The aquifer diffuse recharge is herein considered negligible since most of River Rise discharge originates from the concentrated recharge at River Sink.

3.4.3 Initial parameter estimates and dimensionless system

The average area of the conduits A_* is between 290 and 380 m^2 from field observations [Screaton *et al.*, 2004; Bailly-Comte *et al.*, 2011]. Previous studies in karst caves and conduits estimate the ratio β_*/A_* to vary between 1.5 and 50 m/s [Jeannin, 2001]. For the Santa Fe system, the range of β_* becomes 1450 to 19,000 m^3/s . The calculated transmissivity values from previous aquifer tests were found between 950 and 160,000 m^2/day and the specific yield between 0.2 and 0.4 [Martin and Dean, 2001; Screaton *et al.*, 2004]. The resulting ratio σ_* varies between 0.03 and 9 m^2/s . The hydraulic conductivity was estimated from slug tests and found between 1.5 and 1600 m/day [Langston *et al.*, 2012]. Therefore, the exchange parameter κ_* is between 0.001 and 0.8 m^2/s if the height of the interface D is set equal to 22 meters (i.e. equal to the conduit diameter). An initial estimate of $\beta_l = \beta^2/2Q_m$ is obtained by calculating Q_m for each flood using Equation (2-36).

The Santa Fe system is hereby modeled in dimensionless form by setting the characteristic time equal to the time of the input pulse's peak for Flood A $t_0 = 3.57$ days and the characteristic length equal to $d_0 = 4000m$. These values help scaling the parameters for a more effective optimization. Consequently, the dimensionless ranges of the parameters become: $\beta = 0.007 - 0.1$, $\kappa = 2 \times 10^{-5} - 0.015$ and $\sigma = 6 \times 10^{-4} - 0.2$. For the linear conduit parameter, the range is $\beta_l = 0.03 - 6$. It follows that the coalesced parameter ω ranges between 0.003 and 4.5.

By assuming a zero aquifer recharge, the two optimizing parameters β_l and ω are needed in order to simultaneously fit the downstream water levels and discharge using UU (or Equations 2-29 and 2-30). As initial estimates, the following values were

selected: $\beta_l = 4$ and $\omega = 0.02$. Their range is set between 0 and 10 in the optimization procedure.

3.4.4 *Model results and analysis*

3.4.4.1 Flood A

Flood A is characterized by a single peak followed by long recession (Figure 11). The total loss of water is calculated as $V_{loss} = V_{out} - V_{in} = -2.2 \times 10^7 \text{ m}^3$ which is very close to the value obtained by *Langston et al.* [2012] ($2.5 \times 10^7 \text{ m}^3$). According to previous interpretations, the mass imbalance is attributed to unmapped high-conductivity pathways. The latter's potential presence is explained by higher transmissivities over large scale measurements [*Martin et al.*, 2006; *Langston et al.*, 2012]. Since the existence of bypasses or side conduit networks is not verified in the field, it is hereby assumed that the mass imbalance is caused by water being sequestered in the very wide and highly conductive surrounding matrix. A summary of the model's input data is provided in Table 2 below.

Given that both downstream discharge and water levels are available, they are simultaneously fitted in order to obtain better estimates of the model's main parameters. The parameter values are presented in Table 3 and the results plotted in Figure 11. The simulated River Rise hydrographs show a good correlation to observed ones and the goodness of fit is found high for UU (N-S = 0.98). In addition to UU, the data was simulated using the bound conduit model BB given a fixed downstream boundary condition H_d . The results show that UU has a better performance as compared to BB and that the downstream boundary condition is most likely free discharge.

UU's ratio $\kappa/\sqrt{\sigma} = \omega^2\beta_l = 0.05$ is given in dimensional form as $\kappa_* = 0.007\sqrt{\sigma_*}$. For a hydraulic conductivity that is equal to the average slug tests value of 12m/day [Langston *et al.*, 2012] and an interface height of 22m, the matrix parameter σ_* becomes $0.762 \text{ m}^2/\text{s}$. Finally, the linearizing coefficient Q_m is found equal to 6.7×10^{-4} from Equation (2-36). Therefore, the dimensionless conduit's conductivity β^2 is equal to $3.87 \times 2 \times 6.7 \times 10^{-4} = 0.0048$ and the dimensional ratio $\beta_*/A_* = \frac{\sqrt{0.0048*Q_0^2}}{[290;380]} = [38 - 49] \text{ m/s}$ falls within the acceptable range for large and smooth conduits as reported by Lauritzen [1985].

Table 2. Input data for Santa Fe River Sink and Rise karst system

| | Flood A | Flood B | Flood C |
|---------------------|---------------------|------------------------|---------------------|
| Model Domain | | | |
| L_c | 8000 m | 8000 m | 8000 m |
| $L_r = L_m$ | 8000 m | 8000 m | 8000 m |
| Initial Conditions | | | |
| Q_i | 4 m ³ /s | 1.65 m ³ /s | 0 m ³ /s |
| H_i | 9.93 m | 9.57 m | 9.46 m |
| Simulation duration | 56.11 days | 787 days | 130 days |

Table 3. Estimated dimensionless parameters for Flood A and Flood C

| | Flood A | Flood C |
|----------------------------|---------|---------|
| UU | | |
| β_l | 3.08 | 3.876 |
| ω | 0.228 | 0.11 |
| Nash-Sutcliffe coefficient | 0.98 | 0.98 |
| BB | | |
| β_l | 5.07 | |
| ω | 0.527 | |
| Nash-Sutcliffe coefficient | 0.89 | |

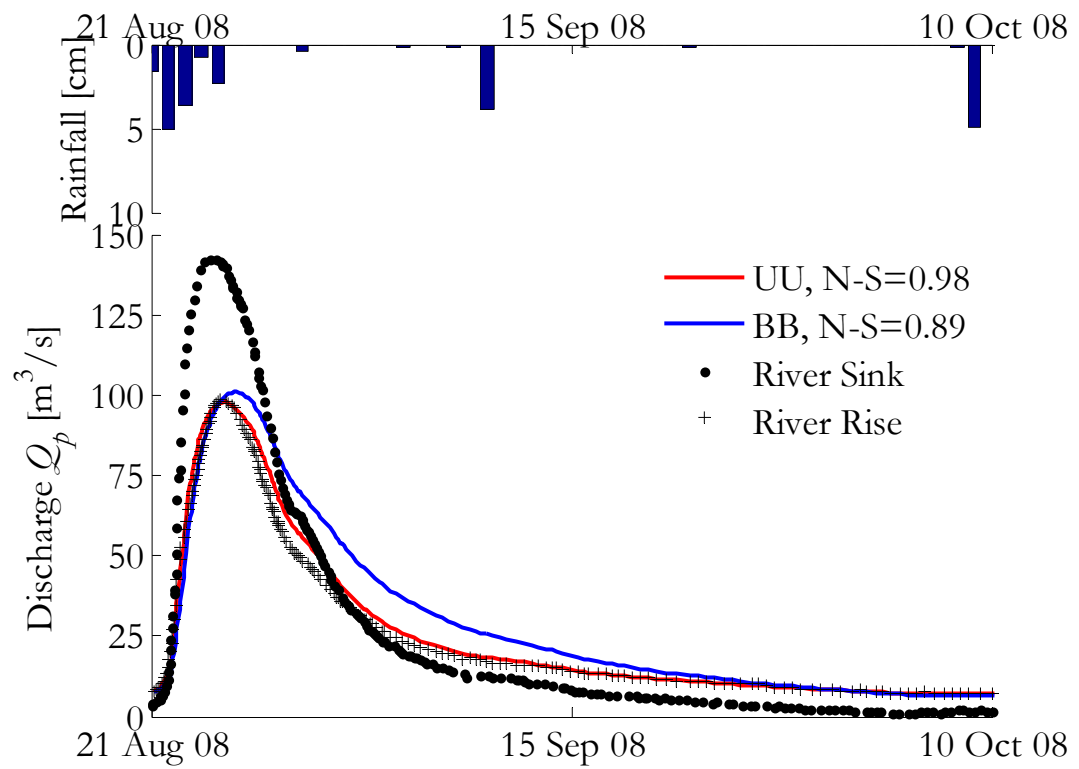


Figure 11. Observed and simulated discharge of the Santa Fe karst system for Flood A. The UU model is able to simulate the observed River Rise with a high goodness of fit and shows a better performance than BB.

3.4.4.2 Flood B

The optimized parameters from Flood A are used to simulate Flood B for model calibration purposes. Flood B represents the hydrological years 2008-2009 (Figure 12) and covers a longer time range than Flood A. It thus shows the prevailing recharge conditions before the occurrence of the August 2008 flood or Flood A. The latter is preceded by nearly 110 days of constant River Rise discharge with zero input at River Sink. The results show that the UU model is able to simulate the behavior of the Santa Fe system for a long period of time using the same optimized parameters from Flood A and has thus the capacity to predict the hydrological response of the system.

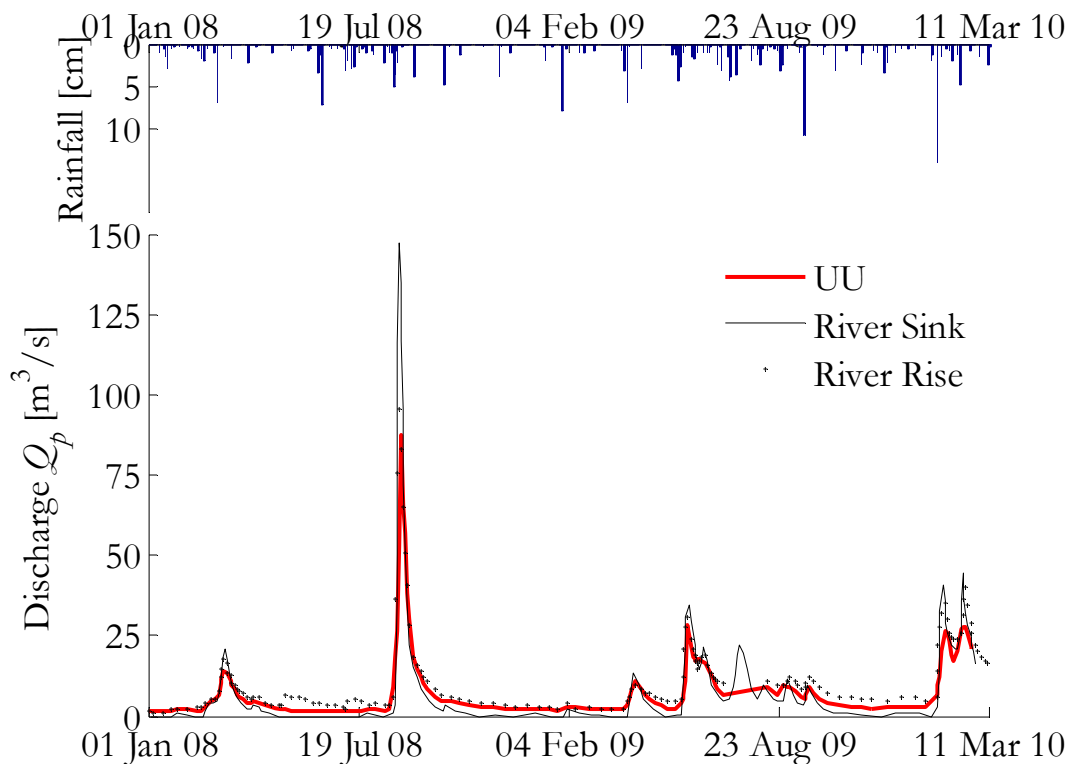


Figure 12. Observed and simulated discharge of the Santa Fe karst system for Flood B using optimized parameters from Flood A. Note that Flood A is also featured (between July 08 and February 09 time ticks).

3.4.4.3 Flood C

The March 2003 event or Flood C is also simulated using UU. The results are presented in Table 3 and Figure 13. One notices a good agreement between simulated and observed hydrographs with UU capturing three consecutive peaks given an acceptable range of the parameters. However, the latter slightly differ than the ones obtained for Flood A. Incorporating the effect of diffuse recharge through hydrological models might improve the model calibration in the future.

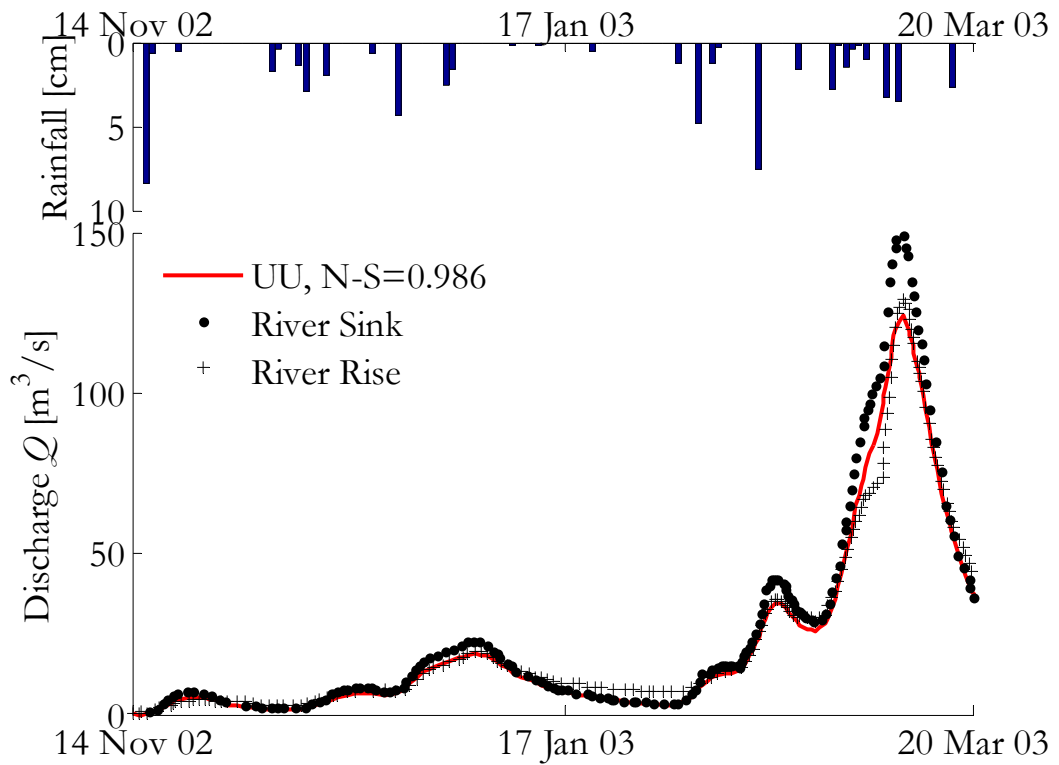


Figure 13. Observed and simulated discharge of the Santa Fe karst system for Flood C.

3.5. Summary of Important Results

The process-based pipe models are capable of simulating the shape of a typical spring hydrograph that is characterized by a rapid response to a recharge event followed by a long recession limb. The different models' responses are almost instantaneous given the pressurized pipe flow conditions while the conduit/aquifer interaction has the ability to dampen the peak of an input flood and to release the stored water as the event recedes. The nonlinear numerical model compared well to its linearized simplification. Furthermore, the semi-infinite aquifer solution was a good approximation to the more complex finite aquifer case for a defined range of aquifer widths. The conduit's downstream boundary condition had a significant effect on the extent of interface exchange and consequently the simplified unbound conduit models (UU) were not able to reproduce the more general bound conduit model results (BB).

Finally, the proposed models were successfully applied to a sink and rise karst system that is subject to a concentrated type of pulse while the conduits are located below the water table and are flowing under pressurized conditions. The optimized parameters were obtained by simultaneously fitting the system discharge and downstream water levels and compared well to reported ones from the literature and field observations. Given that the system discharges freely, the unbound conduit model UU was more successful than the bound one (BB) in capturing the observed hydrograph, particularly its recession.

CHAPTER 4

CHANNEL FLOW MODEL – THEORY

The main objective of this chapter is to derive process-based flow models that account for unpressurized flow conditions in a karst conduit. Conversely to the pipe flow models, the aim herein is to simulate a delay in pulse arrival to the spring. The different flow processes are defined as open-channel, matrix and interface exchange. As a result, the kinematic wave approximation is used to simplify the open-channel flow equation. Consequently, a coupled system of differential equations is derived to simulate the flow in a simplified two-dimensional karst aquifer domain. A numerical solution is provided for the nonlinear model and is followed by an analytical one for the linearized system of equations. Finally, an optimal linearizing coefficient relating the parameters of the linear analytical and nonlinear numerical models is derived by minimizing the difference between the two models.

4.1. Flow Processes

The conceptual framework is similar to the one proposed for the pipe flow models in Section 2.1 where a single conduit is located at the center of a matrix with the two interacting at their common interface. However, the main difference herein is that the conduit is flowing under open-channel rather than pressurized conditions.

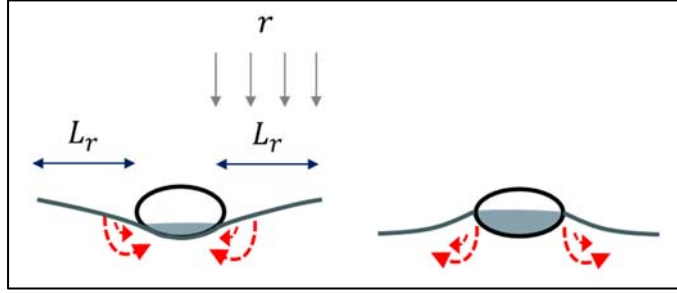


Figure 14. Open-channel conduit cross section. The conduit either drains the surrounding aquifer (right) or acts as a source (left).

The continuity equation for open-channel flow is given by

$$\frac{\partial A_*}{\partial t} + \frac{\partial Q_*}{\partial x} = 2q_{ex} \quad 4-1$$

where A_* is the channel wetted cross-sectional area [L^2] q_{ex} is the exchange flow [L^2/T] and the coefficient 2 is added to account for exchange on both sides of the conduit. The channel discharge is given by

$$Q_* = u_* A_* = w_* \alpha_* h_c^m \quad 4-2$$

where w_c is the channel width [L] and h_c the conduit head measured from the conduit's bottom [L]. The channel velocity u_* [L/T] is given by the expression $u_* = C_c \sqrt{S_0 R_h}$ with C_c being Chezy's coefficient [$L^{1/2}/T$] and R_h the hydraulic radius [L]. for a flow width larger than the flow height, $R_h = h_c$ and $m = 3/2$. The parameter α is $C_c \sqrt{S_0}$. In the current formulation, the friction slope is set equal to the bedslope and this simplification is known as the kinematic wave approximation.

The flow in the aquifer is one-dimensional and is perpendicular to the conduit's centerline. The governing equation is expressed by Equation (2-4). The interface exchange term is a function of the interface hydraulic gradient and is given by Equation (2-6).

4.2. Combined Channel-Aquifer Flow

The channel model's governing equation consists of combining equations (4-2) and (2-6) with (4-1). The resulting nonlinear equation for the coupled channel and aquifer model becomes

$$\frac{\partial h_c}{\partial t} + m\alpha_* h_c^{m-1} \frac{\partial h_c}{\partial x} = \kappa_* \frac{\partial h_m}{\partial y} \Big|_{y=0} \quad 4-3$$

where $\kappa_* = 2K_m D/w_*$. The term on the right-hand side of the equation is the coupling or exchange flux at $y = 0$ where the conduit and matrix heads are equal $h_m = h_c$.

The linearized form of the conduit flow equation becomes

$$\frac{\partial h_c}{\partial t} + c_* \frac{\partial h_c}{\partial x} = \kappa_* \frac{\partial h_m}{\partial y} \Big|_{y=0} \quad 4-4$$

where $c_* = m\alpha_* h_o^{m-1}$ and h_o is a linearizing term.

4.3. Auxiliary Conditions

4.3.1 Boundary conditions in the conduit domain

The conduit is subject to an arbitrary input pulse and a free downstream discharge. The upstream boundary condition is

$$Q_*(0, T) = w_* \alpha_* G_*^m \quad x = 0 \quad 4-5$$

where G_* are the upstream water levels that can be expressed as linear interpolation between two datapoints (see Appendix A).

4.3.2 Boundary conditions in the aquifer domain

The aquifer is considered either semi-infinite or finite. At the interface or $y = 0$, the heads in the aquifer are equal to the ones in the conduit. The boundary conditions become

$$h_m = h_c \quad y = 0 \quad 4-6$$

$$h_m = h_i \quad y \rightarrow \infty \quad 4-7$$

$$dh_m/dy = 0 \quad y = l_m \quad 4-8$$

4.3.3 Initial conditions

Assuming a uniform and constant initial head distribution h_i in both conduit and aquifer, one gets

$$h_c = h_m = h_i \quad t = 0 \quad 4-9$$

4.4. Dimensionless Forms

The following dimensionless variables are used

$$\frac{x}{X} = \frac{y}{Y} = \frac{h}{H} = d_0; \frac{t}{T} = t_0; u = \frac{u_*}{u_0}; Q = \frac{Q_*}{Q_0}; u_0 = \frac{Q_0}{d_0^2}; t_0 = \frac{d_0^3}{Q_0} = \frac{d_0}{u_0} \quad 4-10$$

where d_0 [L], t_0 [T] and u_0 [L/T] are the characteristic depth, time and velocity respectively and Q_0 is the normalizing flow [L^3/T]. The dimensionless aquifer flow Equation (2-4) becomes

$$\frac{\partial H_m}{\partial T} = \sigma \frac{\partial^2 H_m}{\partial Y^2} + \frac{r}{S_y} \quad 4-11$$

where $\sigma = T_m / (u_0 d_0 S_y)$ and $r = r_* / u_0$. The nonlinear conduit flow Equation (2-7) is written in dimensionless form as

$$\frac{\partial H_c}{\partial T} + m\alpha H_c^{m-1} \frac{\partial H_c}{\partial X} = \kappa \frac{\partial H_m}{\partial Y} \Big|_{Y=0} \quad 4-12$$

where $\kappa = \kappa_* / u_0$ and $\alpha = \alpha_* d_0^{m-1} / u_0$ and the dimensionless linear conduit flow equation becomes

$$\frac{\partial H_c}{\partial T} + c \frac{\partial H_c}{\partial X} = \kappa \frac{\partial H_m}{\partial Y} \Big|_{Y=0} \quad 4-13$$

where $c = m\alpha H_0^{m-1}$. The dimensionless discharge expression in terms of the hydraulic heads is thus given by

$$Q = w\alpha H_c^m \quad 4-14$$

Similarly to the pipe models' dimensionless system, one can get a simplified physical domain with $d_0 = l_c$ or a fraction of l_c and a simplified timeframe with $t_0 = t_p$ where t_p is the time to peak of an input pulse. Therefore, one ends up with $L_c = 1, 10, etc \dots$ and $T_p = 1$.

4.5. Numerical Solution

The nonlinear conduit model consisting of the coupled equations (4-11) and (4-12) is solved numerically. The MacCormack and Crank-Nicolson schemes are used to solve the channel and aquifer governing equations respectively. The aquifer finite difference equation has a tridiagonal form that is efficiently solved using the Thomas algorithm. The discretized forms of the equations are presented in Appendix B.

The coupling of the two equations (4-11) and (4-12) is performed according to the following algorithm. At each time step, the heads in the conduit are calculated by updating the upstream boundary condition and using the computed conduit heads and exchange flux from the previous time step. Therefore, a first iteration of the conduit head profile at the current time step is completed and set as the new boundary condition in the aquifer at the interface or $Y = 0$. A new exchange flux is then calculated from the updated aquifer heads and replaced into the conduit subroutine to obtain a new head

distribution. It is noticed that one to two iterations are enough for the solution to converge. The calculations are repeated for all time steps.

The numerical solution serves to simulate the nonlinear conduit flow coupled to the linearized Boussinesq equation. Therefore, it shows the effect of the conduit nonlinearity on the spring hydrograph. However, the numerical solution can be computationally expensive especially for fast flows or high α values where very small time discretizations are required for better results. Moreover, the correctness of the solution is sensitive to the value of the interface discretization. Alternately, one can linearize the conduit flow equation and derive analytical solutions that are both computationally advantageous and exact. However, these solutions' main limitation is the under-representation of the conduit nonlinearity and system heterogeneity.

4.6. Karst Channel Flow Models

For a constant channel velocity coefficient c , analytical solutions are derived for the system of equations (4-11) and (4-13) under various initial and boundary conditions.

4.6.1 *Semi-infinite aquifer solution (KWU)*

Solving the coupled system of equations (4-11) and (4-13) for the boundary conditions in (4-5), (4-6) and (4-7), one gets the Laplace transform solution

$$\bar{H}_c = \bar{H}_i + (\bar{G} - \bar{H}_i)e^{-ap-b\sqrt{p}} + \frac{\bar{r}\omega}{S_y} \left[\frac{1 - e^{-L_m\sqrt{p}/\sigma}}{\sqrt{p}} \right] \left[\frac{1 - e^{-ap-b\sqrt{p}}}{(p + \omega\sqrt{p})} \right] \quad 4-15$$

where $\omega = \kappa/\sqrt{\sigma}$, and the parameters a and b are defined as $a = X/c$ and $b = a\omega$. \bar{G} and \bar{r} is the Laplace transform of the upstream boundary condition and aquifer recharge respectively. They are expressed in function of the complex parameter p as shown in Appendix A. Equation (4-15) is also found in *Hunt* [1990] without the recharge term. It is analytically inverted as

$$\begin{aligned}
H_c(X, T) = & H_i + \int_0^T [G(T - \tau) - H_i] \frac{b}{2\sqrt{\pi(\tau - a)^3}} e^{-b^2/4(\tau - a)} \mathcal{U}(\tau - a) d\tau \\
& + \int_0^T R_c(T - \tau) \operatorname{erfcx}(\omega\sqrt{\tau}) d\tau \\
& - \int_0^T R_c(T - \tau) e^{-b^2/4(\tau - a)} \operatorname{erfcx} \left[\omega\sqrt{\tau - a} + \frac{b}{\sqrt{4(\tau - a)}} \right] \mathcal{U}(\tau - a) d\tau
\end{aligned} \tag{4-16}$$

where

$$\begin{aligned}
R_c(T) = & \frac{r_0\omega}{S_y} \left\{ \sqrt{\frac{4(T - T_0)}{\pi}} [1 - e^{-L_r^2/4\sigma(T - T_0)}] + \frac{L_r}{\sqrt{\sigma}} \operatorname{erfc} \left(\frac{L_r}{\sqrt{4\sigma(T - T_0)}} \right) \right\} \mathcal{U}(T \\
& - T_0) \\
& + \sum_{i=1}^n \frac{(r_i - r_{i-1})}{S_y} \omega \left\{ \sqrt{\frac{4(T - T_i)}{\pi}} [1 - e^{-L_r^2/4\sigma(T - T_0)}] \right. \\
& \left. + \frac{L_r}{\sqrt{\sigma}} \operatorname{erfc} \left(\frac{L_r}{\sqrt{4\sigma(T - T_i)}} \right) \right\} \mathcal{U}(T - T_i)
\end{aligned}$$

and $\operatorname{erfcx}(\chi) = \exp(\chi^2)\operatorname{erfc}(\chi)$.

Equation (4-16) provides a relationship between the water levels at the spring and model parameters (ω , a and b), diffuse recharge (r), recharge length L_r as well as the upstream boundary conditions $G(T)$. The spring discharge is obtained by replacing (4-16) into (4-14). The integrals are evaluated numerically using the ‘*integral*’ function in MATLAB.

4.6.2 Finite aquifer solution (KWB)

For a finite aquifer with $L_m = L_r$, the solution becomes

$$\begin{aligned} \bar{H}_c = \bar{H}_i + [\bar{G} - \bar{H}_i] e^{-ap - b\sqrt{p} \tanh(\sqrt{p/\sigma} L_m)} \\ + \frac{\bar{r}\omega}{S_y p} \tanh(\sqrt{p/\sigma} L_m) \left[\frac{1 - e^{-ap - b\sqrt{p} \tanh(\sqrt{p/\sigma} L_m)}}{\sqrt{p} + \omega \tanh(\sqrt{p/\sigma} L_m)} \right] \end{aligned} \quad 4-17$$

The above Laplace transform solution expresses the spring water levels in terms of the model parameters ω , a and b as well as the aquifer width. It is numerically inverted using the *Hollenbeck* [1998] routine.

4.7. Optimal Coefficient

The linear equation (4-13) is a useful approximation of its nonlinear form (4-12) because it facilitated the derivation of the computationally advantageous analytical and Laplace transform solutions KWU and KWB. However, the linearized velocity parameter c should be related to the nonlinear $m\alpha H_c^{m-1}$ in order to facilitate the interpretation of the results. The latter is achieved through minimizing the difference between the nonlinear equation and its approximation

$$R = \left(\frac{\partial H_c}{\partial T} + \alpha m H_c^{m-1} \frac{\partial H_c}{\partial X} \right) - \left(\frac{\partial H_c}{\partial T} + c \frac{\partial H_c}{\partial X} \right) = 0 \quad 4-18$$

Minimizing the above residual by integrating over space and time, one gets

$$\int_0^T \int_0^{L_c} \left[(\alpha m H_c^{m-1} - c) \frac{\partial H_c}{\partial X} \right] dX dT = 0 \quad 4-19$$

Integrating Equation (4-19) over space, one gets

$$c = \alpha \frac{\int_0^T H_c^m(L_c, T) - H_c^m(0, T) dT}{\int_0^T H_c(L_c, T) - H_c(0, T) dT} \quad 4-20$$

The above relationship is well-defined because it is a function of the boundary values at $X = 0$ and $X = L_c$ which are known in inverse problems. Equation (4-20) can be rewritten in terms of the upstream and downstream discharge as

$$c = \alpha (\alpha w)^{\frac{1-m}{m}} \frac{Q(L_c, T_m) - Q(0, T_m)}{Q^{1/m}(L_c, T_m) - Q^{1/m}(0, T_m)} \quad 4-21$$

A simpler relationship can be obtained by solving $R = 0$ in Equation (4-18) as

$$H_c = \left[\frac{\alpha m}{c} \right]^{1/(1-m)} \quad 4-22$$

Rewriting Equation (4-22) in terms of Q , one gets

$$c = \alpha m \left[\frac{Q(X_m, T_m)}{\alpha w} \right]^{(m-1)/m} \quad 4-23$$

where $Q(X_m, T_m)$ is the discharge at point X_m and time T_m .

4.8. Summary of Important Results

This chapter presents process-based models that simulate the outflow from a karst aquifer where unpressurized conduit conditions prevail. The conceptual model consists of a single conduit flowing under open-channel conditions and interacting with the surrounding aquifer at their common interface. The governing system of equations couples the kinematic wave approximation of conduit flow to the linearized Boussinesq equation via Darcy's law. The result is a two-dimensional coupled system of nonlinear differential equations that is solved numerically. The conduit flow linearization facilitated the derivation of analytical and Laplace transform solutions for a semi-infinite (KWU) and finite (KWB) aquifer boundaries respectively. Similarly to the pipe flow models, the solutions combine the different karst flow processes into one single equation. As a result, KWU and KWB express the spring discharge in terms of the model parameters, model domain (L_c, L_m), aquifer diffuse recharge (r) and concentrated upstream recharge (G). In contrast to pipe flow models, an additional parameter is introduced and consists of the conduit velocity coefficient α (nonlinear) or c (linear). Finally, optimal relationships between the linear and nonlinear conduit velocity parameters (α and c) were obtained by minimizing the difference between the two models' governing equations.

CHAPTER 5

CHANNEL FLOW MODEL – ANALYSIS AND RESULTS

In this chapter, the performance of the process-based open channel models is evaluated by simulating their outflow for given concentrated and diffuse recharge pulses. The Laplace transform solution obtained for finite aquifers is compared to the fully nonlinear numerical model. Also, the semi-infinite aquifer simplification is assessed by comparing the model's output to the more complex finite aquifer solution. Consequently, the proposed models are compared to existing lumped models as well as to the pressurized pipe flow models presented in the current study. The latter serves to highlight the effect of the conduit flow conditions (i.e. pressurized versus open channel) on the spring hydrograph. Finally, the models are applied to two aquifer systems subject to different recharge conditions.

5.1. Salient Results

5.1.1 Key model parameters

The open channel models KWU and KWB's main parameters are the matrix-related exchange coefficient κ , aquifer coefficient σ and drainable porosity S_y as well as the linear channel flow velocity c that is a function of α and w (Equations 4-21 and 4-23). A coalesced parameter ω was also introduced and combines all three matrix-related parameters κ , σ and S_y . The equations were further simplified by introducing $a = X/c$ and $b = a\omega$. For a zero aquifer recharge, the semi-infinite aquifer model becomes a function of ω and c (or a and b) and the finite aquifer solution becomes in

terms of ω , c and σ (or a , b and σ). The interface depth D should be less or equal to the average depth in the aquifer in case of diffuse recharge. After algebraic manipulations of the parameters, one finds that the parameter κ should be less or equal to $2\sigma S_y/w$.

5.1.2 Hypothetical Scenario

In order to generate the output of the different models, the following hypothetical setup is proposed. A single conduit of length $L_c = 10$ and width $w = 0.2$ is coupled to a matrix of half width $L_r = 10$ and is subject to an isosceles triangular pulse. All model parameters are summarized in Table 4.

Table 4. Parameter values of open channel flow models' hypothetical run

| Dimensional Parameter | Value | Dimensionless Parameter | Dimensionless Value |
|-------------------------------|--------------------------|------------------------------------|---------------------|
| l_c | 1000m | L_c | 10 |
| l_m | 1000m | L_r | 10 |
| $K_m D$ | $0.01m^2/s$ | | |
| T_m | $0.01m^2/s$ | | |
| w_* | 20m | w | 0.2 |
| $\alpha_* = C_c \sqrt{S_0}$ | $0.022 m^{1/2}/s$ | $\alpha = \alpha_* d_0^{m-1}/u_0$ | 200 |
| $\kappa_* = 2K_m D/w_*$ | $0.011m/s$ | $\kappa = \kappa_*/u_0$ | 10 |
| $\sigma_* = T_m/S_y$ | $0.1m^2/s$ | $\sigma = T_m/S_y u_0 d_0$ | 10 |
| d_0 | 100m | S_y | 0.1 |
| t_0 | 86400s | | |
| Q_0 | $11.57 m^3/s$ | | |
| u_0 | $1.1 \times 10^{-3} m/s$ | | |
| Diffuse Pulse Characteristics | | Concentrated Pulse Characteristics | |
| Type | Rectangular | Type | Isosceles triangle |
| T_p | 1 | T_p | 1 |
| T_d | 1 | T_d | 1 |
| r | 0.01 | Q_i | 0.1 |
| | | Q_{max} | 1 |

5.1.3 Spring hydrograph

5.1.3.1 Concentrated recharge

Figure 15 shows the nonlinear numerical model's outflow for the selected parameters in Table 4 as well as a doubled exchange coefficient κ . The numerical solution of the linearized system of equations is successfully compared to the numerically inverted Laplace transform solution thus validating the coupling algorithm proposed in Section 4.5. The discretization values are as follows: $\Delta X_i = 0.05$; $(\Delta Y_{j+1/2})_{j=1} = 0.05$ at the interface and gradually increases as one moves away towards the boundary with $(\Delta Y_{j+1/2})_{max} = 0.13$ and $\Delta T = 1 \times 10^{-4}$.

Similarly to the pipe flow models, the interaction between the conduit and aquifer modifies the shape of the concentrated input pulse into a fast flood followed by a slow baseflow recession. The two dimensionless parameters κ and σ control the extent of exchange while α (nonlinear) or c (linear) regulate the time of peak's arrival to the spring. As the exchange coefficient κ increases, the spring outflow peak is reduced and the duration of the baseflow recession becomes longer. Additionally, the exchange coefficient κ has the ability to delay the input pulse arrival and therefore affects the time to peak along with α (Figure 15).

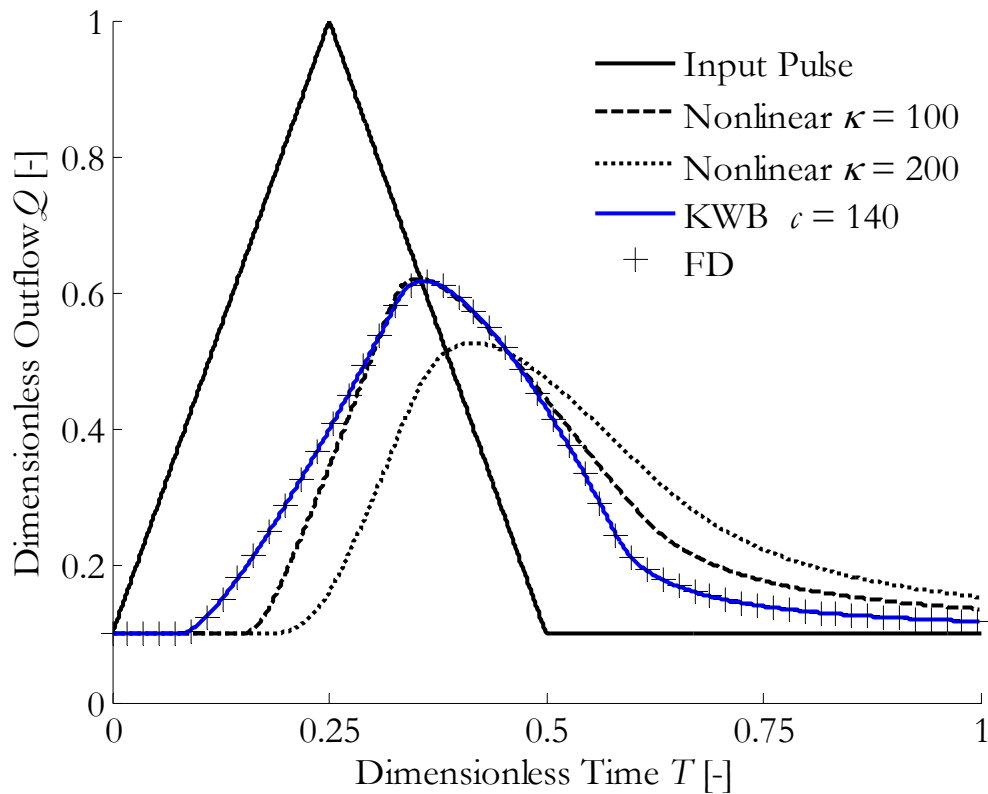


Figure 15. KWB (linear) and numerical (nonlinear) model predictions for a concentrated recharge event for selected values of the exchange parameter κ . As the exchange parameter increases, the peak is reduced and the pulse arrival is further delayed. Also shown is the finite difference solution (FD) for the linear model. KWB fails to capture the rising limb and recession period of the nonlinear model.

5.1.3.2 Diffuse aquifer recharge

For a rectangular diffuse recharge of duration $T_r = 1$ and intensity $R_r = 0.01$, the results are shown in Figure 16. The different values of the matrix parameters κ , σ and S_y have a similar effect on the hydrograph as discussed in the pipe flow model. The conduit nonlinearity is further discussed in Section 5.1.5.

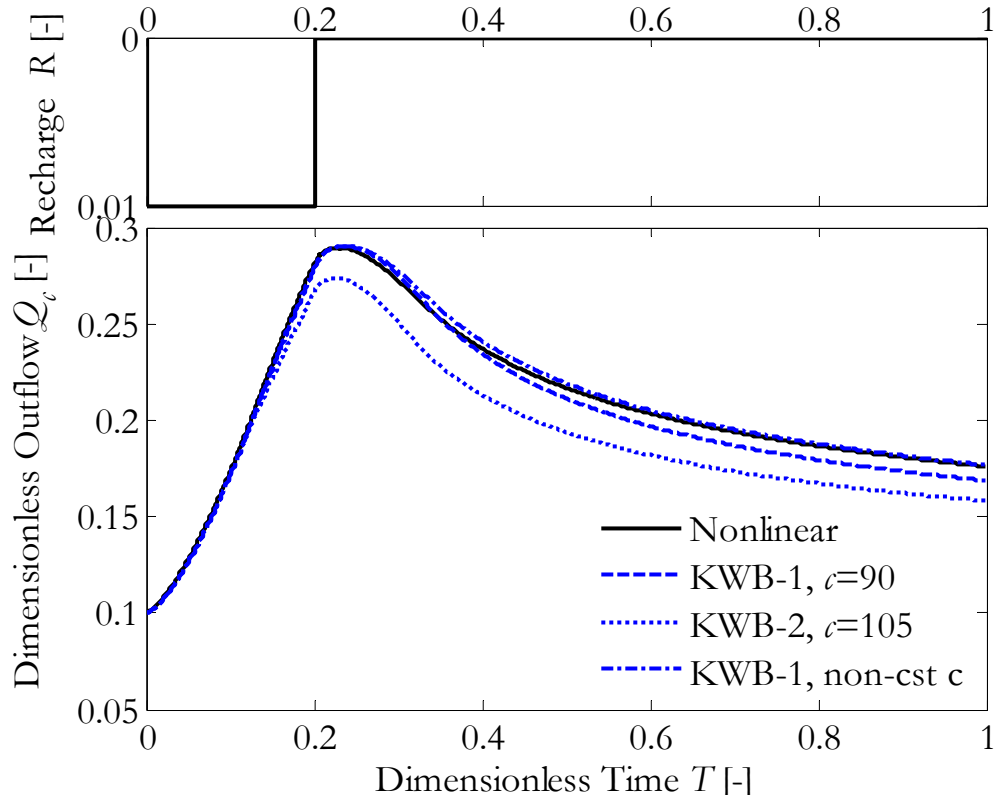


Figure 16. KWB (linear) and numerical (nonlinear) model predictions for a diffuse recharge event. The linear model with a constant conduit velocity can capture either the peak or the whole hydrograph using the selected minimizing equations (KWB-1 corresponds to 4-21, and KWB-2 corresponds to 4-23)

5.1.4 Sensitivity analysis

The sensitivity of the model to the parameters κ , σ , S_y , α and w is hereby assessed in terms of change in peak outflow, peak arrival (i.e. delay) and outflow volume. The model KWU with a constant velocity is used to generate the standard scenario presented in Table 4 as well as the simulated ones. The value of c is expressed in terms of α and w according to Equation (4-23) with $Q(X_m, T_m)$ being equal to the peak outflow of the standard case (0.614 from Figure 15).

For a concentrated recharge, Figure 17 shows that the hydrograph peak is most sensitive to κ and least sensitive to σ . On the other hand, the peak arrival is most

sensitive to the velocity coefficient α followed by κ (Figure 18). The change in volume retrieved at the spring is less sensitive to the change in parameters as compared to the peak and peak arrival (Figure 19). For a diffuse recharge, the model is most sensitive to the specific yield S_y in terms of peak outflow and outflow volume (Figure 20 and Figure 22). Yet, when it comes to peak arrival, the model is most sensitive to α and completely insensitive to S_y (Figure 21).

One concludes that the most sensitive parameters are α , κ and S_y depending on the model evaluation criteria. The conduit-related parameter α mostly governs the time of peak arrival while κ and S_y affect the amount of water reaching the spring and the peak outflow. Similarly to the pipe flow models, the effect of $\pm 10\%$ change in the parameters values on the model's output was minimal.

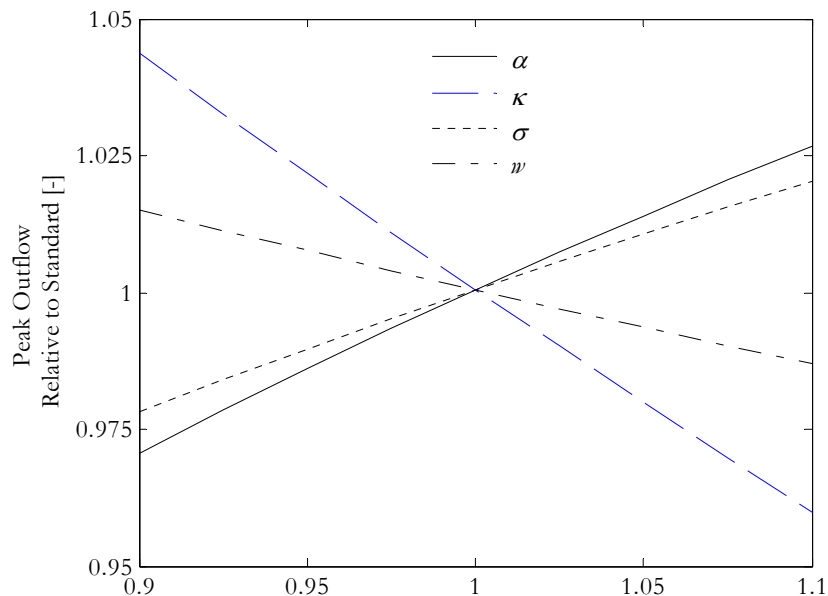


Figure 17. Sensitivity of the model to the parameters in terms of peak outflow for a concentrated recharge. The model is most sensitive to the exchange parameter κ .

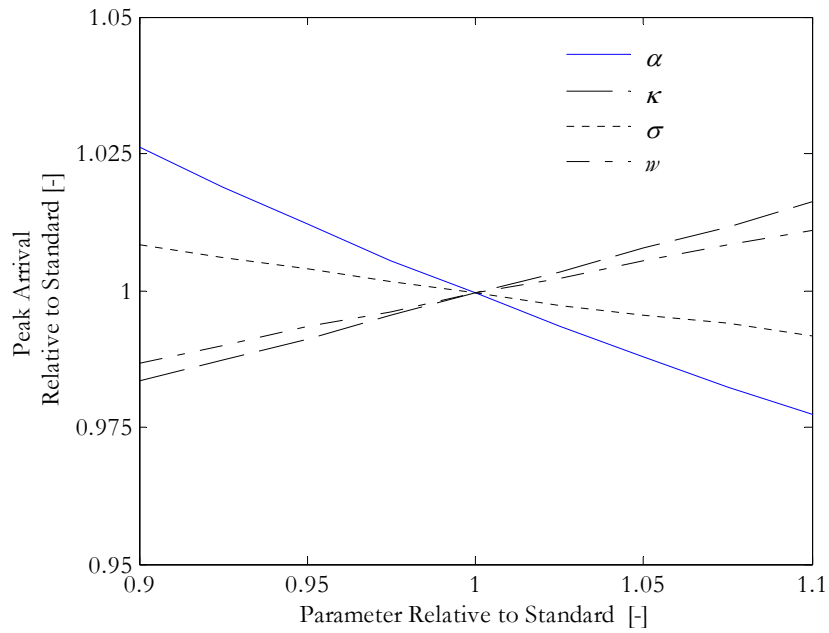


Figure 18. Sensitivity of the model to the parameters in terms of peak arrival for a concentrated recharge. The velocity parameter α has the highest influence on the peak delay.

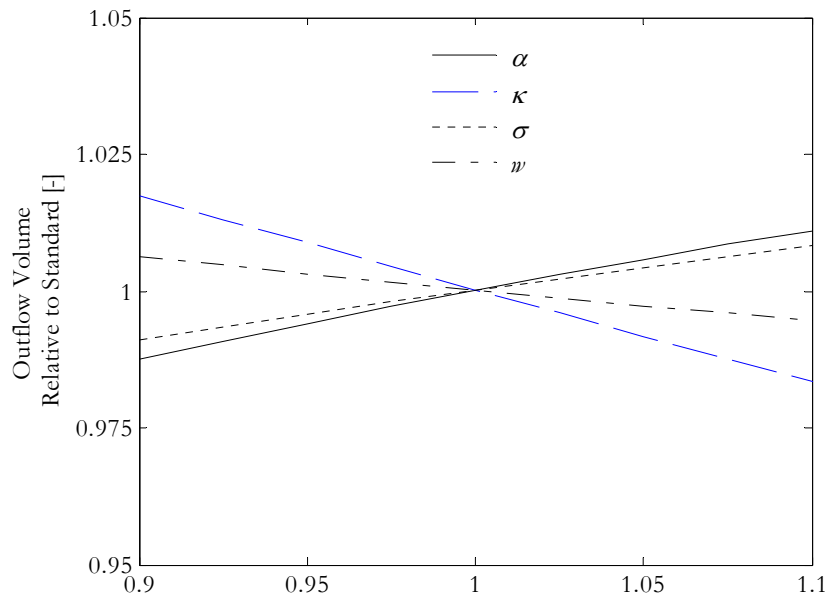


Figure 19. Sensitivity of the model to the parameters in terms of outflow volume for a concentrated recharge. The exchange parameter κ is the most sensitive. The change in volume is not as significant as the one observed for the hydrograph peak and peak delay because the volume recovered during the recession compensates the volume lost due to peak reduction.

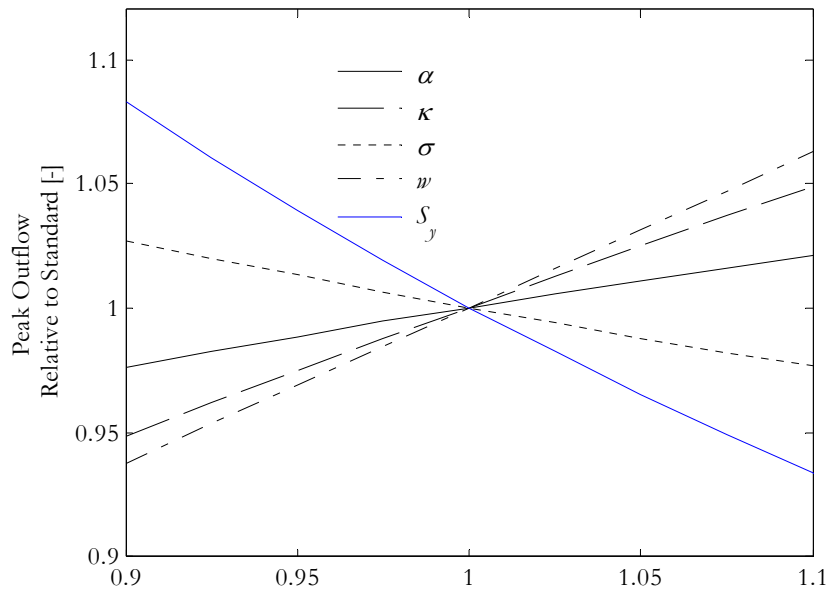


Figure 20. Sensitivity of the model to the parameters in terms of peak outflow for a diffuse recharge. The model is most sensitive to the specific yield.

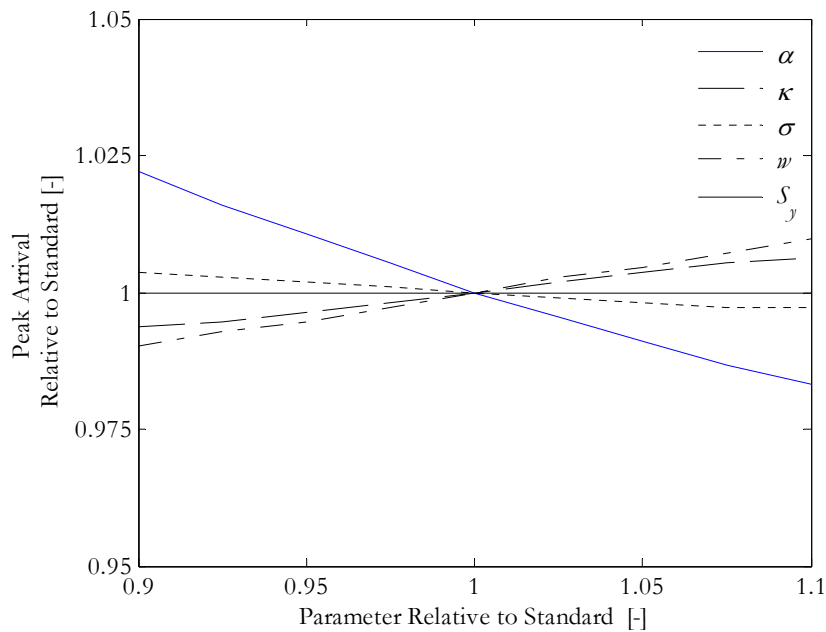


Figure 21. Sensitivity of the model to the parameters in terms of peak arrival for a diffuse recharge. The model is insensitive to S_y but most sensitive to α .

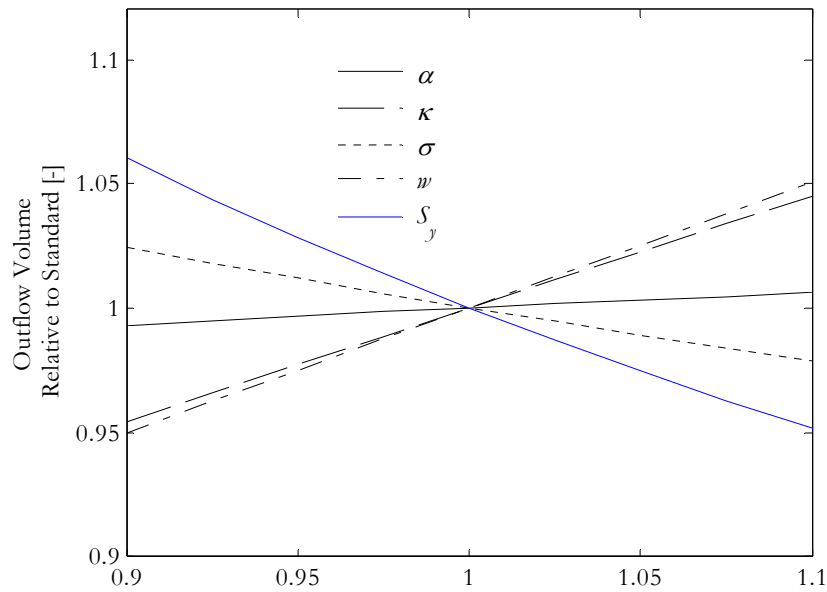


Figure 22. Sensitivity of the model to the parameters in terms of outflow volume for a diffuse recharge. The specific yield has the most influence on the volume of water reaching the spring from the diffuse recharge.

5.1.5 Effect of conduit nonlinearity

The feasibility of the linear conduit flow simplification is assessed by comparing the output of the nonlinear model to its linear approximation KWB. This is achieved by estimating KWB's parameters using the optimal relationships derived in Section 4.7. The model results where KWB's linear velocity is calculated using Equations (4-21) and (4-23) are referred to as KWB-1 and KWB-2 respectively.

For a concentrated recharge, a constant velocity KWB fails to capture the long recession of the hydrograph as well as its rising limb (Figure 15). In order to improve its performance, a temporally varying but spatially constant c is hereby suggested. The latter is a function of both $Q(L_c, T)$ and $Q(0, T)$ for KWB-1 and $Q(L_c, T)$ for KWB-2.

Consequently, the parameter c is updated at each time step in KWB-1 and KWB-2 and is a function of the nonlinear model's discharge values.

As shown in Figure 23, this assumption improved KWB's ability in capturing the nonlinear model's recession with KWB-1 (errors in peak and volume are 0.2% and 2.4%) having similar accuracy to KWB-2 (errors in peak and volume are 1% and 2.4%). However, the advantage of KWB-2 over KWB-1 is that it is only a function of the downstream discharge values.

For a diffuse recharge, Figure 16 shows that KWB-1 is a better approximation of the nonlinear model (errors in peak and volume are 0.22% and 2.0%) as compared to KWB-2 (errors in peak and volume are 5.5% and 8.3%). Furthermore, the KWB model results improved when a non-constant velocity was introduced.

In summary, the linear model KWB is successful in approximating the nonlinear model given both diffuse and concentrated types of recharge. Equation (4-21) is more adequate for diffuse pulses while (4-23) is used for concentrated recharge cases. A non-constant velocity parameter significantly improves the ability of the linear model in capturing the response of the nonlinear one.

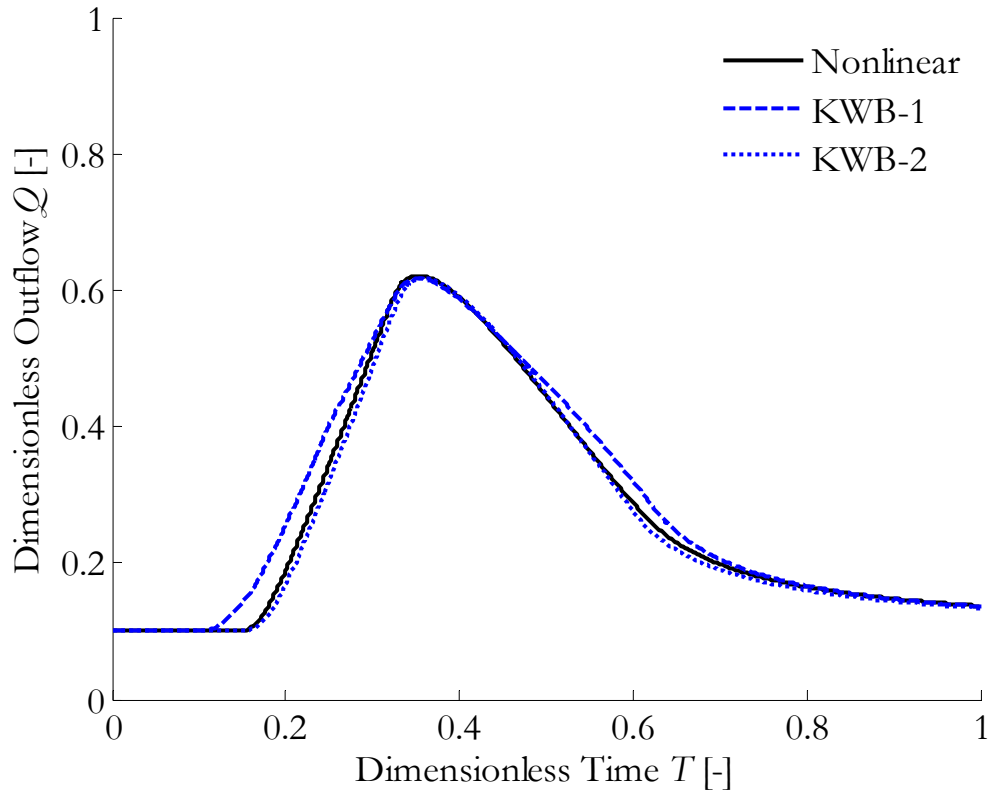


Figure 23. Comparison between KWB (linear) and numerical (nonlinear) models for a concentrated input pulse. The linear model with a non-constant conduit velocity can capture the whole shape of the hydrograph using the selected minimizing equations (KWB-1 corresponds to 4-21, and KWB-2 corresponds to 4-23)

5.1.6 Effect of boundary conditions

Comparisons between the finite KWB and semi-infinite KWU aquifer models are shown in Figure 24 and Figure 25 for concentrated and diffuse recharge types respectively. The effect of the aquifer boundary on the spring hydrograph is similar to the one observed for the pipe flow models in Section 3.1.5.

The semi-infinite assumption is valid for $L_m > 7$ for the concentrated type of recharge. This value compares well to the condition set by *Hunt* [1990] where $\sigma T_p / L_m^2 < 0.2$ or $L_m > \sqrt{50} = 7$ (with $T_p = 1$). Depending on the matrix parameter σ

and the time to pulse's peak T_p , one can thus calculate the aquifer width for which semi-infinite conditions prevail.

As for diffuse recharge, its spatial distribution is important in shaping the hydrograph as shown in Figure 25. As the recharge length increases, the less volume is recovered at the spring with KWB showing higher recovery rates than KWU. The length over which semi-infinite conditions prevail ($L_r = L_m$) > 10 is higher than the requirement for concentrated recharge $L_m > 7$ because the matrix is no longer acting as a storage but rather as a source of water.

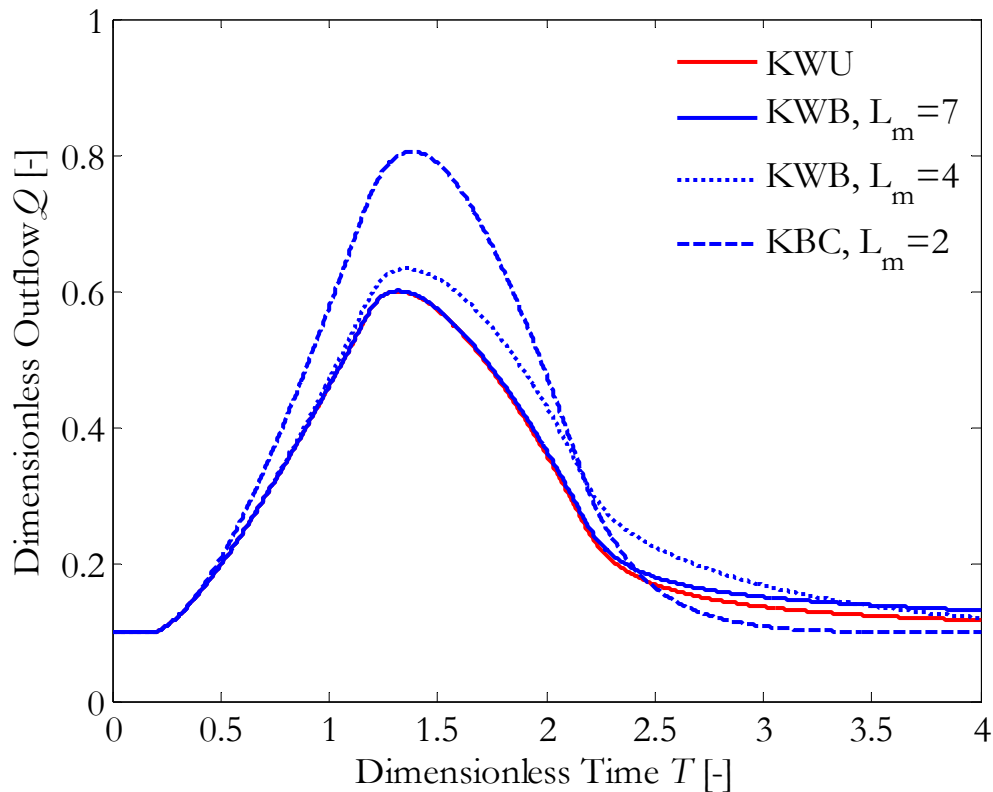


Figure 24. Comparison between the bound (KWB) and unbound (KWU) channel models for a concentrated recharge. The results are simulated for a constant conduit velocity $c = 65$. The aquifer boundary either affects the recession ($L_m = 7$), the peak and recession ($L_m = 4$) or the whole shape of the hydrograph ($L_m = 2$). The semi-infinite aquifer simplification is valid for $L_m > 7$ where the two models are nearly superimposed.

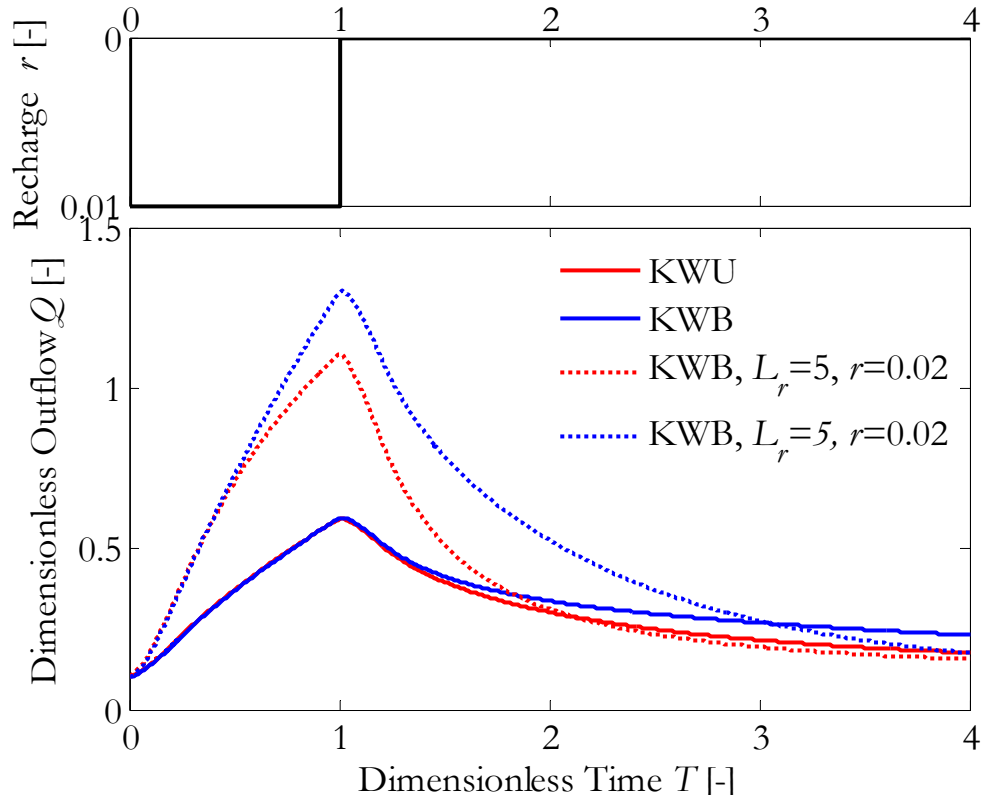


Figure 25. Comparison between the finite (KWB) and semi-infinite (KWU) aquifer models for a diffuse aquifer recharge. The results are simulated for a constant conduit velocity $c = 65$. The finite aquifer model is a good approximation of the unbound one for $L_r = L_m > 10$. As the recharge is applied over larger widths, the volume of water recovered at the spring decreases while KWB shows a greater recovery than the semi-infinite aquifer model KWU.

5.2. Comparison to existing models

The proposed process-based channel models have the same advantages over lumped models as discussed in Section 3.2 for the pipe flow models. They are able to simulate the whole spring hydrograph and are a function of physically meaningful parameters instead of empirical ones.

However, KWU and KWB can only simulate open-channel conditions and do not handle transitions to pressurized conditions such as the CDC distributive models DisCo [de Rooij *et al.*, 2013] or ModBrac [Reimann *et al.*, 2011b]. They also assume

that the conduit is wide enough to approximate the hydraulic radius as $R_h = H_c$ which is not a limitation in existing numerical models. Nonetheless, they offer a computationally advantageous approach to simulate delayed karst system responses. Their results can be used as preliminary estimates in more sophisticated distributive models for further refinement.

5.3. Parameter Estimation

The range of the matrix parameters is discussed in Chapter 3, Section 3.4. As for Chezy's coefficient, it is related to the friction factor as $C_c = \sqrt{8g/f}$. In karst conduits, friction factors range from low values of 0.12 and can be as high as 340 [Springer, 2004]. Therefore, Chezy's coefficient varies between 0.5 and 25 m^{1/2}/s. Assuming a minimum and maximum bed-slopes of 0.01% and 10%, the parameter α ranges between 0.0015 and 8 m^{1/2}/s.

The five model parameters α , w , κ , σ and S_y are optimized using the nonlinear least-square fitting and compared to physical ranges found in the literature. The two parameters α and w are required to calculate the water levels in the system using Equation (4-5). An enhanced estimation of these two parameters is possible when both water levels and spring discharge are measured in the field. For diffuse recharge applications, the relationship between the nonlinear parameter α and linear velocity c is obtained from Equation (4-21). Otherwise, Equation (4-23) is used for concentrated recharge. The initial parameter estimates are based on available field observations, literature ranges or preliminary manual fitting.

5.4. Model Applications and Results

The proposed semi-infinite aquifer model KWU is hereby applied to the Bluegrass [Winston and Criss, 2004], and Lurbach [Mayaud *et al.*, 2014] karst systems. The first site is subject to a diffuse aquifer recharge. The second one consists of a conduit that is receiving a concentrated recharge from a sinking stream.

5.4.1 Bluegrass Spring, Missouri

The Bluegrass spring is located in east central Missouri, USA. The area where the spring emerges has extensive karst features including losing streams, caves and sinkholes. The recharge mainly occurs from precipitation that averages 97 cm a year. The surficial recharge area is approximated as $R_A = 0.8 \text{ km}^2$ and has no runoff features [Winston and Criss, 2004]. However, the groundwater recharge area is believed to be larger from tracer tests. The rainfall events occurring in February and March 2001 are used to validate the KWU model. The main objective of this model application is to show the capability of the proposed model in simulating a spring hydrograph resulting from a diffuse aquifer recharge. Another objective is to compare the results to an existing lumped model by Criss and Winston [2003] as well as the pressurized pipe model UU.

Since the model domain and recharge conditions are unknown, they are hereby subject to the following assumptions that are summarized in Table 5:

(1) The conduit length and contributing recharge semi-length are set to $L_c = 1200 \text{ m}$ and $L_r = R_A/2L_c = 335 \text{ m}$ respectively.

(2) The diffuse recharge pulse is approximated from mass balance calculations such that $V_r R_A = V_{BG} - V_{baseflow}$. It is important to note that the diffuse recharge

herein refers to the recharge to groundwater since the proposed process-based models neglect the surface water to groundwater (or infiltration) process. As a result, the diffuse aquifer recharge is assumed as a delayed fraction of rainfall and its intensity is determined from mass balance calculations. A better estimate of r is achieved by incorporating the models into more complex hydrological ones.

(3) The delays in diffuse pulse arrivals are assumed equal to the ones proposed by *Criss and Winston* [2003].

(4) The velocity is a function of the two optimizing parameters α and w and is obtained from Equation (4-21).

The optimization gives acceptable values of the parameters as shown in Table 6. The maximum simulated head in the conduits was less than the conduit width which is in line with the model's assumption of wide flow. The transmissivity value is greater for the higher intensity flood (i.e. February 2001) because more rainfall was observed and as a result, a higher aquifer depth is expected. The hydraulic conductivity can be obtained from $\kappa_* = 2K_m D/w_*$ (where D is the calculated depth in the conduit) and is equal to 0.028 m/s and 0.02 m/s for February and March 2001 events respectively. The range of the transmissivities and hydraulic conductivity indicate the presence of a fractured system that facilitates the flow towards the conduit.

KWU is then compared to another process-based model developed by *Criss and Winston* [2003] that is a function of a single lumped parameter “ b ” [T] representing the matrix properties. The model simulates the peak by shifting the simulated curve to match the peak of the measured ones. Therefore, the physical processes that cause a pulse arrival delay are neglected. Although C&W and KWU have a similar

performance in simulating the Bluegrass spring hydrograph (Figure 26 and Figure 27), KWU is more advantageous because it is a function of physically significant parameters.

For comparison purposes, the system is also simulated using the pressurized pipe flow model UU. The latter's optimized parameters are $\beta_l = 5,000 \text{ m}^3/\text{s}$, $\kappa = 0.063 \text{ m}^2/\text{s}$, $\sigma = 0.474 \text{ m}^2/\text{s}$ and $S_y = 0.067$ for the February 2011 event and $\beta_l = 5,001 \text{ m}^3/\text{s}$, $\kappa = 0.1 \text{ m}^2/\text{s}$, $\sigma = 0.292 \text{ m}^2/\text{s}$ and $S_y = 0.17$ for the March 2011 event. As shown in Figure 26 and Figure 27, the pipe model is not able to capture the observed recession period and has a lower performance than KWU.

One concludes that conduit hydraulics play an important role in shaping spring hydrographs and the CDC modeling approach proves effective in analyzing karst systems. A better estimate of the parameters can be achieved by incorporating KWU into more sophisticated hydrological models that allow an enhanced estimation of the recharge term r .

Table 5. Input data for Bluegrass karst system

| | February 2001 | March 2001 |
|--|---------------------------------|---------------------------------|
| Model Domain | | |
| L_c | 1200 m | 1200 m |
| L_m | 340 m | 340 m |
| Initial Conditions | | |
| $(Q_{BG})_{t=0}$ | 5.27 L/s | 5.5 L/s |
| T_{sim} | 11 days | 20 days |
| Initial time | Day 72 of Year 2001 | Day 54 of Year 2001 |
| Mass Balance | | |
| V_{BG} | $19.75 \times 10^3 \text{ m}^3$ | $14.25 \times 10^3 \text{ m}^3$ |
| $V_{rainfall} = R_A \int_0^{T_{sim}} RF dt$ | $60.2 \times 10^3 \text{ m}^3$ | $41.08 \times 10^3 \text{ m}^3$ |
| Recharge Pulse(s) | | |
| Lag of pulse or starting time after Initial Time | 1.9 days | 2.9 days |
| Duration of pulse | 0.2 days | 0.2 days |
| Intensity of pulse | 0.52 cm/hr | 0.26 cm/hr |

Table 6. KWU results for the Bluegrass karst system

| | w [m] | α [m ^{1/2} /s] | κ [m/s] | σ [m ² /s] | S_y [-] | T_m [m ² /d] | $\max(H_c)$ | K_m [m/s] |
|----------------------|------------|-----------------------------------|-------------------|---------------------------------|--------------|------------------------------|-------------|----------------|
| Feb 2001 | | | | | | | | |
| Initial Estimates | 5 | 0.065 | 0.012 | 2 | 0.04 | | | |
| Optimized Parameters | 4.12 | 0.031 | 0.0182 | 4.28 | 0.0087 | 3,242 | 1.33 | 0.028 |
| Mar 2001 | | | | | | | | |
| Initial Estimates | 5 | 0.065 | 0.012 | 2 | 0.007 | | | |
| Optimized Parameters | 3.57 | 0.019 | 0.014 | 3.61 | 0.007 | 2,219 | 1.25 | 0.02 |

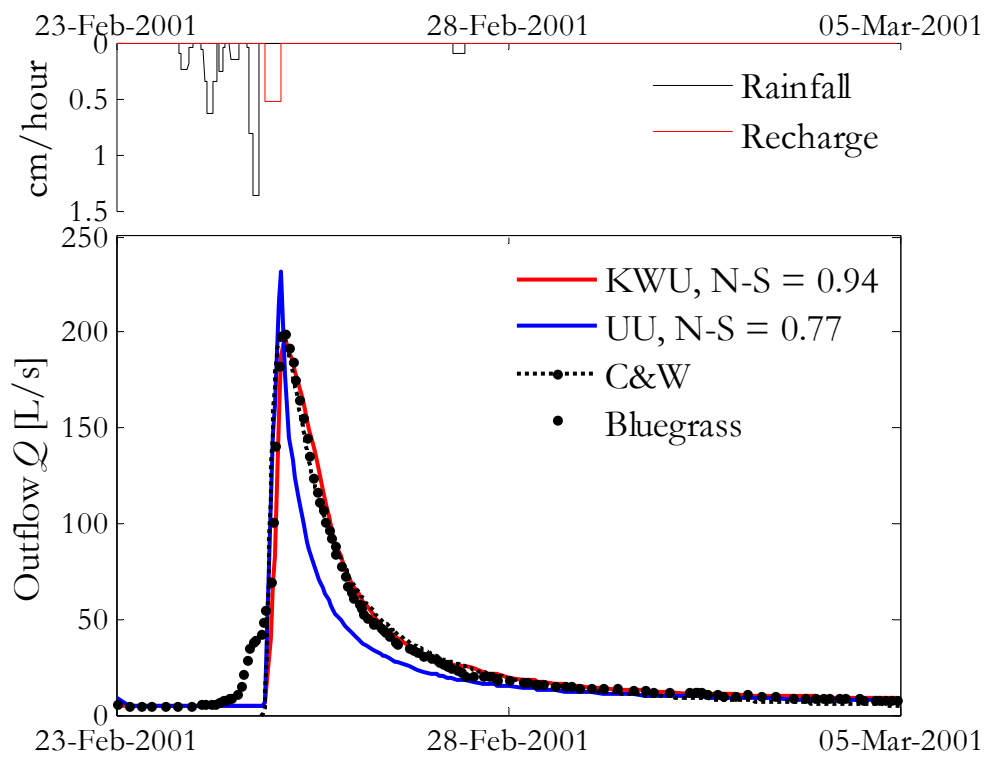


Figure 26. Observed vs. simulated discharge at the Bluegrass spring for the February 2001 event. KWU is more effective than UU in simulating the long recession. It also compares well to another process-based model (C&W) that simplifies the conduit hydraulics and recharge conditions.

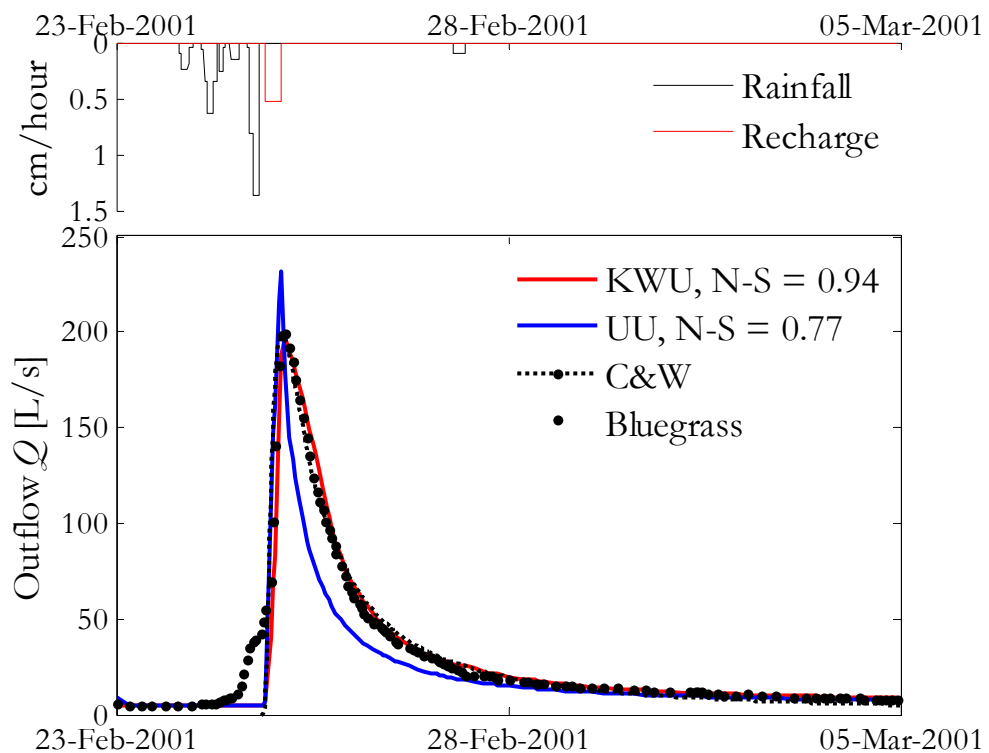


Figure 27. Observed vs. simulated discharge at the Bluegrass spring for the March 2001 event.

5.4.2 *Lurbach Karst System, Austria*

5.4.2.1 Area description

The Lurbach karst system is located in the Styria region, Austria. The system consists of a stream that drains the upper catchment of the Lurbach (LB) watershed and then disappears into a sinkhole located at a cave's entrance. The stream resurges further downstream as two springs named Hammerbach (HB) and Schmelzbach (SB). The complexity of the Lurbach system is captured by hydrological studies and tracer tests [Mayaud *et al.*, 2013; 2014]. During low to medium flow conditions, the LB stream only discharges into the HB spring. As the water levels exceed a certain threshold at

HB, an overflow is activated towards SB. A schematic of the system is presented in Figure 28.

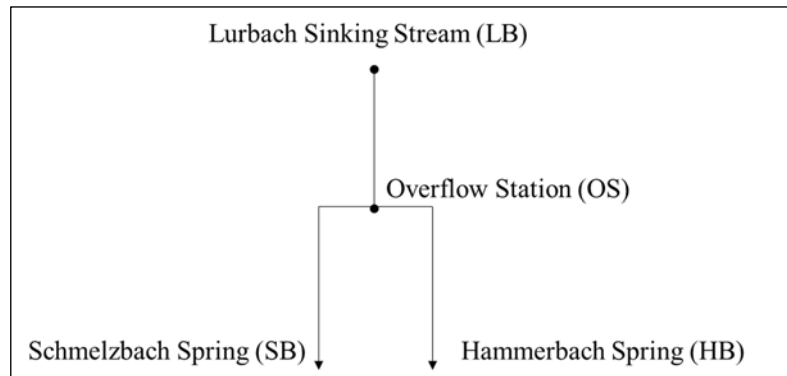


Figure 28. Schematic representation of the Lurbach karst system

A field campaign comprising a tracer test was conducted from November 28th until December 30th, 2008 with the tracer being released in the Lurbach cave near the sinking stream location. The three stations LB, HB and SB were monitored for discharge and Uranine concentrations. Within this period, two floods with a total duration of 32 days were observed. The first flood has a single peak, a duration of 13 days and is hereby used to validate the KWU model. Note that the data for LB, SB and HB is digitized from *Mayaud et al.* [2014, Figure 3].

5.4.2.2 Model Assumptions

This system is considered uncharted due to the limited information available about the conduits' sizes as well as the location of the overflow station. Consequently, the main objectives of this application are to apply the model on a system that is subject to a concentrated recharge in the form of a sinking stream. Another objective is to simplify the conceptual framework of the Lurbach system based on a set of sound assumptions in order to apply the proposed process-based KWU.

Consequently, the following assumptions are made and summarized in Table 7:

(1) The model aims to simulate the SB spring outflow rather than HB's

because there is a strong correlation between their hydrographs (Figure 29). Indeed, SB's and LB's hydrographs are characterized by a fast rising limb followed by a long recession. Conversely, HB's outflow rises abruptly after the flood event and remains constant afterwards.

(2) The overflow contribution to SB is zero for $T < 2.8$ days while it is equal to LB's minus HB's spring discharge for $T > 2.8$ days. This value was selected because it is equal to the time the tracer released at LB was detected at SB. Therefore, the overflow discharge equation becomes

$$Q_{OS} = \begin{cases} 0, & T < 2.8 \text{ days} \\ [Q_{LB} - (Q_{LB})_{t=0}] - [Q_{HB} - (Q_{HB})_{t=0}], & T \geq 2.8 \text{ days} \end{cases} \quad 5-1$$

where $(Q_{LB})_{t=0}$ and $(Q_{HB})_{t=0}$ are the baseflow of LB and HB springs respectively. Note that Q_{LB} , Q_{SB} and Q_{HB} represent the observed discharge at Lurbach, Schmelzbach and Hammerbach stations respectively.

(3) The overflow location is assumed close to the Lurbach sink as discussed in *Mayaud et al.* [2014]. Therefore, the distance between OS and SB is $L_c = 3,000$ m and the diffuse recharge length is equal to $L_r = 350$ m.

(4) Once LB, SB and HB baseflows are removed, mass balance should be satisfied between the overflow station and SB ($V_{SB} = \int_0^{T_{sim}} [Q_{SB} - (Q_{SB})_{t=0}] dt = 20,237 \text{ m}^3$ and $V_{OS} = \int_0^{T_{sim}} Q_{OS} dt = 18,341 \text{ m}^3$). Since the SB spring drains an additional watershed, the diffuse aquifer recharge is calculated from mass balance as

$r = \frac{V_{SB} - V_{OS}}{2L_c L_r T_d} = 8 \times 10^{-10} \text{ m/s}$ where $T_r = 13 \text{ days}$. As mentioned for the Bluegrass

spring system, the diffuse aquifer recharge refers to the direct recharge to the groundwater while the infiltration process is neglected in this work.

(5) The non-constant velocity parameter is calculated using Equation (4-23)

(6) The channel width is set equal to 10 meters as assumed by *Mayaud et al.*

[2014]

5.4.2.3 Model results

The KWU optimized parameters are found equal to: $\alpha = 0.5 \text{ m}^{1/2}/\text{s}$, $\sigma = 0.5 \text{ m}^2/\text{s}$, $\kappa = 0.0033 \text{ m/s}$ and $S = 0.01$, and $w = 10\text{m}$. The resulting transmissivity and hydraulic conductivity are equal to $430 \text{ m}^2/\text{day}$ and 0.01 m/s , All model parameters fall within the acceptable range set for karst aquifers.

As shown in Figure 29, the proposed KWU model is able to capture the peak and time to peak of SB's hydrograph although the goodness of fit is reduced during the recession period. The reason may be attributed to the discharge calculations at the overflow station as detailed in model assumption (2). The latter states that the HB station is receiving water solely from LB whereas it can originate from both concentrated LB and diffuse aquifer recharge. In this case, the discharge at the OS could be higher than the one shown in Figure 29 during the recession period. Improved recession fitting can thus be achieved by combining the proposed model with an infiltration module that calculates the amount of infiltrated water in HB's watershed. The latter will help in determining the mass balance at the overflow station and consequently improve the estimation of the model parameters.

Finally, KWU is compared to the pipe flow model UU. As shown in the figures, the proposed model KWU is more successful in simulating the pulse arrival delay at the Schmelzbach spring (with) as compared to the pressurized pipe model UU.

Table 7. Input data for Lurbach karst system

| | Event 1 |
|---------------------|-------------------------|
| Model Domain | |
| L_c | 3000 m |
| L_m | 350 m |
| Initial Conditions | |
| $(Q_{LB})_{t=0}$ | 6.46 L/s |
| $(Q_{HB})_{t=0}$ | 95.3 L/s |
| $(Q_{SB})_{t=0}$ | 16.9 L/s |
| T_{sim} | 13 days |
| Recharge Conditions | |
| T_r | 13 days |
| $L_r = L_m$ | 350m |
| V_{OS} | $18.0 \times 10^3 m^3$ |
| V_{SB} | $20.2 \times 10^3 m^3$ |
| V_{loss} | $0 m^3$ |
| V_r | $1.9 \times 10^3 m^3$ |
| r | $8 \times 10^{-10} m/s$ |

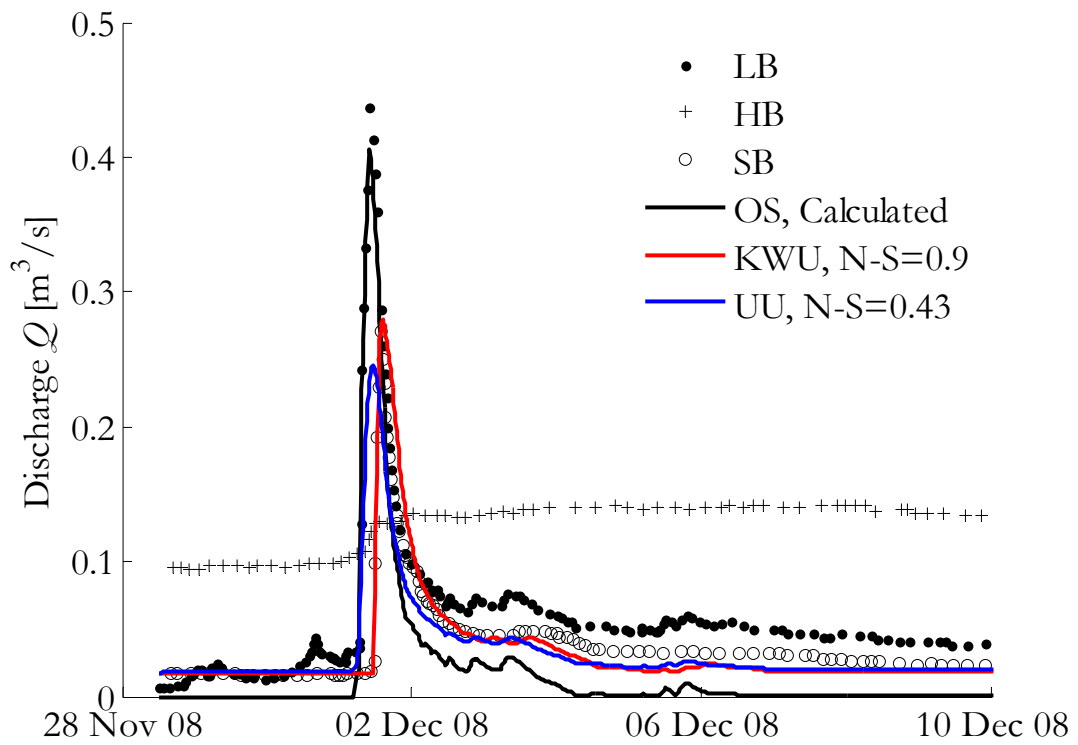


Figure 29. Simulated and observed discharge values at Schmelzbach spring for Event 1. The KWU model is able to simulate the SB's spring hydrograph and is particularly able to capture the delay in pulse arrival from the overflow station (OS). The pressurized pipe model UU simulated an instantaneous response and had a lower performance than KWU's.

5.5. Summary of Important Results

The proposed linear models KWU and KWB are able to simulate a system's delayed response to a recharge event and reproduce the shape of a typical hydrograph that is characterized by a fast followed by a slow spring recession. They also capture the more general behavior of the nonlinear model using the linearizing optimal coefficient obtained in the previous chapter. Furthermore, the semi-infinite aquifer model KWU is found as an acceptable approximation of the finite aquifer model KWB under various recharge conditions. The models' limitations include the inability to simulate transitions from pressurized to unpressurized flows and the handle spatially variable diffuse aquifer recharge.

The models were successfully applied to two real karst systems subject to different recharge conditions. The analytical solutions were computationally effective in the optimization process and the parameters compared reasonably well to literature ranges. Also, the performance of the open channel models was compared to the pressurized flow model UU that failed to capture delay in peak arrival to the spring.

CHAPTER 6

TRANSPORT MODEL – THEORY

This chapter presents the theoretical background and governing equations of the transport model. First, the different transport processes in the system are defined. The advection-diffusion equation is used to describe the solute transport in the conduit and aquifer while the interface exchange is governed by . The combined two-dimensional system of equations is consequently solved using the Laplace transform method and analytical solutions are obtained for arbitrary and Dirac-type input pulses.

6.1. Transport Processes

This study considers a single conduit of length l_c [L] located at the center of an aquifer of width w_m [L]. The conduit is connected to a sinkhole on one end while the other is considered a perennial spring representing the system's output. A mass of artificial tracer m [W] is released into the sinkhole and later recovered at the spring. The temporal distribution of the solute concentration c [W/L³] at the spring is considered the system's output and is referred to as the tracer breakthrough curve.

6.1.1 Conduit transport

The one-dimensional advection-dispersion equation with a source term describes the transport of a conservative solute in a wide conduit of constant width w [L] as

$$\frac{\partial c}{\partial t} = -u \frac{\partial c}{\partial x} + D_x \frac{\partial^2 c}{\partial x^2} + \frac{2J_{ex}}{w} \quad 6-1$$

where c is the solute concentration in the conduit [W/L^3], u is the velocity in the conduit flow direction [L/T], D_x is the conduit's dispersion coefficient [L^2/T], J_{ex} is the source term and represents the conduit/matrix interface flux [W/L^2T], x is the Cartesian coordinate in the conduit flow direction [L] and t is the time [T]. The coefficient 2 is added to account for solute exchange on both sides of the conduit.

6.1.2 Matrix transport

The transport in the surrounding aquifer is assumed to be one-dimensional in the lateral y -direction that is perpendicular to the conduit centerline. The transport equation in the aquifer is given by

$$\frac{\partial c_m}{\partial t} = -v \frac{\partial c_m}{\partial y} + D_y \frac{\partial^2 c_m}{\partial y^2} \quad 6-2$$

where c_m is the aquifer solute concentration, D_y is the dispersion coefficient in the aquifer flow direction [L^2/T] and v is the aquifer velocity [L/T].

6.1.3 Exchange solute flux

The solute exchange flux at the interface J_{ex} is given by the advective-dispersive mass flux equation [e.g. *Houseworth, 2006*]

$$J_{ex} = -q_m c_m|_{y=0} + D_y \theta \left. \frac{dc_m}{dy} \right|_{y=0} \quad 6-3$$

where θ is the aquifer or matrix effective porosity [-] and q_m is the Darcy flow rate and is equal to

$$q_m = v\theta \quad 6-4$$

6.2. Combined Conduit-Aquifer Transport

By coupling Equations (6-3) and (6-4) with Equation (6-1), one gets the combined conduit-aquifer transport governing equation

$$\frac{\partial c}{\partial t} = -u \frac{\partial c}{\partial x} + D_x \frac{\partial^2 c}{\partial x^2} + \frac{2\theta}{w_c} \left(-v c_m|_{y=0} + D_y \left. \frac{dc_m}{dy} \right|_{y=0} \right) \quad 6-5$$

6.3. Boundary Conditions

The boundary conditions in the conduit are defined as

$$c = c_0(t) \quad x = 0 \quad 6-6$$

$$c = 0 \quad x \rightarrow \infty \quad 6-7$$

The matrix concentrations at the interface or $y = 0$ are equal to the ones in the conduit. The matrix is either semi-infinite or finite. Therefore, the matrix boundary conditions become

$$c_m = c \quad y = 0 \quad 6-8$$

$$c_m = 0 \quad y \rightarrow \infty \quad 6-9$$

$$dc_m/dy = 0 \quad y = l_m \quad 6-10$$

The initial conditions are

$$c = c_m = 0 \quad t = 0 \quad 6-11$$

In the absence of upstream measured concentrations, c_0 is often assumed as an instantaneous upstream pulse (Dirac-type input function) and is written as

$$c_0 = i_0 \delta(t - t_0) \quad 6-12$$

where $\delta(t - t_0)$ is the Dirac-delta function and t_0 is the time at which the tracer is released [-]. Depending on the input data, the pulse intensity i_0 is either a function of the flow area A_c [L²] and conduit velocity or the conduit discharge Q [L³/T].

6.4. Dimensionless System

Define the following dimensionless variables

$$C = \frac{c}{c_0}; X = \frac{x}{d_0}; Y = \frac{y}{d_0}; T = t \frac{u}{d_0} \quad 6-13$$

where d_0 is the characteristic length which is generally equal to l_c and c_0 is the normalizing concentration. The conduit and matrix dimensionless equations become

$$\frac{\partial C}{\partial T} = -\frac{\partial C}{\partial X} + \frac{1}{P_{ex}} \frac{\partial^2 C}{\partial X^2} + S \left(-VC + D_Y \frac{dC_m}{dY} \Big|_{Y=0} \right) \quad 6-14$$

$$\frac{\partial C_m}{\partial T} = -V \frac{\partial C_m}{\partial Y} + D_Y \frac{\partial^2 C_m}{\partial Y^2} \quad 6-15$$

where $P_{ex} = \frac{ud_0}{D_x}$; $D_Y = \frac{D_y}{ud_0}$; $V = \frac{v}{u}$ and $S = \frac{2\theta d_0}{w}$. For $d_0 = l_c$, the parameter P_{ex} becomes equal to the Péclet number which is a measure of the relative importance of advection to dispersion inside the karst conduit.

The Dirac pulse is defined in dimensionless form as

$$I_0 = \frac{mu}{Qc_0d_0} \text{ or } I_0 = \frac{m}{A_c c_0 d_0} \quad 6-16$$

6.5. Karst Transport Models

In this section, the Laplace transform and analytical solutions of the system of governing equations (6-14) and (6-15) are derived for a semi-infinite as well as a bound aquifer. Although the governing equations have appeared in fractured media related research [e.g. *Tang et al.*, 1981; *Sudicky and Frind*, 1982; *van Genuchten et al.*, 2013], the boundary conditions and physical processes are different than the ones considered in this work. For example, the aforementioned references solely consider a diffusive interface flux and neglect the advective flux that is of primary importance herein. Others, neglect the fracture and matrix dispersion and take into consideration advective-dispersive exchange [e.g. *Houseworth et al.*, 2013]

The solution methodology consists of applying the Laplace transform to the aquifer solute transport Equation (6-15) and solving the ensuing ordinary differential equation for the given boundary conditions. The expression is then differentiated to obtain the concentration gradient at the interface which in its turn is replaced into (6-14). The conduit transport equation is subsequently solved and the ensuing Laplace transform solution is inverted either analytically or numerically.

Applying the Laplace transform to Equation (6-15) gives

$$p\bar{C}_m + V \frac{\partial \bar{C}_m}{\partial Y} - D_Y \frac{\partial^2 \bar{C}_m}{\partial Y^2} = 0 \quad 6-17$$

where \bar{C}_m is the Laplace transform of C_m such that

$$\bar{C}_m = \int_0^{\infty} e^{-pT} C_m dT \quad 6-18$$

6.5.1 *Semi-infinite aquifer (KTM)*

Following the solution methodology outlined above, the conduit concentration become

$$\bar{C} = \bar{C}_0 \exp\left(\frac{P_{ex} L_c}{2}\right) \exp\left(-\frac{P_{ex} L_c}{2} \sqrt{1 + \frac{4}{P_{ex}} [p + \alpha + \sqrt{\alpha^2 + \beta p}]}\right) \quad 6-19$$

with $\alpha = SV/2$ and $\beta = S^2D_y$. The parameter α represents advective exchange being a function of v while β represents diffusive exchange being a function of D_y .

Equation (6-19) is analytically inverted as

$$C(L_c, T) = \frac{2}{\pi^{1/2}} \exp\left(\frac{P_{ex}L_c}{2}\right) \int_0^T \int_l^\infty C_0(T - \tau) \frac{\gamma}{\xi^2} \left[\frac{4\pi}{\beta} \left(\tau - \frac{\gamma}{\xi^2} \right)^3 \right]^{-1/2} \exp\left[-\xi^2 - \frac{\gamma}{\xi^2} \left(\frac{P_{ex}}{4} + \alpha \right) - \frac{\beta}{4} \left(\frac{\gamma}{\xi^2} \right)^2 \left(\tau - \frac{\gamma}{\xi^2} \right)^{-1} - \frac{\alpha^2}{\beta} \left(\tau - \frac{\gamma}{\xi^2} \right) \right] d\xi d\tau \quad 6-20$$

where $\gamma = L_c^2 P_{ex}/4$, $l = \sqrt{\gamma/\tau}$ and $\beta > 0$. For a Dirac-type input condition I_0 , Equation (6-20) reduces to

$$C(L_c, T) = \frac{2 I_0}{\pi^{1/2}} \exp\left(\frac{P_{ex}L_c}{2}\right) \int_l^\infty \frac{\gamma}{\xi^2} \left[\frac{4\pi}{\beta} \left(\tau - \frac{\gamma}{\xi^2} \right)^3 \right]^{-1/2} \exp\left[-\xi^2 - \frac{\gamma}{\xi^2} \left(\frac{P_{ex}}{4} + \alpha \right) - \frac{\beta}{4} \left(\frac{\gamma}{\xi^2} \right)^2 \left(\tau - \frac{\gamma}{\xi^2} \right)^{-1} - \frac{\alpha^2}{\beta} \left(\tau - \frac{\gamma}{\xi^2} \right) \right] d\xi \quad 6-21$$

Equations (6-20) and (6-21) express the breakthrough curve $C(L_c, T)$ in terms of the model parameters P_{ex} , α and β as well as the upstream boundary condition while the dimensionless time T is a function of the conduit velocity u . The single and double integrals are numerically integrated using the MATLAB functions ‘*integral*’ and ‘*integral2*’ respectively.

6.5.2 Finite aquifer (KTMB)

For the aquifer condition in Equation (6-8), the solution becomes

$$\bar{c} = \bar{c}_0 \exp\left(\frac{P_{ex} L_c}{2}\right) \exp\left[-\frac{P_{ex} L_c}{2} \sqrt{1 + \frac{4p}{P_{ex}} + \frac{4}{P_{ex}} \left(2\alpha + \frac{\beta p}{\alpha + \sqrt{\beta p + \alpha^2} \coth\left(L_m \frac{S}{\beta} \sqrt{\beta p + \alpha^2}\right)}\right)}\right] \quad 6-22$$

Equation (6-22) simulates the breakthrough curve resulting from a finite aquifer of width L_m . It is used to verify the range of aquifer widths for which (6-20) and (6-21) are valid. The solution is numerically inverted using the routine developed by *Hollenbeck* [1998].

6.6. Summary of Important Results

A process-based transport model is proposed to simulate tracer breakthrough curves. The conceptual model consists of a single conduit embedded in a porous aquifer with the two exchanging solute at their common interface. The advection diffusion equation governs the solute transport in both conduit and matrix while the interface solute exchange is described by the advective-dispersive mass flux equation. The coupled system of governing equations is consequently solved using the Laplace transform method and an analytical solution is obtained for semi-infinite and finite aquifers. The transport model provides a relationship between the breakthrough curve, upstream boundary condition (arbitrary or instantaneous), Péclet number and interface exchange coefficients α (advective exchange) and β (diffusive exchange).

CHAPTER 7

TRANSPORT MODEL – ANALYSIS AND RESULTS

In this chapter, the process-based transport model is discussed and used to simulate real breakthrough curves. First, the effect of the key parameters and simplifications are discussed. Those include a semi-infinite aquifer approximation and a Dirac-type input pulse. Consequently, the proposed KTM is applied to several karst systems with the aim of simulating real breakthrough curves and capture their long tailing using physically meaningful parameters.

7.1. Salient Results

7.1.1 Key model parameters

The KTM model parameters are the conduit velocity u , Péclet number P_{ex} and exchange coefficients α and β . A relationship between the conduit width w , exchange parameters and aquifer dispersivity ($\alpha_L = \theta D_y / v$) is given as $\alpha_L = \beta w / 4\alpha$. This relationship is of interest in inverse problems because it facilitates the estimation of both conduit and aquifer physical properties.

The effect of each KTM model parameter is hereby investigated for a conduit of length $L_c = 1$ subject to an instantaneous pulse of intensity $I_0 = 10$. The model's variables have the following values: $P_{ex} = 20$, $\alpha = 0.5$ and $\beta = 1$. The results are shown in Figure 30. The Péclet number P_{ex} simulates the extent of the spill while the parameters α and β control the conduit/aquifer solute exchange. For smaller values of P_{ex} (i.e. < 6), a strong skewness in the breakthrough curve is witnessed because the conduit transport process is dominated by dispersion rather than advection.

When α is zero, there is no advective interface exchange and the conduit interacts with the matrix through a diffusive flux only. As α increases, the solute leaves the conduit towards the matrix through the one-directional advective flow (or v) and the recovery rate at the spring is reduced. Conversely, when β increases, the conduit recovers solute later on and longer tailing is observed.

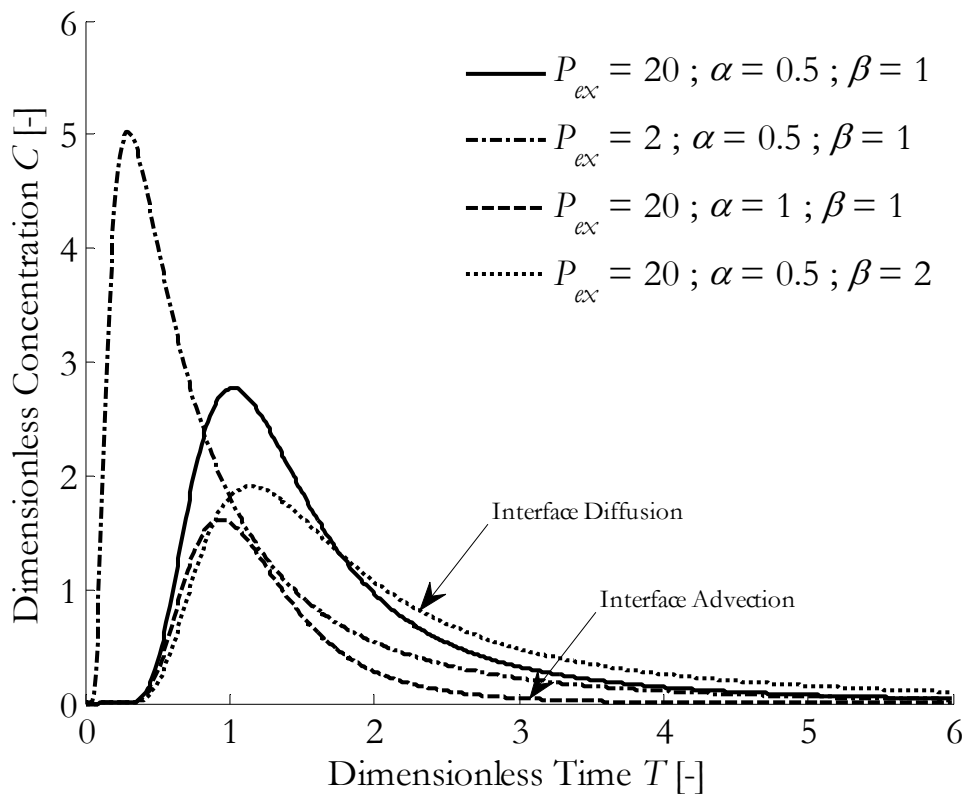


Figure 30. Effect of the model parameters on the breakthrough curve. When the advective exchange parameter α increases, the solute mass is lost to the aquifer (compare solid line to coarsely dotted line). Conversely, the diffusive exchange parameter β shows a later recovery of solute (compare solid line to finely dotted line).

7.1.2 Effect of non-constant velocities

As mentioned in the flow-related chapters, exchange flow is generally caused by the occurrence of a flood event where the conduit initially loses a certain volume of

water to the aquifer and slowly recovers it during the recession period. Subsequently, the advective interface flux becomes bidirectional such that it is positive throughout the flood event and negative during the recession period. Additionally, the conduit velocity u becomes affected by the upstream boundary condition as well as the conduit/aquifer exchange of flow. When the conduit is losing water to the matrix, the velocity is reduced along its length and the reverse is true when the conduit is draining the surrounding matrix. Hence, the variation of u in both space and time affects the extent of exchange and consequently the shape of the resulting breakthrough curve.

However, the proposed KTM model assumes constant conduit and aquifer velocities u and v and does not handle interface hydraulic gradient inversions. Therefore, the KTM model applications are limited to systems flowing under baseflow conditions where temporal and spatial variations of conduit velocities can be neglected.

Moreover, tracer tests are generally released as a pool dump into a sinkhole which causes an increase in the karst conduit's hydraulic heads with respect to the matrix after the pool release [Luhmann *et al.*, 2012]. As a result, interface exchange is induced and water/solute leaves the conduit towards the aquifer at a velocity v . The proposed KTM makes the assumption that this flow is one-directional, constant and positive towards the matrix (i.e. positive α) when simulating breakthrough curves.

7.1.3 Effect of boundary conditions

7.1.3.1 Aquifer

The finite aquifer model KTMB (Equation 6-22) helps analyzing the effect of the aquifer width (L_m) on breakthrough curves. As shown in Figure 31 ($P_{ex} = 20$, $\alpha = 0.5$, $\beta = 1$ and $S = 200$), it has the ability to modify the shape of the curve depending

on the available area for the solute to spread into the matrix. However, one notices that the aquifer width required to make major changes is significantly lower than the conduit's length, L_c (i.e. $L_m > 0.02$). Therefore, the semi-infinite approximation (KTM) is valid in most inverse problems since aquifers are generally much wider than the embedded karst conduits.

7.1.3.2 Instantaneous input pulse

In field applications, tracers are generally released instantaneously into a karst conduit and the input pulse is often approximated as a Dirac-type. In order to assess this simplification, the output of equations (6-20) and (6-21) is compared using a short rectangular input pulse of duration T_{pulse} and intensity $C_{pulse} = I_0/T_{pulse}$. As shown in Figure 32, the Dirac-type model is able to reproduce the more general case of a rectangular input pulse up to a duration that is 100 times smaller than the total simulation time. However, it loses accuracy as the upstream pulse duration increases (see $T_{max}/T_{pulse} \leq 50$).

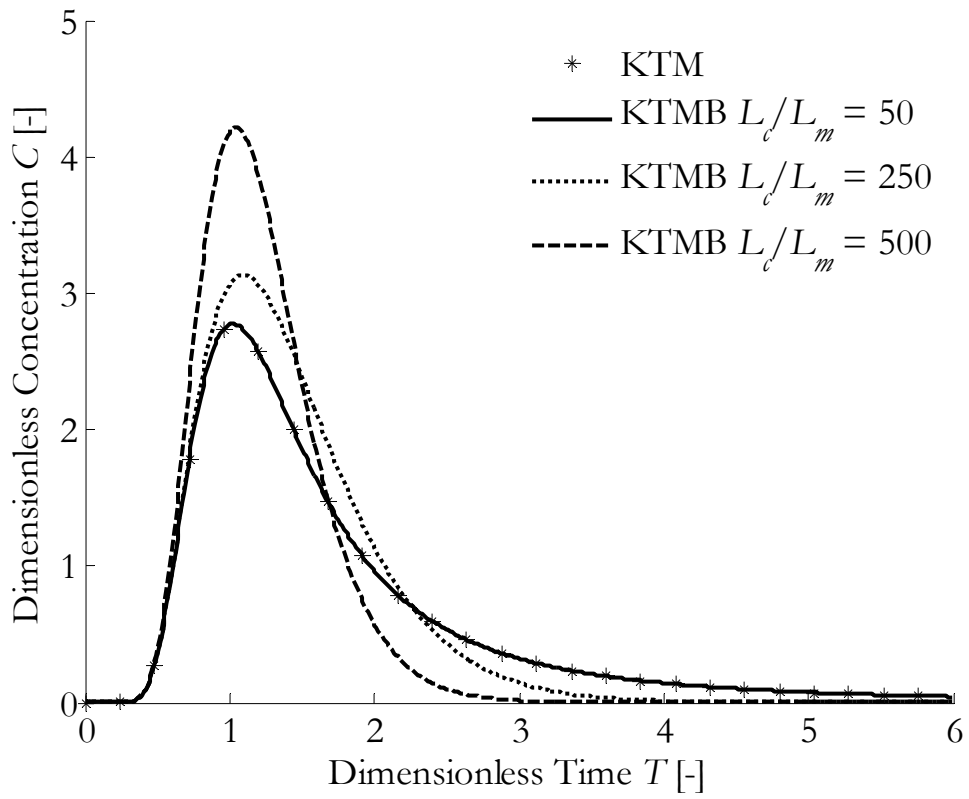


Figure 31. Comparison between the unbound and bound aquifer models for $S = 200$. The unbound aquifer model is found valid for small aquifer widths that are at least 50 times shorter than the conduit length.

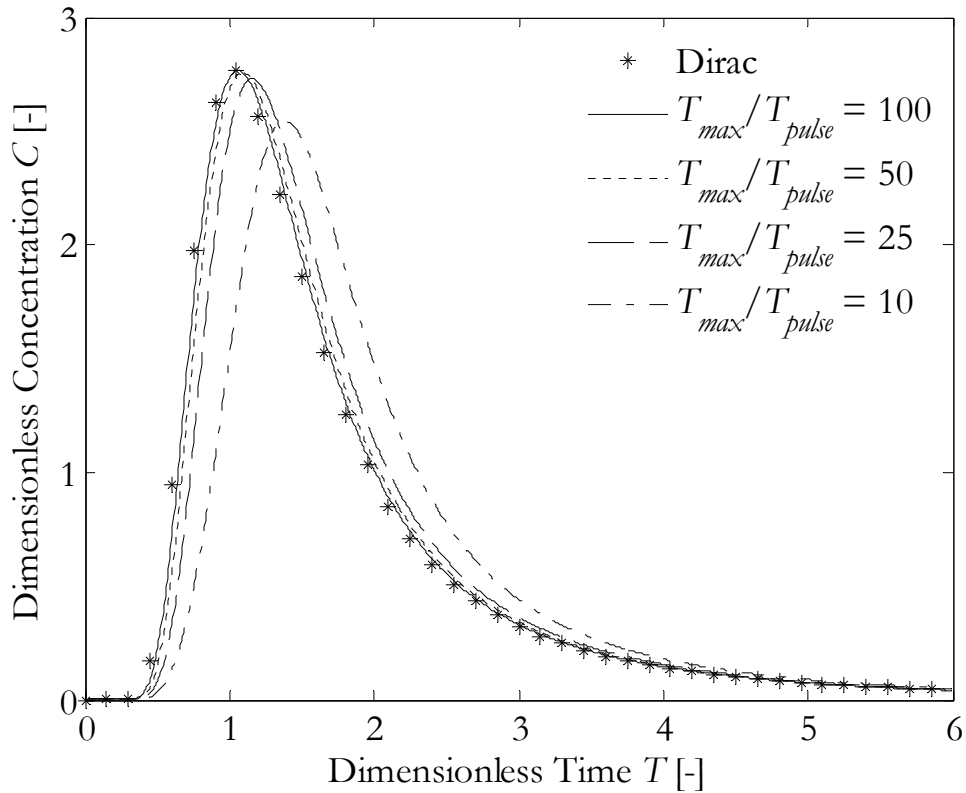


Figure 32. Comparison between a Dirac-type and short-pulse rectangular input functions. The Dirac-type input approximation is found acceptable for a wide range of pulse durations.

7.2. Comparison to other models

Existing process-based models for simulating breakthrough curves mostly adopt a partitioning approach and have been particularly selected to simulate the long tailing. As previously mentioned in the introductory section of this thesis, the two-region non-equilibrium model 2RNE [Toride *et al.*, 1993] has been widely applied to karst systems although its parameters have little physical meaning in a karst context. In fact, 2RNE was originally intended for porous media and its parameters are a function of the retardation, dispersion and advection processes in the mobile region as well as the first-order exchange between mobile and immobile regions. The mobile region parameters can be compared to KTM's Péclet number P_{ex} , conduit velocity u and flow

area A . On the other hand, 2NRE's exchange parameters do not represent actual karst aquifer properties and physical processes.

In comparison to partitioning models, KTM adopts the more physical ADE approach instead of non-equilibrium solute partitioning and is a function of both conduit and aquifer physical parameters. Yet, the KTM model is not able to handle non-constant conduit and aquifer velocities and is not as flexible as distributive numerical transport models in representing the system's heterogeneities.

7.3. Parameter Estimation

The Peclet number P_{ex} is expected to be higher than 6 in karst conduits [*Field and Nash, 1997*] and indicates predominant advective transport when it is greater than 100. The aquifer dispersivity is generally reported as α_L/θ and varies between 0.02 and 250 meters depending on the scale of observation and type of aquifer (i.e. porous versus fractured) [*Gelhar et al., 1992*]. Since the drainable porosity θ (or S_y) has a large range in karst aquifers [*Baedke and Krothe, 2001*], it is difficult to compare the calculated dispersivity values (α_L) using KTM to the ones reported in literature (α_L/θ). Therefore, the latter is possible if the drainable porosity θ of the matrix or aquifer is known or simulated from flow models.

As for the parameter estimation procedure, the conduit velocity u is a good choice of a non-fitted parameter because it can be initially estimated from the time to the breakthrough curve's peak and the distance between the sink and spring resurgence. By initially fixing the conduit velocity u , the model parameters P_{ex} , α , β and A are optimized using the nonlinear least-square fitting. The process is repeated for different values of the conduit velocity until an acceptable goodness of fit is reached. The flow

area A later gives a rough estimate of the conduit dimension by assuming a circular conduit of diameter w .

7.4. Model Applications

The analytical transport model KTM is used to simulate the breakthrough curves of the following karst systems: the Dyers and Quarry springs [*Field and Pinsky, 2000*], the Sagebach spring [*Göppert and Goldscheider, 2008*], the Olaorta spring [*Morales et al., 2010*] and the Villanueva del Rosario spring [*Marín et al., 2015*]. These experiments represent different field conditions, tracer quantities and conduit velocities. They all consist of an almost instantaneous release of tracer at a karst window or sinking location.

7.4.1 Dyers and Quarry springs

The Dyers Spring (Elizabethtown, Kentucky) test consists of releasing 3.57 grams of Rhodamine WT dye into the karst window located 1,372 meters away from the spring while the Quarry Spring (Tennessee) tracer test involves an injection of 0.7 g of Uranine in a monitoring well located 450 meters away [*Field and Pinsky, 2000*]. Four parameters are hereby fitted: P_{ex} , α , β and A with u being manually set. The characteristic lengths for Dyers and Quarry are 1372 and 450 meters respectively. The tracer test simulations are shown in Figure 33 and Figure 34.

For Dyers, the optimized parameters are $P_{ex} = 450$, $\alpha = 0.923$, $\beta = 0.39$, $A = 0.308 \text{ m}^2$ and the conduit velocity is $u = 101 \text{ m/hour}$. A rough estimate of the conduit dimension is found from the area A as $w \approx 0.63 \text{ m}$ and the aquifer dispersivity $\alpha_L = \beta w / 4\alpha$ is found equal to 0.066 m. As for the Quarry Spring tracer test, the KTM

optimized parameters are $P_{ex} = 113.18$, $\alpha = 0.6193$, $\beta = 1.038$, $A = 0.1974 \text{ m}^2$ and $u = 77 \text{ m/hour}$. Consequently, the aquifer dispersivity is equal to 0.16 meters with $w \approx 0.4 \text{ m}$. The recovery rates indicate that interface exchange is governed by advection for Dyers (62.5%) and by diffusion for Quarry (98%). This also explains the long tailing of Quarry's breakthrough curve as compared to the sharper recession of Dyer's.

Both springs' breakthrough curves were previously fitted using a mobile/immobile model (MIM) and a combined physical/chemical non-equilibrium model (PCNE) [Field and Leij, 2014]. Yet, MIM and PCNE required seven and twelve parameters respectively in order to simulate Dyers' breakthrough curve. In comparison, KTM's required a significantly less number of parameters to match their accuracy and adopted the more physical ADE approach instead of non-equilibrium solute partitioning.

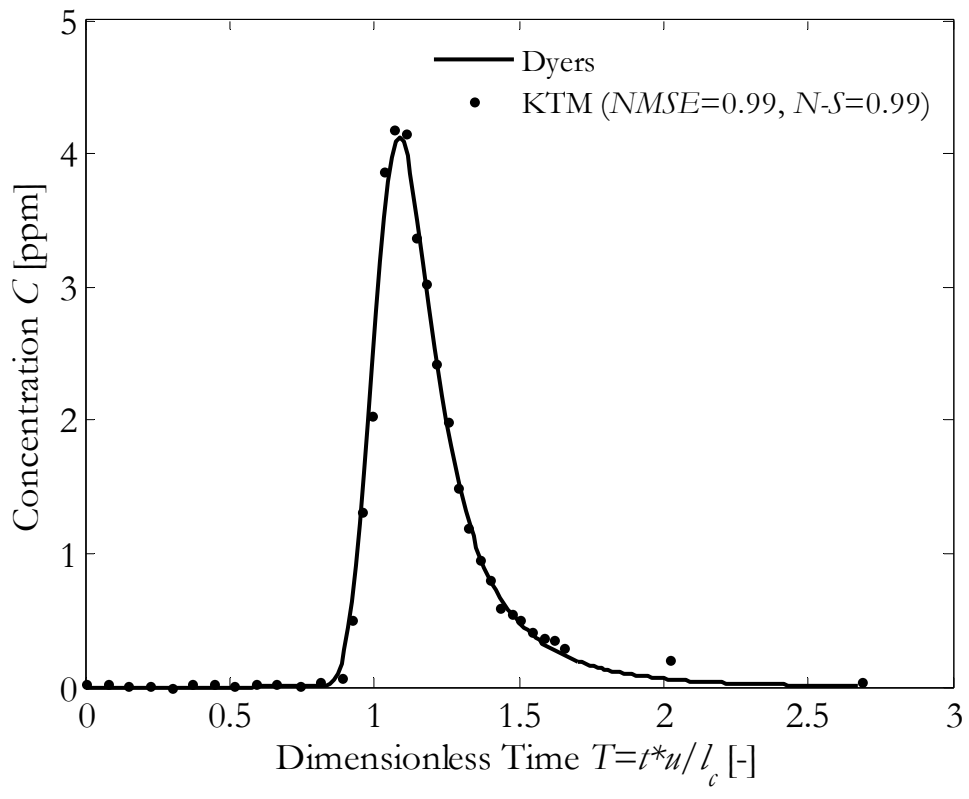


Figure 33. Observed vs. simulated Dyers Spring breakthrough curve.

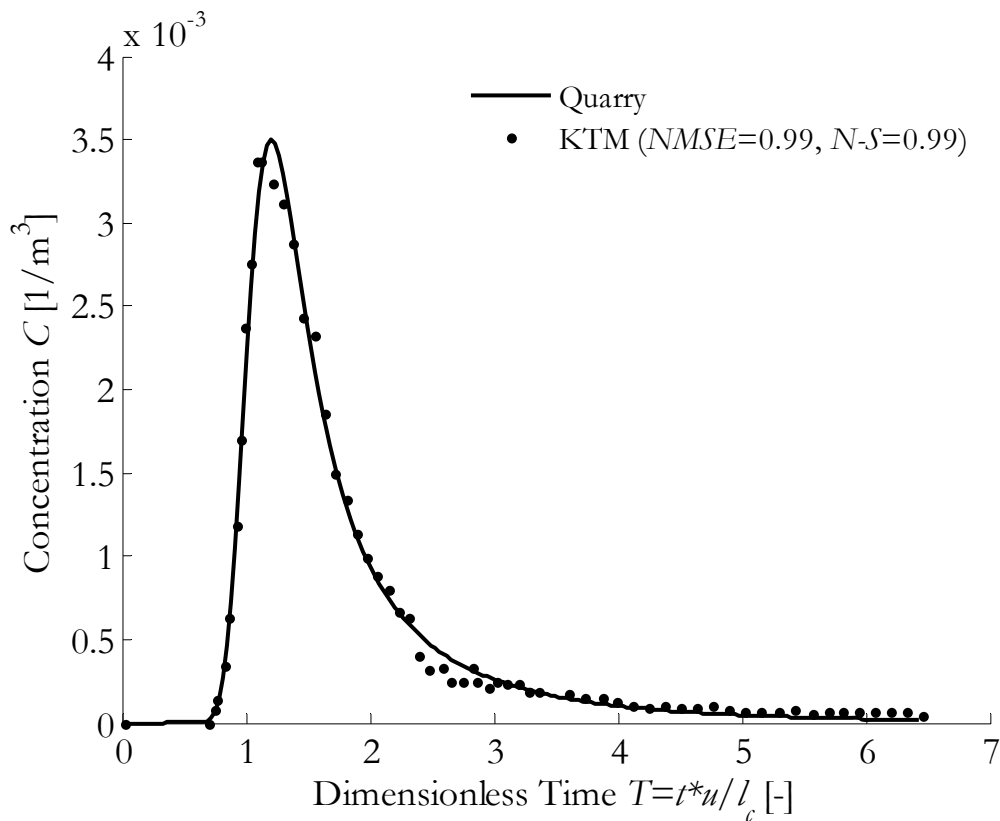


Figure 34. Observed vs. simulated Quarry Spring breakthrough curve.

7.4.2 Sagebach spring

A tracer test was conducted during low-flow and constant discharge conditions at a karst spring in the vicinity of the Hölloch cave, Switzerland [Göppert and Goldscheider, 2008]. Two hundred grams (200 g) of Uranine were injected into the cave's stream and recovered 2,500 kilometers downstream at the Sagebach spring. The recovery rate was 99.8%.

Using the same fitting methodology outlined above, Sagebach's optimized parameters are $P_{ex} = 179.4$, $\alpha = 0.0431$, $\beta = 0.0498$ and $A = 20.54 \text{ m}^2$. The conduit velocity is $u = 26.2 \text{ m/hour}$. As shown in Figure 35, the proposed KTM model is able to simulate the measured data with a perfect goodness of fit ($NMSE = 0.998$) and is particularly capable of capturing the long tail of the breakthrough curve. The

optimized area is within range of $Q_{avg}/u = 23.63 \text{ m}^2$. The $\beta/\alpha = 0.703$ ratio and average conduit radius $w \approx 5.1 \text{ m}$ result in an aquifer dispersivity of $\alpha_L = 0.9 \text{ m}$.

Previously, *Göppert and Goldscheider* [2008] used the one-dimensional ADE model and the two-region non-equilibrium model 2RNE to fit Sagebach's breakthrough curve with 2RNE being more successful in simulating the long tailing. In contrast, the proposed KTM model follows the physical ADE approach, is able to link the exchange parameters to the matrix properties and has an equal performance to 2RNE's.

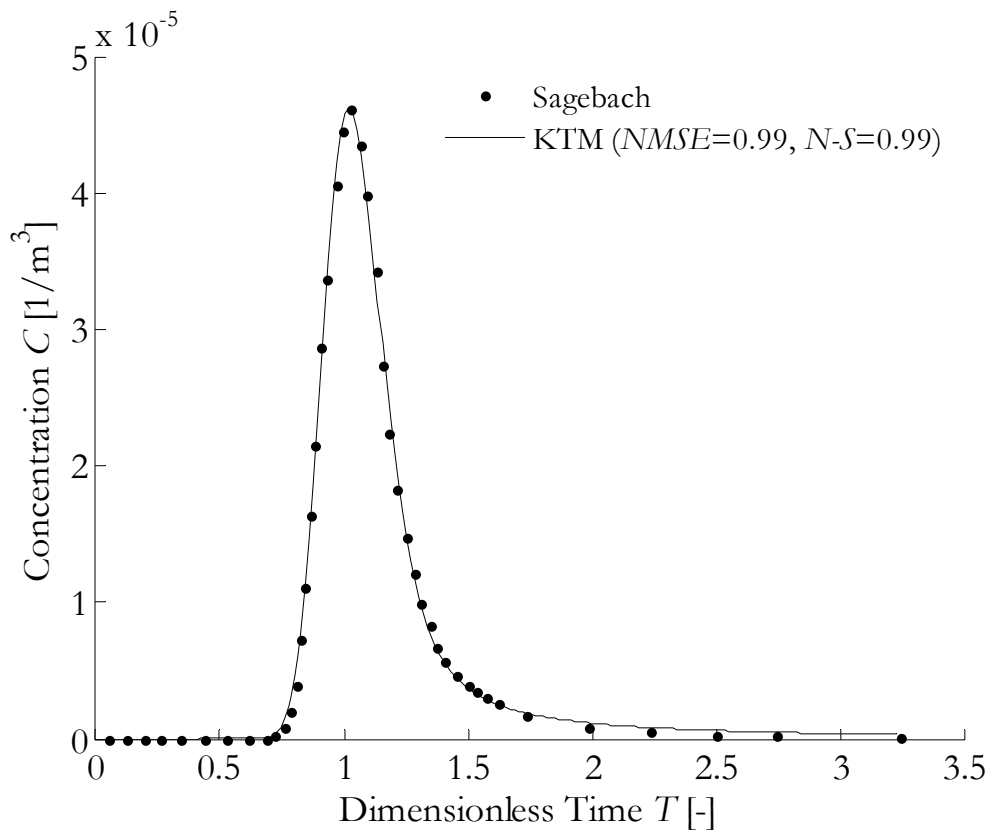


Figure 35. Observed vs. simulated Sagebach spring breakthrough curve.

7.4.3 Olaorta spring

The Olaorta Spring is located in the Santa Eufemia-Ereñozar karst unit in the Basque County, Spain. It is connected to a karst window that is located 450 meters

upstream of the spring. The detailed hydrological and geological information is available in [Morales *et al.*, 2007; Morales *et al.*, 2010]. Several tracer tests were conducted in the area using lithium which is not present in natural waters and allows the generation of well-defined recovery curves. A tortuosity factor of 1.3 is also assumed (i.e. $L_c = 1.3 \times 475m$).

KTM was able to simulate the resulting breakthrough curves of two independent tracer tests Olaorta Test 1 (91% recovery) and Olaorta Test 2 (86% recovery) as shown in Figure 36 and Figure 37 with a goodness of fit exceeding 99%. The following parameters were obtained for Test 1: $P_{ex} = 53.33$, $\alpha = 0.00512$, $\beta = 0.081$ and $u = 56.5$ m/s and Test 2: $P_{ex} = 69.62$, $\alpha = 0.069$, $\beta = 0.11$ and $u = 42$ m/hour.

When two tracer tests are conducted, one can take advantage of the relationship $v = [4\theta D_y/w] \frac{\alpha}{\beta}$ in order to determine which test exhibits a higher advective interface velocity. Indeed, $4\theta D_y/w$ is constant because it is a function of physical conduit/matrix parameters. As a result, the test with a higher α/β ratio undergoes more advective exchange with the surrounding matrix. For Tests 1 and 2, the α/β ratios were 0.0632 and 0.627 respectively. Therefore, more solute is leaving the conduit during Test 2 as compared to Test 1 which explains the lower recovery rate during Test 2 (i.e. 86% vs. 91%).

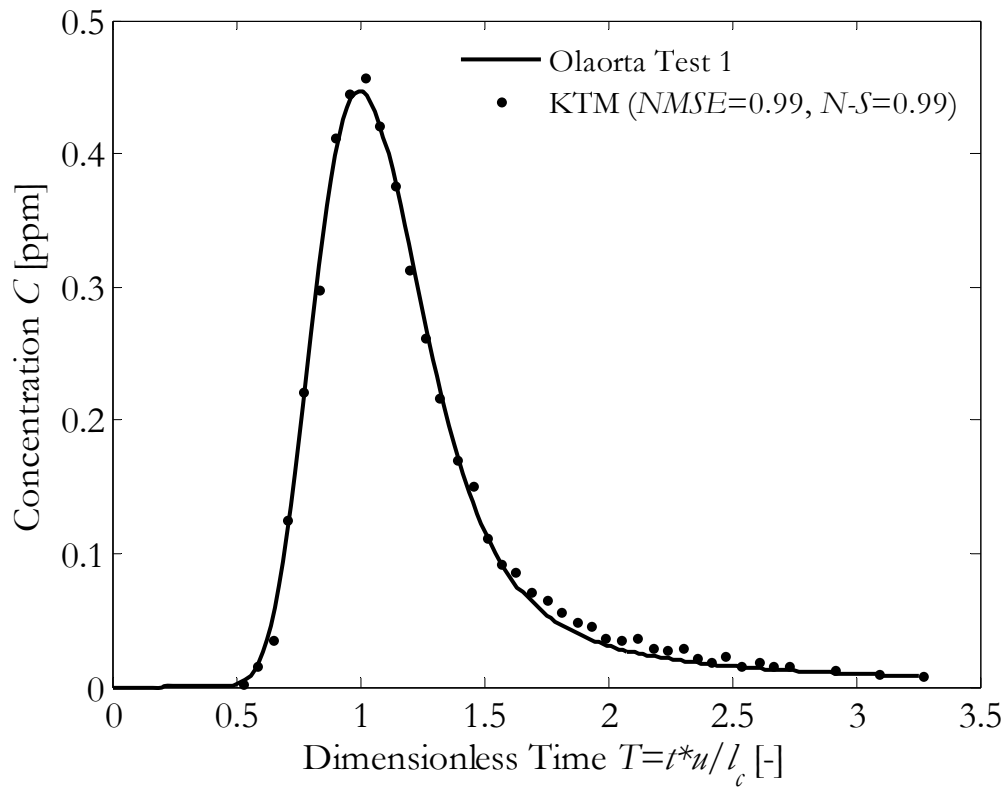


Figure 36. Observed vs. simulated Olaorta, Test 1 spring breakthrough curve.

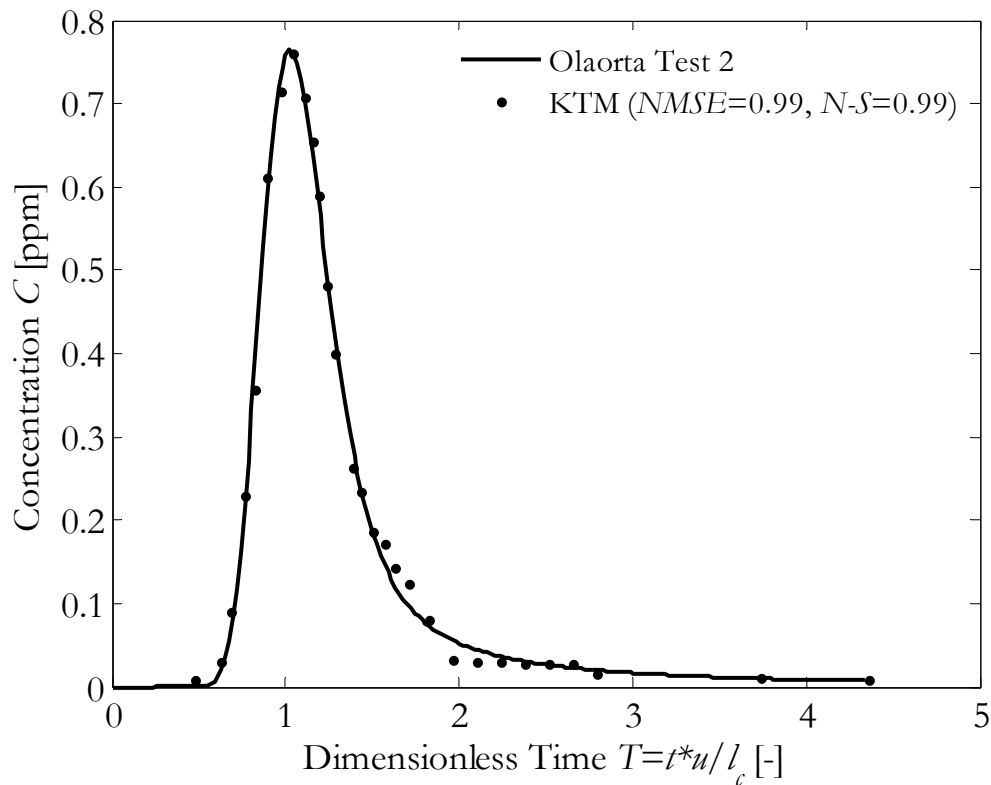


Figure 37. Observed vs. simulated Olaorta, Test 2 spring breakthrough curve.

7.4.4 Villanueva del Rosario spring

The Villanueva del Rosario spring is located nearly 30 km north of the city of Malaga, Southern Spain. The spring drains the Sierra Camarolos and Sierra del Jobo karst aquifers. A detailed geological description of the site is available in *Marín et al.* [2015]. Several tracer tests were carried out with each tracer being released in a different swallow hole. The purpose was to map underground connections in the aquifer and reduce the uncertainty regarding conduits' lengths, sizes and locations (Figure 38). A summary of input data is available in Table 8.

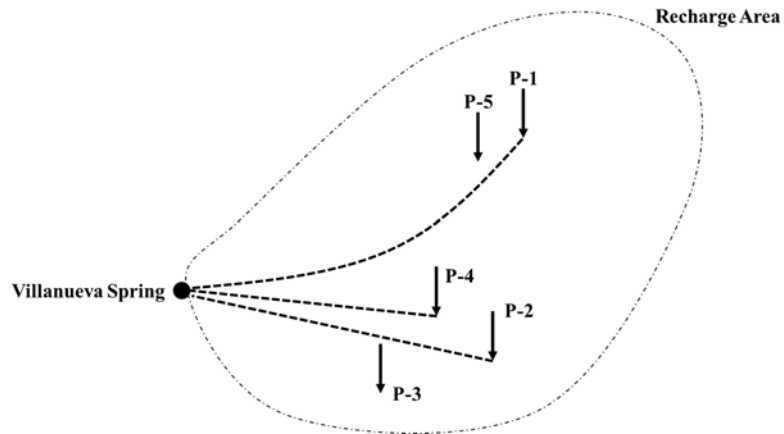


Figure 38. Schematic representation of the Villanueva del Rosario Spring. Tracers are released in swallow holes (P-arrows) at five locations. Connections were proven between the designated karst windows and spring (i.e. dotted lines).

Table 8. Input data for Villanueva del Rosario Spring tracer tests

| | T-1 | T-2 |
|--------------------------------------|----------------------------|----------------------------|
| Tracer | Pyranine (P-1) | Sulforhodamine-B (P-4) |
| Distance to Spring L_c (m) | 6,600 | 2,810 |
| Tracer Test Day | May 2 nd , 2011 | May 2 nd , 2011 |
| End of Injection | 8:35 | 8:45 |
| Mass Injected (kg) | 2 | 2 |
| Average Discharge at Spring (L/s) | 925 | 925 |
| Recovery Rate (%) | 42.4 | 54.2 |

KTM was able to simulate the breakthrough curves of two simultaneous tracer tests as shown in Figure 39 and Figure 40 with a goodness of fit exceeding 95%. The following parameters were obtained for Sulforhodamine-B (T-1 released in P-1): $P_{ex} = 794.31$, $\alpha = 0.212$, $\beta = 0.29$, $A = 23.05 \text{ m}^2$, and $u = 215.5 \text{ m/s}$ and Pyranine (T-2 released in P-4): $P_{ex} = 309.34$, $\alpha = 0.319$, $\beta = 0.6$, $A = 14.95 \text{ m}^2$ and $u = 160.5 \text{ m/hour}$.

Using the relationship $v = [4\theta D_y/w] \frac{\alpha}{\beta}$, one can express the advective velocity in conduit P-1 (Pyranine) in function of the one in conduit P-4 (Sulforhodamine-B) while assuming constant matrix properties θ and D_y . Therefore, $v_{P-1} \approx 1.1v_{P-4}$ with $w_{P-1}/w_{P-4} = \sqrt{A_{P-1}/A_{P-4}}$. The two advective velocities are nearly equal thus indicating similar hydraulic fluxes at the interface. They also must be significant due to the low recovery rates at the spring (42.4% for P-1 and 54.2% for P-4).

One observes though that the goodness of fit is herein lowered as compared to the other tracer tests especially in the recession period. This is explained from the effect of the conduit velocity u variation during the flood conditions under which the two tests were carried out. A better fit would thus be achieved by deriving a synthesized flow and transport model that simulates both discharge and breakthrough curves.

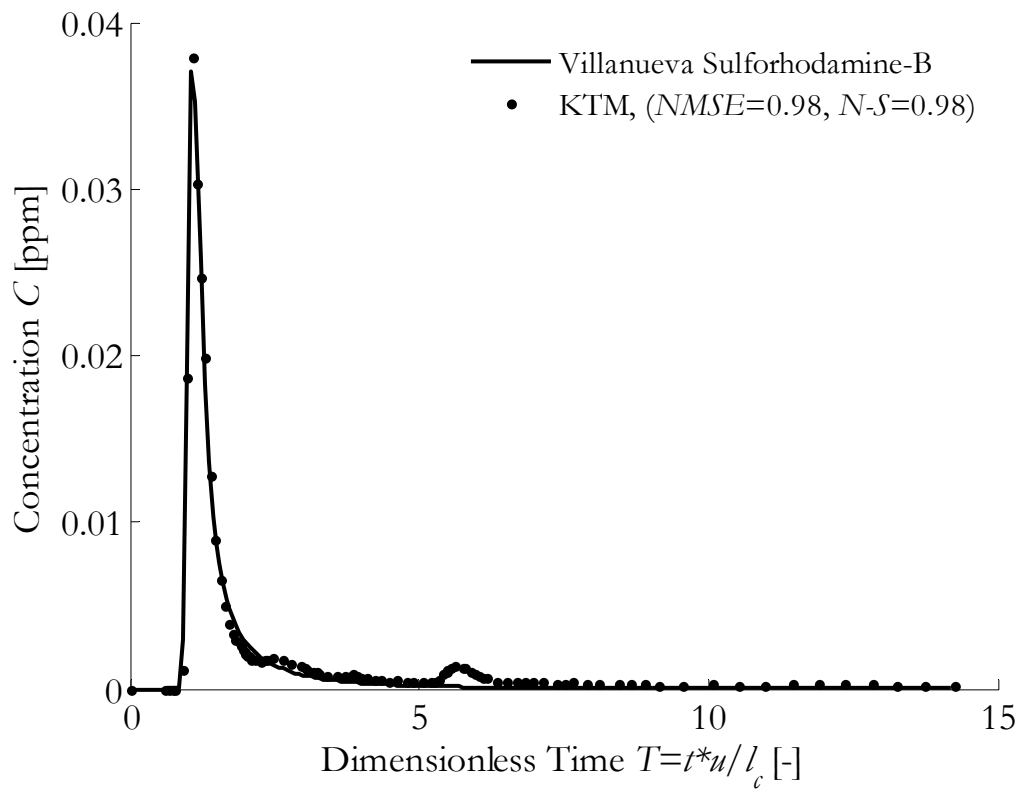


Figure 39. Computed and measured concentrations for the Sulforhodamine-B tracer test

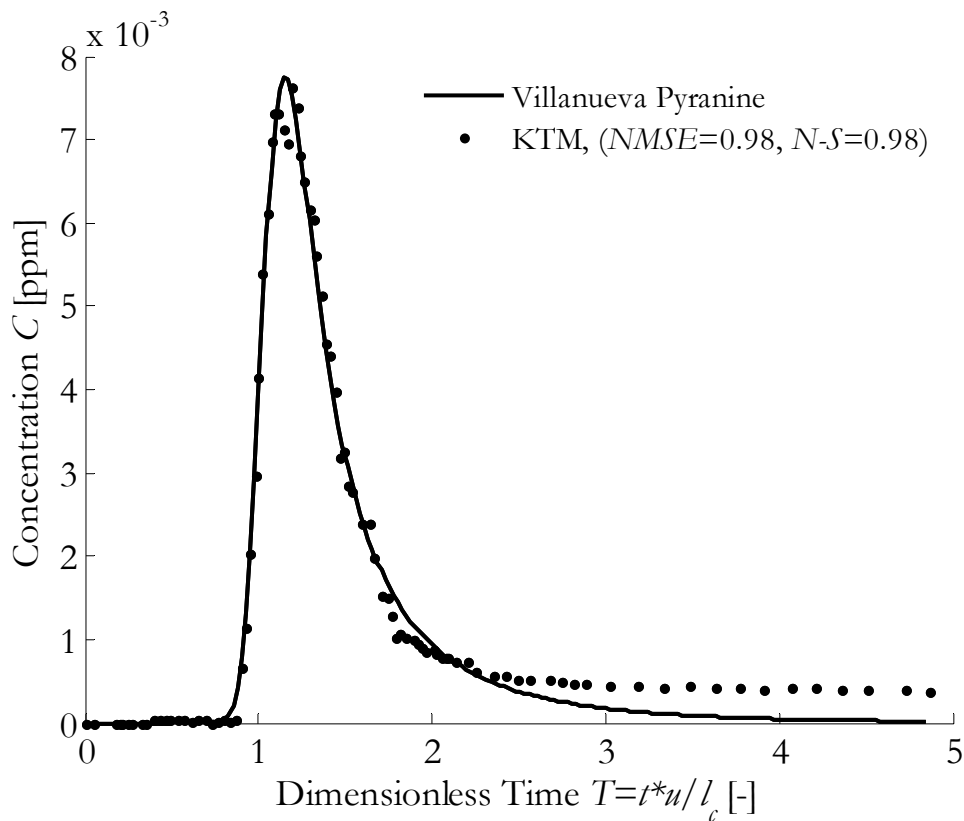


Figure 40. Computed and measured concentrations for the Pyranine tracer test.

7.5. Summary of Important Results

The proposed KTM model's key parameters and main simplifications were discussed. The Dirac-type input pulse was found as a good approximation for short duration pulses while the semi-infinite aquifer simplification was successfully tested against the more complex finite aquifer solution. The model was also compared to existing partitioning models in terms of its usefulness and physical meaning. The model's limitations were also discussed namely the constant conduit and aquifer velocities assumption. Finally, KTM was successfully applied to simulate several real breakthrough curves while capturing their long tailing using physically meaningful parameters. For all tests, the Péclet number was within the expected range for karst conduits and referred to a predominant advective transport.

CHAPTER 8

CONCLUSIONS

Simplified process-based flow and transport models capable of simulating the outflow of real karst aquifers were developed. The models' conceptual framework is physically sound and represents the different processes occurring in a karst system. The models' domain consists of a one-dimensional conduit embedded in a two-dimensional matrix with the two elements exchanging fluid and solute at their common interface. The important conclusions drawn from the models' results and recommended future work are discussed below.

8.1. Important Conclusions

With respect to the flow models:

- 1) The process-based approach allowed the derivation of computationally advantageous solutions that express the spring discharge in terms of recharge conditions (diffuse and concentrated), domain boundaries (conduit length and aquifer width), boundary conditions and physical properties of the system.
- 2) All flow models can replicate the typical shape of a spring hydrograph that is characterized by a fast rising limb followed by a long recession curve. However, the pipe flow models simulate an almost instantaneous response to a recharge event while the open-channel models can simulate a pulse arrival delay.

- 3) An optimal parameter estimation method was proposed to relate the linear and nonlinear model parameters. Hypothetical runs showed the effectiveness of this method in approximating the nonlinear numerical flow models with the computationally advantageous linear ones.
- 4) The semi-infinite aquifer assumption was found as a good approximation of the more complex finite aquifer case.
- 5) The flow models were able to simulate the response of the more complex three-dimensional dual-hydraulic models and are a function of more physically sound parameters than lumped or empirical models.
- 6) The fully unbound pipe flow model was successfully applied to a sink and rise karst aquifer system subject to a concentrated recharge pulse. The model was able to simulate the outflow of this karst system for long periods of time and thus showed its predicting capability.
- 7) The open-channel flow model was used to simulate the outflow of a karst system subject to a diffuse aquifer recharge and another that consists of a sinking stream where delays were observed between upstream and downstream boundaries.

With respect to the transport models:

- 8) The process-based transport model expresses the tracer breakthrough curve in terms of the mass of tracer released and the physical properties of the system. The parameters include the conduit velocity, Péclet number and advective/diffusive interface exchange parameters.

- 9) The transport model was effectively able to simulate real tracer breakthrough curves using the advection-diffusion equation rather than a partitioning approach. However, a better interpretation of the aquifer dispersivity parameter can be achieved by knowing the drainable porosity of the aquifer.

8.2. Future Work

Recommended future work includes:

8.2.1 *Branched systems solutions*

In karst systems, underground conduit networks are often encountered [*Perrin et al., 2007; Chen and Goldscheider, 2014*]. However, the simulation of such systems is very challenging in the absence of information about conduits' location and the relative contribution of each tributary. A process-based approach to simulating branched conduit systems might prove useful especially for large systems where recharge heterogeneities might be encountered. The branched solution will consist of conduit branches draining sub-catchments and connected to a main spring conduit. This approach has been already proposed in a DC context by *Cornaton and Perrochet [2002]* while neglecting the contribution of diffuse recharge. For a CDC approach, the flow in each branch will be a function of its own recharge and physical conditions including diameter, friction factor and matrix properties. The number of parameters will increase as compared to the models presented herein but the solution will still be simpler than existing distributive models. The latter can serve as a further refinement of the parameter values.

8.2.2 Matrix water levels simulation

The aim of the proposed process-based flow models was to simulate a spring discharge given a concentrated or diffuse aquifer recharge as an input. A better validation and calibration of the model is achieved by simulating the water levels in the adjoining matrix. The expressions of matrix water levels can be easily derived by using the Laplace transform method introduced in this work: one only has to replace the obtained water levels (H_c) into the solution of the aquifer flow equation (or linearized Boussinesq).

8.2.3 Hydrological models

The proposed flow models can be integrated into more complex hydrological ones that provide a better estimate of the recharge to groundwater term r . Consequently, future research should focus on modeling the flow through the epikarst layer [e.g. *Hartmann et al.*, 2012] and incorporating the results into the proposed models in order to achieve a better estimation of the parameters.

8.2.4 Synthesized flow and transport modeling approach

A synthesized flow and transport model can analyze spring hydrographs and breakthrough curves simultaneously if sufficient data is gathered from the field and aims on achieving a better estimation of model parameters. The transport model will be a function of the non-constant velocities obtained from the associated flow model and will be able to handle bi-directional fluxes at the interface.

In order to validate the synthesized model, field work should focus on conducting tracer tests during flood conditions. Consequently, the effect of

conduit/aquifer exchange is analyzed by comparing simulated to monitored values at the spring (discharge and breakthrough curve) and observation wells (water levels and solute concentrations). An extension of this work is to conduct tracer tests in pressurized and unpressurized karst conduits during flood conditions and study the effect of conduit flow hydraulics on solute transport.

APPENDIX A RECHARGE EXPRESSIONS

The arbitrary recharge functions are defined as a linear relationship between two data points

$$G(t) = \begin{cases} g_0(t) & t_0 \leq t < t_1 \\ \dots & \dots \\ g_{n-1}(t) & t_{n-1} \leq t < t_n \\ g_n(t) & t \geq t_n \end{cases}$$

where n is the number of data points and $g_{n-1}(T) = \frac{G(T_n) - G(T_{n-1})}{T_n - T_{n-1}}(T - T_{n-1}) + G(T_{n-1})$ for $T_{n-1} < T$ and $g_n(T) = G(T_n)$ for $T > T_n$.

The above arbitrary (G) and piecewise (R) recharge conditions are written in terms of the unit step function as

$$G(T) = g_0(T)\mathcal{U}(T - T_0) + g_n(T)\mathcal{U}(T - T_n) + \sum_{i=2}^n [g_{i-1}(T) - g_{i-2}(T)]\mathcal{U}(T - T_{i-1}) \quad \text{Arbitrary}$$

$$R(T) = r_0\mathcal{U}(T - T_0) + \sum_{i=1}^n (r_i - r_{i-1})\mathcal{U}(T - T_i) \quad \text{Piecewise}$$

Taking the Laplace transform on T for the above two equations, one gets

$$\bar{G} = \frac{e^{-pT_0}}{p^2} [I_1 + pG(T_0)] + G(T_n) \frac{e^{-pT_n}}{p} + \sum_{i=2}^{n-1} (I_i - I_{i-1}) \frac{e^{-pT_{i-1}}}{p^2} \quad \text{Arbitrary}$$

$$\bar{R} = r_0 \frac{e^{-pT_0}}{p} + \sum_{i=1}^n (r_i - r_{i-1}) \frac{e^{-pT_i}}{p} \quad \text{Piecewise}$$

where $I_i = [G(T_i) - G(T_{i-1})]/[T_i - T_{i-1}]$ and p is a complex number.

The expressions of \bar{G} and \bar{R} are replaced into the Laplace transform equations presented in this dissertation for model evaluation.

APPENDIX B FINITE DIFFERENCE EQUATIONS

- Pipe Flow

The finite difference solution to the nonlinear pipe flow model is hereby presented (i.e. Equations 2-19 and 2-7). First, a fictitious time-dependent term is introduced and the nonlinear pipe flow equation (2-7) is rewritten as

$$\epsilon \frac{dH_c}{dT} = m\beta \left(-\frac{\partial H_c}{\partial X} \right)^{m-1} \frac{\partial^2 H_c}{\partial X^2} + \kappa \frac{\partial H_m}{\partial Y} \Big|_{Y=0}$$

where ϵ is a fictitious term that is introduced to fasten the convergence process.

Using the Crank-Nicolson scheme, the finite difference solution to the above equation becomes

$$\begin{aligned} E_i^{n+1} H_{i+1}^{n+1} - \left(\frac{2\epsilon \Delta X_i^2}{m\beta \Delta T} + 2E_i^{n+1} \right) H_i^{n+1} + E_i^{n+1} H_{i-1}^{n+1} \\ = -E_i^n H_{i+1}^n + \left(2E_i^n - \frac{2\epsilon \Delta X_i^2}{m\beta \Delta T} \right) H_i^n - E_i^n H_{i-1}^n \\ - \frac{\kappa \Delta X_i^2}{m\beta} \left(\frac{H_{j=2}^{n+1} - H_{j=1}^{n+1}}{\Delta Y_{j=1}} + \frac{H_{j=2}^n - H_{j=1}^n}{\Delta Y_{j=1}} \right) \end{aligned}$$

where $E_i^n = \left(\left| -\left(\frac{H_{i+1}^n - H_{i-1}^n}{2\Delta X_i} \right) \right| \right)^m \left[-\left(\frac{H_{i+1}^{n+1} - H_{i-1}^n}{2\Delta X_i} \right) \right]^{-1}$. The i and j indices

represent the flow in the X and Y directions respectively. Therefore, ΔX_i is the cell discretization in the X -direction and ΔY_j in the Y -direction. H_i and H_j are the conduit and matrix heads respectively. For stability, the Courant number must be satisfied such

that $C_o = \frac{m\beta}{\epsilon} \frac{\Delta T}{\Delta X^2} \leq \frac{1}{2}$.

- **Matrix Flow**

The aquifer flow equation (2-19) is discretized using the Crank Nicolson scheme as

$$\begin{aligned} \frac{1}{\Delta Y_{j+1/2}} H_{i,j+1}^{n+1} - \left(\frac{2\Delta Y_j}{\sigma_d \Delta T} + \frac{1}{\Delta Y_{j+1/2}} + \frac{1}{\Delta Y_{j-1/2}} \right) H_{i,j}^{n+1} + \frac{1}{\Delta Y_{j-1/2}} H_{i,j-1}^{n+1} \\ = -\frac{1}{\Delta Y_{j+1/2}} H_{i,j+1}^n + \left(-\frac{2\Delta Y_j}{\sigma_d \Delta T} + \frac{1}{\Delta Y_{j+1/2}} + \frac{1}{\Delta Y_{j-1/2}} \right) H_{i,j}^n \\ - \frac{1}{\Delta Y_{j-1/2}} H_{i,j-1}^n - \frac{2\Delta Y_j}{\sigma_d} \frac{R_{i,j}^n}{S_y} \end{aligned}$$

- **Open Channel Flow**

The channel flow equation is discretized using the MacCormack scheme which is an explicit, two-step predictor and corrector scheme. It is second order accurate in space and time. Forward finite differences are used to calculate the predictor step values and backward finite differences are utilized for the corrector step.

The predictor step is given as follows

$$H_{i,n+1}^* = H_{i,n} - \alpha \frac{\Delta T}{\Delta X} (H_{i+1,n}^m - H_{i,n}^m) + \Delta T \kappa \left(\frac{H_{i,j=2}^{n+1} - H_{i,j=1}^{n+1}}{\Delta Y_{j=1}} \right)$$

where i, j and n are the conduit, matrix and time indices respectively.

The value at the last node ($N_n + 1$) is calculated using the backward finite difference method

$$\begin{aligned} H_{N_n+1,n+1}^* = H_{N_n+1,n} - \alpha \frac{\Delta T}{\Delta X} (H_{N_n+1,n}^m - H_{N_n,n}^m) \\ + \Delta T \kappa \left(\frac{H_{N_n+1,j=2}^{n+1} - H_{N_n+1,j=1}^{n+1}}{\Delta Y_{j=1}} \right) \end{aligned}$$

The corrector step is

$$H_{i,n+1}^{**} = H_{i,n+1}^* - \alpha \frac{\Delta T}{\Delta X} [(H_{i,n}^*)^m - (H_{i-1,n}^*)^m] \\ + \Delta T \kappa \left(\frac{H_{i,j=2}^{n+1} - H_{i,j=1}^{n+1}}{\Delta Y_{j=1}} \right)$$

The value at the current time step is the average of the corrector and previous time step values

$$H_{i,n+1} = \frac{1}{2} (H_{i,n} + H_{i,n+1}^{**})$$

BIBLIOGRAPHY

- Baedke, S. J., and N. C. Krothe (2001), Derivation of effective hydraulic parameters of a karst aquifer from discharge hydrograph analysis, *Water Resour.Res.*, 37(1), 13.
- Bailly-Comte, V., J. B. Martin, and E. J. Sreaton (2011), Time variant cross correlation to assess residence time of water and implication for hydraulics of a sink-rise karst system, *Water Resour.Res.*, 47(5).
- Bakalowicz, M. (2005), Karst groundwater: a challenge for new resources, *Hydrogeol.J.*, 13(1), 148.
- Birk, S., and S. Hergarten (2010), Early recession behaviour of spring hydrographs, *Journal of Hydrology*, 387(1-2), 24.
- Bruggeman, G. A. (1999), *Analytical solutions of geohydrological problems*, Elsevier, Amsterdam, Netherlands.
- Chen, Z., and N. Goldscheider (2014), Modeling spatially and temporally varied hydraulic behavior of a folded karst system with dominant conduit drainage at catchment scale, Hochifen-Gottesacker, Alps, *Journal of Hydrology*, 514, 41.
- Clemens, T., D. Hückinghaus, M. Sauter, R. Liedl, and G. Teutsch (1996), A combined continuum and discrete network reactive transport model for the simulation of karst development, *IAHS-AISH Publication*, 237, 309.
- Cornaton, F., and P. Perrochet (2002), Analytical 1D dual-porosity equivalent solutions to 3D discrete single-continuum models. Application to karstic spring hydrograph modelling, *Journal of Hydrology*, 262(1-4), 165.
- Criss, R. E., and W. E. Winston (2003), Hydrograph for small basins following intense storms, *Geophys.Res.Lett.*, 30(6), 47-41.
- de Hoog, F., J. Knight, and A. Stokes (1982), An Improved Method for Numerical Inversion of Laplace Transforms, *Society for Industrial and Applied Mathematics. SIAM Journal on Scientific and Statistical Computing*, 3(3), 357-366.

- de Rooij, R., P. Perrochet, and W. Graham (2013), From rainfall to spring discharge: Coupling conduit flow, subsurface matrix flow and surface flow in karst systems using a discrete-continuum model, *Adv. Water Resour.*, 61, 29.
- Doummar, J. (2012), Identification of indicator parameters for the quantitative assessment of vulnerability in karst aquifers, Niedersächsische Staats-und Universitätsbibliothek Göttingen.
- Drogue, C. (1972), Analyse statistique des hydrogrammes de décrues des sources karstiques statistical analysis of hydrographs of karstic springs, *Journal of Hydrology*, 15(1), 49-68.
- Field, M. S., and S. G. Nash (1997), Risk assessment methodology for karst aquifers:(1) Estimating karst conduit-flow parameters, *Environmental Monitoring and Assessment*, 47(1), 1-21.
- Field, M. S., and P. F. Pinsky (2000), A two-region nonequilibrium model for solute transport in solution conduits in karstic aquifers, *J.Contam.Hydrol.*, 44(3), 329-351.
- Field, M. S., and F. J. Leij (2014), Combined physical and chemical nonequilibrium transport model for solution conduits, *J.Contam.Hydrol.*, 157, 37-46.
- Fu, T., H. Chen, and K. Wang (2016), Structure and water storage capacity of a small karst aquifer based on stream discharge in southwest China, *Journal of Hydrology*, 534, 50-62.
- Gelhar, L. W., C. Welty, and K. R. Rehfeldt (1992), A critical review of data on field-scale dispersion in aquifers, *Water Resour.Res.*, 28(7), 1955.
- Göppert, N., and N. Goldscheider (2008), Solute and Colloid Transport in Karst Conduits under Low- and High-Flow Conditions, *Ground Water*, 46(1), 61-68.
- Hartmann, A., J. Lange, M. Weiler, Y. Arbel, and N. Greenbaum (2012), A new approach to model the spatial and temporal variability of recharge to karst aquifers, *Hydrology and Earth System Sciences*, 16(7), 2219.

- Hartmann, A., N. Goldscheider, T. Wagener, J. Lange, and M. Weiler (2014), Karst water resources in a changing world: Review of hydrological modeling approaches, *Rev.Geophys.*, 52(3), 218.
- Hisert, R. A. (1994), *A Multiple Tracer Approach to Determine the Ground and Surface Water Relationships in the Western Santa Fe River, Columbia County, FL.*
- Hollenbeck, K. J. (1998), INVLAP.m: A MATLAB function for numerical inversion of Laplace transforms by the de Hoog algorithm, edited.
- Houseworth, J. E. (2006), An analytical model for solute transport in unsaturated flow through a single fracture and porous rock matrix, *Water Resour.Res.*, 42(1), W01416.
- Houseworth, J. E., D. Asahina, and J. T. Birkholzer (2013), An analytical model for solute transport through a water-saturated single fracture and permeable rock matrix, *Water Resour.Res.*, 49(10), 6317-6338.
- Hunt, B. (1990), An approximation for the bank storage effect, *Water Resour.Res.*, 26(11), 2769.
- Jeannin, P. Y. (2001), Modeling flow in phreatic and epiphreatic Karst conduits in the Hölloch Cave (Muotatal, Switzerland), *Water Resour.Res.*, 37(2), 191.
- Jukić, D., and V. Denić-Jukić (2006), Nonlinear kernel functions for karst aquifers, *Journal of Hydrology*, 328(1), 360.
- Jukić, D., and V. Denić-Jukić (2008), Estimating parameters of groundwater recharge model in frequency domain: Karst springs Jadro and Žrnovnica, *Hydrol.Process.*, 22(23), 4532.
- Katz, B. G., J. S. Catches, T. D. Bullen, and R. L. Michel (1998), Changes in the isotopic and chemical composition of ground water resulting from a recharge pulse from a sinking stream, *Journal of Hydrology*, 211(1), 178-207.
- Kovacs, A., and P. Perrochet (2008), A quantitative approach to spring hydrograph decomposition, *Journal of Hydrology*, 352(1), 16.

- Kovacs, A., P. Perrochet, L. Kiraly, and P. Y. Jeannin (2005), A quantitative method for the characterisation of karst aquifers based on spring hydrograph analysis, *Journal of Hydrology*, 303(1-4), 152.
- Langston, A. L., E. J. Sreaton, J. B. Martin, and V. Bailly-Comte (2012), Interactions of diffuse and focused allogenic recharge in an eogenetic karst aquifer (Florida, USA), *Hydrogeol.J.*, 20(4), 767.
- Lauritzen, S. E. (1985), Morphology and hydraulics of an active phreatic conduit, *Cave Science - Transactions British Cave Research Association*, 12(4), 139-146.
- Luhmann, A. J., M. D. Covington, S. C. Alexander, S. Y. Chai, B. F. Schwartz, J. T. Groten, and E. C. Alexander (2012), Comparing conservative and nonconservative tracers in karst and using them to estimate flow path geometry, *Journal of Hydrology*, 448-449, 201-211.
- Maillet, E. T. (1905), Essais d'Hydraulique souterraine et fluviale, *Nature*, 72(1854), 25-26.
- Mangin, A. (1975), Contribution à l'étude hydrodynamique des aquifères karstiques, *Thèse de Doctorat, Institut des Sciences de la Terre de l'Université de Dijon*.
- Maréchal, J. C., B. Ladouche, N. Doerfliger, and P. Lachassagne (2008), Interpretation of pumping tests in a mixed flow karst system, *Water Resour.Res.*, 44(5).
- Marín, A. I., B. Andreo, and M. Mudarra (2015), Vulnerability mapping and protection zoning of karst springs. Validation by multitracer tests, *Science of the Total Environment*, 532, 435-446.
- Martin, J. (2003), Quantification of the matrix hydraulic conductivity in the Santa Fe River Sink/Rise system with implications for the exchange of water between the matrix and conduits, Gainesville Fla. : University of Florida.
- Martin, J., and R. Dean (2001), Exchange of water between conduits and matrix in the Floridan aquifer, *Chem.Geol.*, 179(1-4), 145.

Martin, J., E. Screamon, and J. Martin (2006), *Monitoring well responses to karst conduit head fluctuations: Implications for fluid exchange and matrix transmissivity in the Floridan aquifer*, 209 pp.

Mayaud, C., T. Wagner, R. Benischke, and S. Birk (2013), Understanding changes in the hydrological behaviour within a karst aquifer (Lurbach system, Austria), *Carbonates and Evaporites*, 1-9.

Mayaud, C., T. Wagner, R. Benischke, and S. Birk (2014), Single event time series analysis in a binary karst catchment evaluated using a groundwater model (Lurbach system, Austria), *Journal of Hydrology*, 511, 628.

Moore, P. J., J. B. Martin, and E. J. Screamon (2009), Geochemical and statistical evidence of recharge, mixing, and controls on spring discharge in an eogenetic karst aquifer, *Journal of Hydrology*, 376(3-4), 443.

Moore, P. J., J. B. Martin, E. J. Screamon, and P. S. Neuhoff (2010), Conduit enlargement in an eogenetic karst aquifer, *Journal of Hydrology*, 393(3-4), 143.

Morales, T., I. Fdez. de Valderrama, J. A. Uriarte, I. Antigüedad, and M. Olazar (2007), Predicting travel times and transport characterization in karst conduits by analyzing tracer-breakthrough curves, *Journal of Hydrology*, 334(1-2), 183-198.

Morales, T., J. A. Uriarte, M. Olazar, I. Antigüedad, and B. Angulo (2010), Solute transport modelling in karst conduits with slow zones during different hydrologic conditions, *Journal of Hydrology*, 390(3-4), 182-189.

Nash, J. E., and J. V. Sutcliffe (1970), River flow forecasting through conceptual models part I — A discussion of principles, *Journal of Hydrology*, 10(3), 282-290.

Perrin, J., P. Y. Jeannin, and F. Cornaton (2007), The role of tributary mixing in chemical variations at a karst spring, Milandre, Switzerland, *Journal of Hydrology*, 332(1), 158.

Powers, J. G., and L. Shevenell (2000), Transmissivity Estimates from Well Hydrographs in Karst and Fractured Aquifers, *Ground Water*, 38(3), 361.

- Reimann, T., and M. E. Hill (2009), MODFLOW-CFP: A new conduit flow process for MODFLOW-2005, *Ground Water*, 47(3), 321.
- Reimann, T., C. Rehl, W. B. Shoemaker, T. Geyer, and S. Birk (2011a), The significance of turbulent flow representation in single-continuum models, *Water Resour.Res.*, 47(9).
- Reimann, T., T. Geyer, W. B. Shoemaker, R. Liedl, and M. Sauter (2011b), Effects of dynamically variable saturation and matrix-conduit coupling of flow in karst aquifers, *Water Resour.Res.*, 47(11).
- Ritorto, M. (2007), Impacts of diffuse recharge on transmissivity and water budget calculations in the unconfined karst aquifer of the Santa Fe River basin, University of Florida.
- Ritorto, M., E. J. Sreaton, J. B. Martin, and P. J. Moore (2009), Relative importance and chemical effects of diffuse and focused recharge in an eogenetic karst aquifer: an example from the unconfined upper Floridan aquifer, USA, *Hydrogeol.J.*, 17(7), 1687.
- Scanlon, B. R., R. E. Mace, M. E. Barrett, and B. Smith (2003), Can we simulate regional groundwater flow in a karst system using equivalent porous media models? Case study, Barton Springs Edwards aquifer, USA, *Journal of Hydrology*, 276(1-4), 137.
- Sreaton, E., J. B. Martin, B. Ginn, and L. Smith (2004), Conduit properties and karstification in the unconfined Floridan Aquifer, *Ground Water*, 42(3), 338.
- Shevenell, L. (1996), Analysis of well hydrographs in a karst aquifer: Estimates of specific yields and continuum transmissivities, *Journal of Hydrology*, 174(3-4), 331.
- Shoemaker, W. B., E. L. Kuniandy, S. Birk, S. Bauer, and E. D. Swain (2008), Documentation of a conduit flow process (CFP) for MODFLOW-2005., in *U.S. Geological Survey techniques and methods, Book 6*, edited, U.S. Geological Survey, Reston, Virginia.
- Springer, G. S. (2004), A pipe-based, first approach to modeling closed conduit flow in caves, *Journal of Hydrology*, 289(1), 178.

Sudicky, E. A., and E. O. Frind (1982), Contaminant transport in fractured porous media: Analytical solutions for a system of parallel fractures, *Water Resour.Res.*, 18(6), 1634-1642.

Tang, D. H., E. O. Frind, and E. A. Sudicky (1981), Contaminant transport in fractured porous media: Analytical solution for a single fracture, *Water Resour.Res.*, 17(3), 555-564.

Toride, N., F. J. Leij, and M. T. van Genuchten (1993), A comprehensive set of analytical solutions for nonequilibrium solute transport with first-order decay and zero-order production, *Water Resour.Res.*, 29(7), 2167.

van Genuchten, M. T., F. J. Leij, T. H. Skaggs, N. Toride, S. A. Bradford, and E. M. Pontedeiro (2013), Exact analytical solutions for contaminant transport in rivers 2. Transient storage and decay chain solutions, *Journal of Hydrology and Hydromechanics*, 61(3), 250.

White, W. B. (2002), Karst hydrology: recent developments and open questions, *Eng.Geol.*, 65(2), 85.

Winston, W. E., and R. E. Criss (2004), Dynamic hydrologic and geochemical response in a perennial karst spring, *Water Resour.Res.*, 40(5), W05106.